Dissertation

submitted to the

Combined Faculty of Natural Sciences and Mathematics

Ruprecht-Karls University Heidelberg, Germany

for the degree of

Doctor of Natural Sciences (Dr. rer. nat.)

Presented by

Dipl.-Chem. Isabel Thome

Born in Heidelberg, Germany

Oral examination: May 31^{st}, 2013

Influence of Surface Conditioning and Morphology on Biofouling

This dissertation was carried out at the

Department of Applied Physical Chemistry

University of Heidelberg

Referees:

Prof. Dr. Michael Grunze

apl. Prof. Dr. Hans-Robert Volpp

Abstract Biofouling, the undesired colonization of surfaces, is a major problem for marine-related industries. To prevent unwanted effects caused by biofouling, suitable non-toxic coatings for the marine environment are required. Conditioning, i.e. the adsorption of proteins and macromolecules influences, as surface chemistry and morphology do, the settlement of fouling oragnisms. Investigating the temporal dynamics of conditioning film formation on functionalized self assembled monolayers (SAMs), it was shown that the obtained film thickness of about 10 Å to 20 Å is independent of the surface chemistry but differences occur concerning the composition of these films. While on hydrophilic surfaces more proteinaceous compounds are detectable, the hydrophobic surfaces show a lower intensity of proteins. Furthermore, is was shown that in standard *Ulva linza* spore settlement assays the influence of a molecular conditioning layer is likely to be small, but by increasing pre-conditioning time this influence gains importance and should be considered in long term experiments. Preconditioning also resulted in detectable surface differences in field studies. It was found that preconditioned samples which contain more proteinaceous compounds seem to be more attractive for settlement. Experiments with matured laboratory biofilms formed by *Pseudomonas aeruginosa* demonstrated that using a protein-rich medium results in conditioning film formation. Conversely, surface conditioning is reduced when a media containing a smaller amount of proteins is utilized. Furthermore, it was observed that surface chemistry has no remarkable effect on the fraction of inoculated bacteria that adhere to a surface.
Finally, inspired by the nanostructured skin of dolphins, electron-beam lithography was utilized to create a honeycomb topography made of poly(*N*-isopropylacrylamide) (PNIPAM). The evaluation showed that structures from 0.75 µm to 2.5 µm in diameter reduce *Ulva* settlement in comparison to a smooth PNIPAM surface. It should be noted, that wet polymer structure heights in the range of only 0.01 µm do have an effect on spores with a body size of around 5 µm.

Kurzfassung

Biofouling, also die unerwünschte Besiedlung von Oberflächen, stellt ein erhebliches Problem in der maritimen Industrie dar. Um die durch den Bewuchs auftretenden unerwünschten Effekte zu unterbinden, werden entsprechende umweltverträgliche Beschichtungen benötigt. Die Konditionierung, d. h. die Adsorption von Proteinen und anderen Makromolekülen, beeinflusst, wie auch die Oberflächenchemie und Morphologie, die Besiedlung durch Fouling -Organismen. Mit der Erforschung des zeitlichen Ablaufs der Bildung dieser Konditionierungsfilme auf selbst assemblierenden Monolagen (SAMs), konnte gezeigt werden, dass die erhaltene Schichtdicke von ungefähr 10 Å bis 20 Å unabhängig von der Oberflächenchemie ist, sich die Filme aber in ihrer Zusammensetzung unterscheiden. Während auf hydrophilen Oberflächen mehr proteinöse Komponenten nachweisbar waren, zeigten hydrophobe Oberflächen eine geringere Proteinintensität. Des Weiteren konnte gezeigt werden, dass in Standard *Ulva linza* Besiedlungs-Assays der Einfluss eines molekularen Konditionierungsfilms gering ist, aber dass durch Erhöhung der Inkubationszeit dieser Einfluss immer drastischer wird und er desshalb bei der Planung von Langzeitexperimenten dementsprechend berücksichtigt werden muss. Präkonditionierung führte auch zu nachweisbaren Oberflächenunterschieden in Feldstudien. Es wurde beobachtet, dass konditionierte Proben mit einem höheren Anteil an proteinösen Komponenten attraktiver für die Besiedlung zu sein scheinen. Experimente mit ausgeprägten Laborbiofilmen, die durch *Pseudomonas aeruginosa* gebildet werden, zeigten, dass bei der Nutzung eines proteinreichen Mediums ein Konditionierungsfilm gebildet wird. Im Gegensatz dazu war bei einem proteinärmeren Medium eine geringere Konditionierung erkennbar. Zusätzlich wurde gezeigt, dass die Oberflächenchemie keinen erheblichen Einfluss auf die an der Oberfläche anhaftenden Bakterien hat.

Schließlich wurde Elektronenstrahllithographie verwendet um eine durch die nanostrukturierte Haut von Delphinen inspirierte Bienenwabenstruktur bestehend aus Poly(*N*-isopropylacrylamid) (PNIPAM) zu generiern. Die Auswertung zeigte, dass Strukturen mit einer Größe von 0.75 µm bis 5 µm Durchmesser die Besiedlung durch *Ulva* im Vergleich zu einer gleichmäßigen PNIPAM Oberfläche reduzieren. Es ist bemerkenswert, dass eine Polymerstrukturhöhe im Bereich von nur 0.01 µm die Besiedlung etwa 5 µm großer Sporenkörper beeinflusst.

Contents

1 Introduction

The term *fouling* refers to an undesired process in which unwanted material from the surrounding environment accumulates to a surface. In the case of *biofouling* this material consists of organisms and their waste products, e.g., extracellular polysaccharides and proteins [1]. Marine biofouling is an omnipresent phenomenon which is known since man-kind started sailing the ocean. Objects get colonized as soon as they are submerged into water leading to a high economic loss in all kinds of involved industries [2]. Actually, the one being most affected is the marine shipping industry, but heat exchangers, oceanographic sensors as well as aquaculture systems are also influenced by this phenomenon [3]. Annually, billions of dollars are spent worldwide to reduce the negative impact of the adhesion of barnacles, macro algae and microbial slime [4]. As a direct consequence of this, the water flow along the immersed object is perturbed and the hydrodynamic drag is increased. This leads to higher fuel consumption at a comparable speed of the vessel [5–7]. Just a small layer of algal slime with a thickness of 1 mm will increase the hull friction by 80 % and cause a 15 % loss in ship speed [8]. It is estimated that the world fleet consumes an additional 300 million tons of fuel annually and international shipping therefore was identified as a factor contributing to the global climate change by being a significant source of air pollution [9]. Besides the environmental issues, the costs for dry-docking and cleaning of the ships and the renewal of the antifouling coatings are immense [10].

So far, biocidal antifouling coatings, systems which kill colonizing organisms, were used to prevent this fouling process. The most common and most effective antifouling paints originated in the 1970s and were based on tributyltin (TBT) [8, 11, 12]. These paints have been used widely on all kinds of ships to prevent —due to their high toxicity— the settlement and growth of marine organisms on the hulls. The application of TBT based paints led to an annual saving of about 5.7 billion US dollars [13]. Unfortunately, paints incorporating TBT have adverse effects on the surrounding environment as they are the most toxic substances ever intensionally introduced to the aquatic environment [14]. TBT has a short residence time of only a few days and degrades rapidly in seawater. However, by adsorbing to particles it can reach the sediments where the degradation is considerably slower. Due to the fact that the molecules have lipophilic and ionic properties, they can easily bind to lipids and macromolecules and get accumulated in the tissue of marine organisms [15]. The turnaround came in the 1980s, when two events were attributed to a TBT contamination. A near-collapse

Figure 1.1: Fouling on a submarine by the seaweed *Ulva linza* [5].

of an oyster farm in Arcachon Bay, western France occured [16], as well as the demise of populations of dogwelks *Nucella* at centers of boating activity in south-west England [17]. These facts forced the International Maritime Organization (IMO) to a restriction of TBT-containing compounds from paints and vessels in 2001 [18]. As a result there is an enormous demand of environmentally acceptable and 'greener' antifouling coatings.

Designing antifouling or foul-release coatings is a major challenge since surfaces can have different variable properties. To get a better understanding of the impact of these physical, chemical, and biological properties influencing the fouling process, model surfaces were required. Self assembled monolayers (SAMs) are a highly multifunctional tool to study the response of marine organisms to a number of physico-chemical properties [19–24]. With these surfaces it is possible to vary, e.g., the surface chemistry and with this the wettability, to study its influence in greater detail [25–27].

Not only marine organisms are responsible for fouling, also the fastest step, the adsorption of proteins, also called conditioning of a surface, is important [28]. Based on this fact the performance of different SAMs with varying surface chemistries, was investigated as a conditioning film was allowed to build up. The changes of the surface properties were followed by different analytical techniques. Additionally, it was determined which influence these rapidly formed conditioning layers have on the succeeding adhesion of marine organisms. Therefore experiments were first performed in the laboratory with model organisms. The green alga *Ulva linza* was chosen since it is the most common fouler worldwide [4]. Like many other marine life forms they need to locate and settle on a surface quickly to complete their life cycle and with this they are perfectly suitable to perform fast screenings of new investigated coatings.

Indeed, these short time laboratory test with model organisms offer a fast possibility to screen potential anti-fouling coatings. However, the real challenge for every developed surface is to resist the everyday changing environmental factors in the ocean. Therefore field studies at important locations where the variation in populations and its influence is well known are required. In the course of this thesis two different test sites on the east coast of Florida were selected to study the formation and influence of a conditioning layer on chemically different surfaces known from laboratory studies.

One drawback of field studies is that they are mainly longterm assays usually performed over a period of several months to years. To overcome this negative impact some more artificial laboratory studies with mature biofilms are required. As bacteria are among the fastest organisms to colonize a surface, the bacterium *Pseudomonas aeruginosa* was chosen as a model for bacterial adhesion. Although this is a freshwater bacterium its behavior is comparable to that of marine species [29]. Another reason for choosing *P. aeruginosa* was its increasing presence in other systems, ranging from heat exchangers to human implants. It plays a major role in the wound healing process where it is necessary to control the adhesion of bacteria to decrease the possible infection rate of wounds.

Not only the chemistry has an influence on the adhesion of organisms, but also the topography of a surface is a major aspect which contributes to the quality of antifouling coatings [2, 24, 30]. By changing the accessible area between the adhesives and the sample, an effective reduction of the adhesion strength could be observed [19]. There are numerous examples in nature, such as the skin of sharks or dolphins, which exemplify that structured surfaces are capable of reducing the settlement of fouling organisms [31–33]. The method of choice was electron beam lithography utilizing SAMs as a resist, which serve as an anchor group for the growing of polymer brush patterns after irradiation. Honeycomb structures, inspired by the nanostructured skin of pilot whales were chosen due to the fact that the structures seem to be able to prevent the growth of biofilms due to their unique topography [24]. In this work patterns of different feature sizes were produced and their influence on the settlement behavior of the zoospore *Ulva linza* was investigated.

2 State of the art

In the following sections the existing knowledge in literature important for this thesis will be reviewed. First, the different stages of the fouling process will be presented and the associated organisms with their special behavior will be introduced. Next, the surfaces used in this work are described and an overview of which surface properties have an influence on the settlement process will be given. In the last subsections the operating modes of the analytical techniques used in this thesis are explained in detail.

2.1 Biofouling

Biofouling is defined as the accumulation of proteins and other organic molecules, microorganisms, plants, algae or animals on wetted surfaces [34]. The organisms which are mainly part of this process live in shallow water along coast lines. So far, more then 4000 different species have been identified on fouled structures [35] but nevertheless this is just a fraction of organisms living in that kind of environment for which the adhesion to a substrate is a major part of their life cycle. This also raises another challenge for the organisms. They need to find ways to stick to the surface without being washed off. Therefore ship hulls are a special habitat and with periodically changing parameters like temperature, flow rate or salinity of the water they build a niche for microorganisms, which can adapt to environmental changes [18].

The fouling process is described to be composed of varying organisms of different sizes which adhere to immersed samples on different timescales (Figure 2.1). The initial step is the adsorption of a 'conditioning' film primarily composed of dissolved organic material [36–38]. This process is mainly driven by physical forces such as electrostatic interactions or van der Waals forces. The following colonization of this conditioned surface is dependent on the availability of the organisms and their demand to explore and attach to it. This is a highly dynamic process which depends on many factors like the geographical location, the season and additionally the competition between different species. Within this pool of organisms they can be distinguished between 'microfoulers' (unicellular microorganisms) such as bacteria, diatoms and protozoa, 'soft macrofoulers' like visible algae and invertabrates (soft corals, sponges, anemones and tunicates) and 'hard macrofoulers' like barnacles, mussels and tubeworms [3, 5].

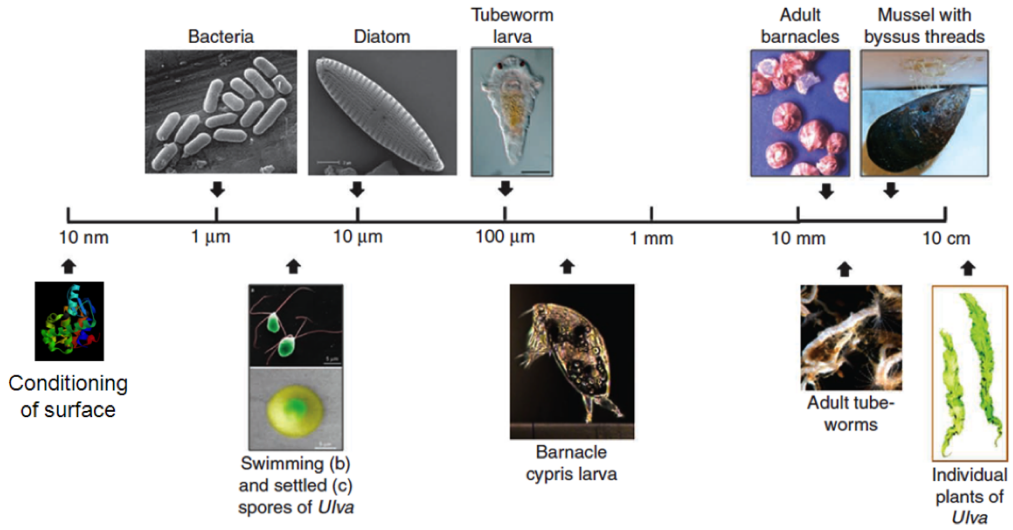

Figure 2.1: Diversity and size of a range of representative fouling organisms ([3] modified).

The entire process is often described as a linear consecutive of different fouling stages where the first bacterial biofilms are followed by alga settlement within one week and this in turn is followed by different macrofoulers [1, 39, 40]. In reality, this view is a significant oversimplification of the occurring events. Spores are able to settle within several minutes to hours on pristine surfaces [41]. The same observation was made for barnacle larvae, bryozoans and hydroids [42]. It is misleading to assume that there is a causal relationship between different 'stages' during colonization processes occurring on surfaces and that the whole biofouling problem could be solved by blocking or even eliminating initial stages [3]. To make research in the field of antifouling coatings more efficient it is necessary to understand the mechanisms which are used by the organisms to locate and attach to a surface as well as the influence of environmental factors. In the next subsections the different processes occurring during the fouling process and the organisms involved, which are relevant for this work will be specified.

2.1.1 Conditioning films

When a surface is exposed to the ocean, immediately after immersion in the water organic and inorganic molecules which are already present in the environment or produced by microorganisms [43] spontaneously adsorb onto it [44, 45]. This so called 'conditioning film' alters the physico-chemical conditions of the surface and provides a nutrient source for the attaching organisms [28].

In various studies using attenuated internal reflection infrared spectroscopy (AT-IR) it could be shown that the formed conditioning films are mainly composed of proteins [43, 46, 47] and glycoproteins [48]. Fluorescence measurements indicated that humic acids may also be present [49]. In addition lipids, nucleic acids, polysaccharides, aromatic amino acids [44] and unspecified macromolecules [50] could be found. In earlier studies it was shown that different chemical and physical properties of the substrates, like charge or wettability, influence the substrate-water interface and thereby the species of adsorbing organic molecules [51]. These adsorbed molecules in turn modify the charge and the free energy of the substrate which play an important role in the subsequent colonization by microorganisms [50, 52, 53].

The chemical nature of this adsorbed layer is still poorly understood [43]. For a detailed understanding of organism settlement, adhesion and colonization, it is desirable to know the kinetics of the formation and the chemical composition of the conditioning layer as well as its impact on following adhesion processes. In order to interpret the results achieved in the laboratory assays it is also important to know which role the conditioning plays.

2.1.2 Bacterial biofilms

A majority of bacteria in the natural or clinical environment accumulate in biofilms, which are usually attached to surfaces. Within these films the bacteria can exist in two different living forms, a free swimming planktonic and a sessile, colony forming form. The structure and mechanical properties of these biofilms are defined by extracellular polymeric substances (EPS), which serve as a glue holding the biofilm together. The life cycle of such biofilms is characterized in five stages (Figure 2.2) beginning with the initial attachment of the planktonic bacteria to the surface. Thereby the bacteria adhere reversibly and are able to explore the surface by type IV pili-mediated twitching movements [54]. In the second step, EPS are produced since they convert the slight attachment into a more 'irreversible' one [54]. For *Pseudomonas aeruginosa* this EPS mainly consists of alginate. The following two stages involve the aggregation of bacteria into microcolonies as well as subsequent growth and maturation. Typically structures are formed consisting of microcolonies containing open water channels for the delivery of nutrients deep into the complex community. In the final step bacteria divide or migrate to cover empty regions of the substrate and produce a mature, thick and spatially inhomogeneous biofilm [55]. During this development process, cell to cell communication plays a major role. This quorum sensing regulates bacterial gene expression in response to a fluctuation in local signal concentrations. Bacteria produce and release signal molecules, autoinducers and if a specific amount is reached, the cells are able to detect them and gene expression of the cells changes, immediately followed by attachment of more bacteria.

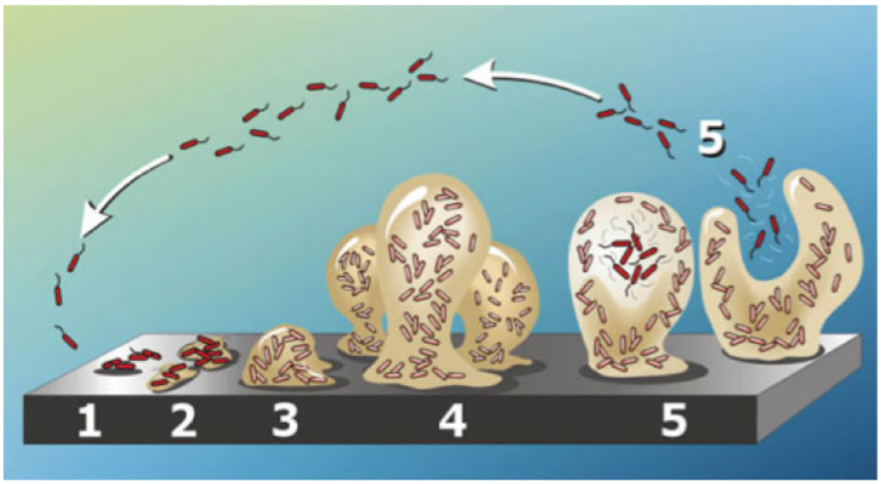

Figure 2.2: Scheme showing the development of a biofilm as a five-stage process: 1) Individual cells populate the surface. 2) EPS is produced resulting in a more firmly adhered attachment. 3)+4) Biofilm architecture develops and matures. 5) Single cells are released from the biofilm [54].

2.1.3 The green alga *Ulva linza*

Model organisms representing the major fouling groups (microfouler, soft- and hard- macrofouler), which pose a challenge to surfaces in their natural environment, are selected to study the performance of potential antifouling coatings. The green alga *Ulva linza* (formerly *Enteromorpha*), or seaweed, is known to be the most common macrofouler in the intertidal zones of seashores all over the world [5]. It is a bright green plant which lives attached to rocks, ship hulls or piers. It propagates by the production of zoospores which are 5 µm and swim by using their four flagella (Figure 2.3a).

Ulva spores run through an antithetic alternation of generations in their life and the sexual and the asexual propagation can be observed. All *Ulva* species alternate between gametophytic and sporophytic life stages with similar morphologies (Figure 2.4). By mitosis (cell division) the haploid gametophytes produce biflagellated, male or female haploid gametes, which are phototacticly positive. If they find each other by swimming around, fusion takes place and the so called syngametes are formed. By fertilization negative phototactic spores are produced which search for surfaces to settle and grow into a plant [56]. In terms of biofouling this is the important step, as like other marine organisms, the zoospores need to locate and settle to a surface in order to complete their life cycle [41]. For this reason these kind of spores are used in order to perform laboratory assays but a major problem is the lack of cultivation methods [57]. Their proliferation is controlled by the lunar cycle and the release of spores follows the gametes a few days later. The process of spore settlement can be divided into two sequential stages:

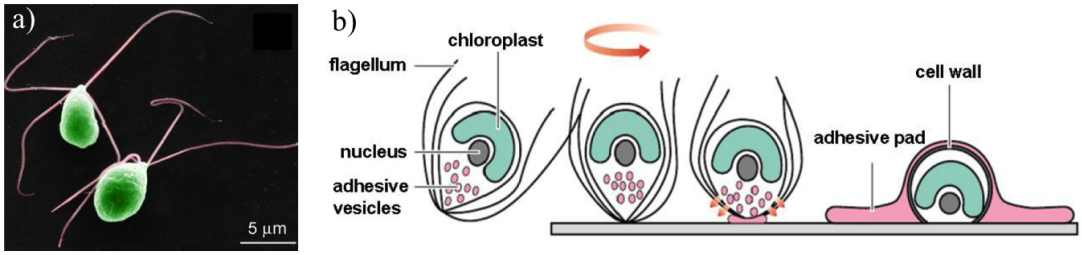

Figure 2.3: a) False coloured SEM image of zoospores of *Ulva linza* [2]. b) Cartoon representation of the different stages involved in *Ulva* zoospore settlement and adhesion [5].

'settlement' or locating of the substrate, and the establishing of surface contact, 'adhesion' [58]. Motile spores swim actively with the help of their flagella and 'sense' the surface. If a surface measures up the expectations for settlement, the diploid spores start to adhere permanently. An irreversible process starts, which includes the spinning on the surface, the discharge of adhesive vesicles containing EPS and the withdrawal of the flagella axonemes into the cell [59]. This process shown in Figure 2.3b only takes about 30 s to 60 s and is followed by the synthesis of a new cell wall [59]. Within the next few hours spore germination occurs, followed by cell division and growth to sporophytes. These young plants then grow to a size visible to the naked eye [59]. The described settlement stage is the most important step in the life cycle of zoospores and it needs to be understood in order to design effective anti algae coatings.

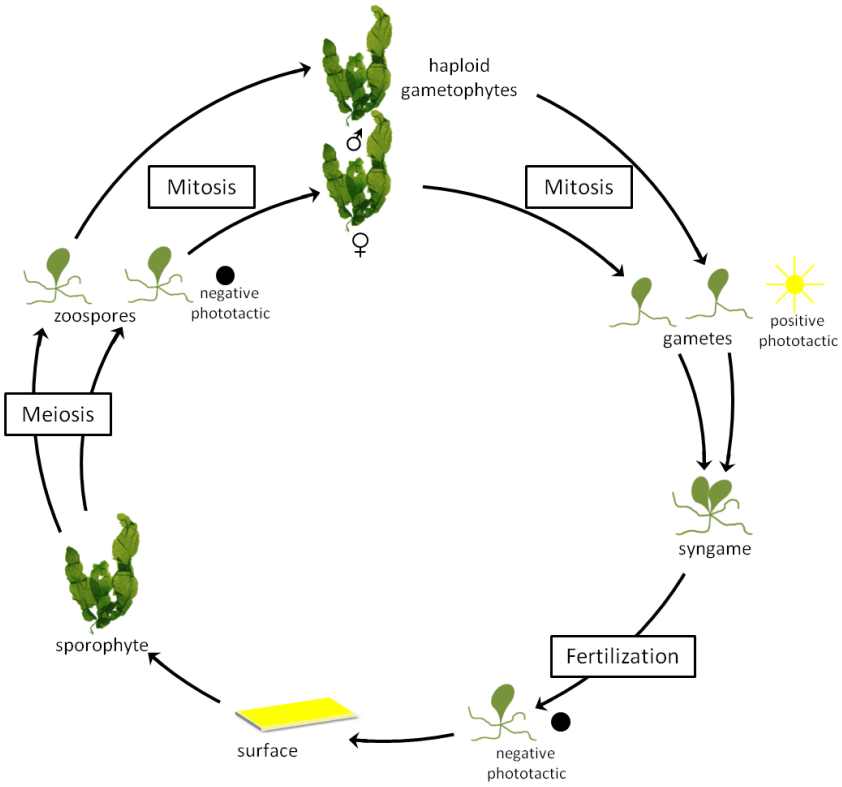

Figure 2.4: Life cycle of *Ulva linza* [3]. Through mitosis, gametes (sexually reproductive cells) are produced by gametophytes. After joining together and settling on a surface they grow into sporophytes. The sporophytes then undergo meiosis, producing zoospores (asexual reproductive cells), and each zoospore grows into a gametophyte. The gametophyte then produces more gametes, and the cycle continues.

2.1.4 Field tests

Controlled short-term laboratory assays with model organisms like the bacterium *P. aeruginosa* or the green alga *Ulva linza* are frequently used to rate different antifouling properties of model surfaces by simply using one certain species. Although the mechanisms involved in the fouling process are not completely understood, some microfoulers like bacteria and diatoms have been reported to regulate the settlement of macrofoulers via chemical cues [60]. Consequently, the formation of a biofilm depends on many factors including interactions between different species and environmental conditions.

Therefore field tests provide the ideal environment to study the performance of model surfaces that pass the laboratory assays. Though these studies have some disadvantages, such as seasonality of many organisms, time and weather dependence of the activity phases of the foulers, they are an important tool to study the behavior of coatings in the 'real world'. Parameters like water temperature, salinity, pH but also wind velocities play a crucial role. Nevertheless, many studies testing the performance of commercial antifouling coatings at test sites where the populations are well known over the whole year have been done over several weeks and months. Swain *et al.* investigated the influence of different static immersion test sites to well known silicone formulations. They showed that there were differences in the type and amount of adhered organisms although the relative performance of the coatings was similar for all sites [61]. In a similar study, Zargiel *et al.* used different commercial foul release coatings to investigate the influence of different locations. In this study they identified 127 species comprising 44 genera and found that the abundance of the diatoms was influenced by the coating composition and the test site [62]. Another interesting point was again evaluated by Swain *et al.*, who had the hypothesis that different colors may have an impact on the settlement behavior of different foulers. The experiments with black and white substrates showed that more spores adhered to the black substrates [63]. This demonstrates a high interest in long term immersion studies. However, there is a deficit concerning the composition of the initial fouling steps and communities in the field on well defined substrates.

2.2 Self assembled monolayers as a research tool for bioadhesion

As described above well defined model surfaces are extensively used to study the influence of different surface properties effecting fouling. With surface coatings these relevant properties can be modified selectively. A reproducible and defined modification of surfaces can be achieved, e.g. by applying an organic monolayer.

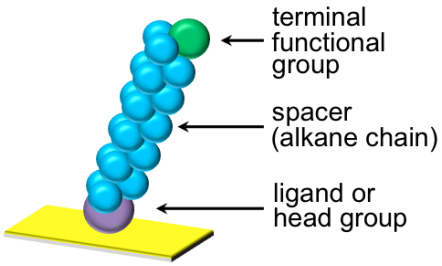

Figure 2.5: Alkanethiol supported on a gold surface.

A well known and extensively studied example for this are the self assembled monolayers (SAMs).

Molecular self assembly is known to be the spontaneous arrangement of molecules under defined conditions. In nature the self assembly mechanism is widely spread. Protein folding to tertiary structures, the DNA double strand formation or the formation of a virus are just a few examples [64].

In 1983 Nuzzo and Allara were among the first who reported the spontaneous self assembly of alkanethiols on surfaces [65]. Many self assembled systems have been investigated over the years, but monolayers of alkanethiols on gold are probably the most studied kind of SAMs [25]. Most of these studies deal with the formation of the alkanethiol monolayer on ultrasmooth thin gold surfaces (Figure 2.5) [66–68]. The most commonly used organo-thiol contains three different parts, a terminal functional group, a spacer and a ligand or head group.

For SAM preparation the substrate is simply immersed into a dilute (ca. 1 mM) solution of the adsorbate at room temperature [69]. The formation of SAMs relies on a strong specific interaction between the head group and the substrate. The main driving force of this accumulation is the formation of the gold-sulfur bond with a binding energy of about 44 kcal mol^{-1} [70]. Within a few seconds to minutes after the immersion in the solution a undefined monolayer is formed. If this process proceeds van der Waals forces between spacers of the molecules —in our case single alkane thiols— cause the aggregation of the molecules and a crystalline monolayer is formed (Figure 2.6) [70]. The spacing between the alkanethiol chains is reported to be 4.97 Å for Au(111) substrates, what is nearly three times the van der Waals diameter of a sulfur atom (1.85 Å) [25, 71]. During the process of ordering dust molecules are displaced and defects in the packing density are reduced [72, 73]. The terminal functional group determines the resulting surface properties of the organic monolayers.

Fourier transform infrared spectroscopy (FTIR) studies revealed that the alkyl chains are tilted about 30° to 35° from the surface normal to maximize their van der Waals interactions [74]. Electron diffraction, low energy and scanning tunneling microscopy studies showed that the thiol bonding on Au(111) is gener-

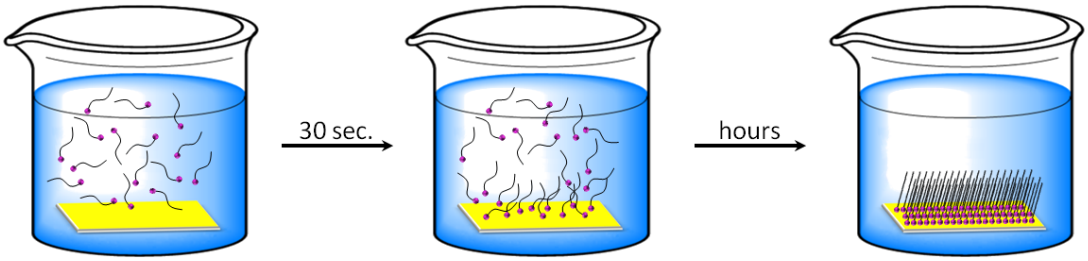

Figure 2.6: SAM formation in the lab.

ally based on a $(\sqrt{3} \times \sqrt{3})$R30° overlayer structure where the sulfur atoms are positioned in the 3-fold hollow of the gold lattice (Figure 2.7) [26, 27, 70]. It has to be noted that the thiol molecules are bound equally to the Au lattice sites but with some variation in the molecular orientation [75]. Camillone *et al.* observed a c(4×2) superlattice structure and proposed a model to explain this observation [76]. In the model, alkanethiol molecules are arranged in a $(\sqrt{3} \times \sqrt{3})$R30° structure where all sulfur headgroups are bound to identical hollow sites of the Au substrate but with alternating twist angles. But not only gold can serve as a substrate for the formation of SAMs, also Ag can be utilized [77]. Unfortunately, compared to Au(111) less is known about the self assembly of thiols on Ag(111). Although the substrates show similarities in the symmetry or lattice spacing, alkanethiol films formed on Ag(111) display differences such as a different packing density of the sulfur atoms. In this case the overlayer structure was found to be $(\sqrt{7} \times \sqrt{7})$R10.9° [71, 78]. Although the range of the reported tilt angle ranges from 0° to 14° [77], it may be concluded that on a Ag(111) substrate the thiols are practically standing upright on the surface [79].

Since surface properties are generally considered to be controlled by the outmost

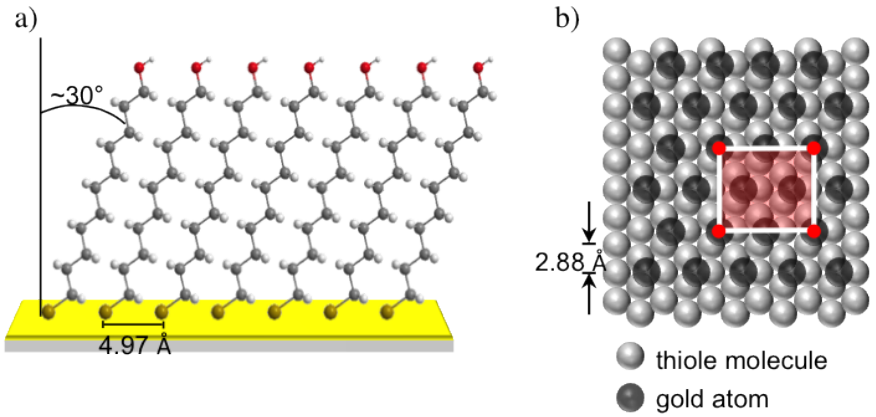

Figure 2.7: a) SAM monolayer anchored to the Au(111) substrate via a sulfur–gold bond, b) Surface structure of undecanethiol SAM on Au(111) [27].

5 Å to 10 Å of a film [80], SAMs are used as well suited model surfaces to study interfacial phenomena due to the ability of fine controlling the surface properties [25]. In the following sections a closer look will be taken on the influence of different surface properties which can have an impact on the biofouling process.

2.3 Surface properties affecting fouling

As described in section 2.1.2 and 2.1.3 it is a major part of the life cycle of marine organisms to adhere to a surface. Most of these foulers are motile organisms, which means that they can swim actively through water and 'explore' surfaces for their suitability for settlement. This process could be influenced by varying chemical and physical cues which guide the biological behavior of individual organisms. In the next sections the influence of surface wettability, hydration, charge, polarity and topography will be summarized.

2.3.1 Wettability

Since wettability is a representative macroscopic physical property of surfaces it has been studied extensively. It is important to understand the microscopic basis of the wetting behavior of substrates since the wettability of flat surfaces is determined by interfacial free energies and hence reflects intermolecular interactions at solid-liquid interfaces [72]. Additionally, it plays a significant role in the adhesion of fouling organisms on surfaces [1]. In the 1960s Baier *et al.* could demonstrate a correlation between relative biological interactions and the free energy of a surface. They showed that the amount of biomass on a surface does not depend linearly on the surface energy of the substrate, but that there is a range of surface energies ($20\,\mathrm{mN\,m^{-1}}$ to $30\,\mathrm{mN\,m^{-1}}$) where the adhesion is minimal [81]. By decreasing the surface free energy, and with this increasing the water contact angle, the adhesion also increases. A minimum of bioadhesion can be explained by changes in dispersion forces as a function of surface energy [82]. The surface energy at which the minimum is detected is approximately equal to the dispersive component for water. If an adhesive starts to bind to a surface in an aquatic system, it first has to 'wet' this surface and whether it does so depends on the competition between the adhesive and the water. The interaction process is complex and includes the displacement of the water from the substrate and the formation of contact between the adhesive and the surface [22]. It has been shown that the *Ulva* spore adhesive has both hydrophobic and hydrophilic functionalities. When a protein comes into contact with a surface, it can undergo a conformational change exposing the functionalities that optimize adhesion to the surface [22]. Hydrophobic interactions assist in the displacement of water molecules at the surface-water

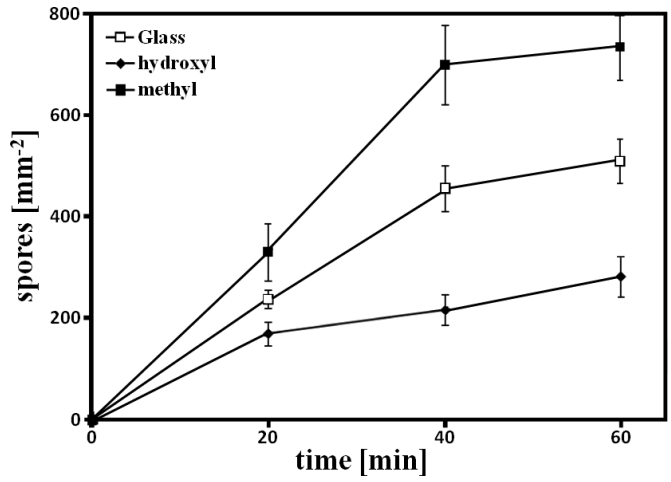

Figure 2.8: Time course for zoospore settlement on glass, a CH_3-terminated SAM, and a OH-terminated SAM [83].

interface and therefore facilitate the substrate-adhesive bonding process resulting in a higher amount of settled spores. Consequently, spores which want to attach to hydrophilic substrates are not able to form a substrate-adhesive bond and thus are easy to remove just by rinsing the test slides with water. This concept has been a major driving force in the development of low adhesion strength foul-release coatings [84].

A change of wettability using alkanethiol SAMs with chemically different end groups (-OH, -CH_3) indicated that *Ulva* zoospores avoided to settle on hydrophilic surfaces [21, 83, 85]. Figure 2.8 depicts one example where surface energy influences settlement. The plot shows the increase of *Ulva* zoospore attachment on surfaces with different contact angles. After 1 h of incubation there were approximately 2.5 times more spores attached to the hydrophobic -CH_3 surface than to the hydrophilic -OH one. The glass substrate, which has an intermediate contact angle, exhibited intermediate levels of zoospore attachment [83]. Although more spores settled on the hydrophobic -CH_3 SAMs, the adhesion strength was higher on the hydrophilic -OH surfaces [85]. But one needs to be careful in generalizing since it is known that the adhesion of diatom cells appears to be different from that of *Ulva* zoospores. The diatom cells adhered more strongly to the hydrophobic methyl-terminated SAM and less strongly to the hydrophilic hydroxyl-terminated SAM. This high adhesion strength was paired with a reduction in motility of the diatoms on the hydrophobic substrates [86].

It also could be shown, that spores can discriminate between hydrophobic and hydrophilic surfaces (Figure 2.9) [87]. Stripe patterns consisting of PEGylated and fluorinated SAMs on silicon were prepared with different stripe width. Up to a stripe width of 5 µm, the spores preferred to settle on the fluorinated areas whereas they avoided the PEGylated counterparts. If the stripe width was set to

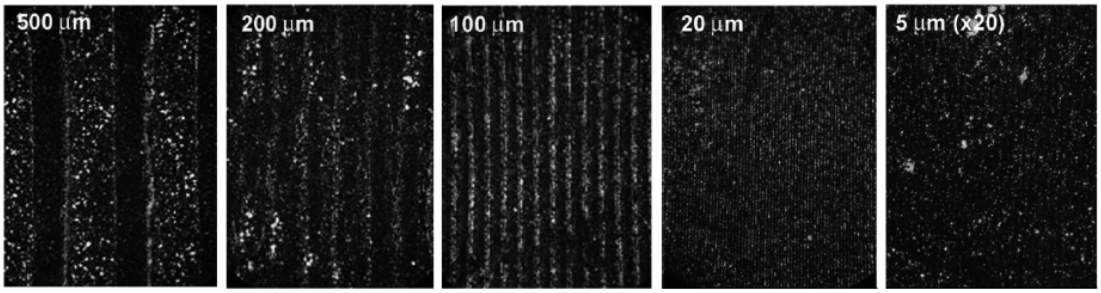

Figure 2.9: Images of spores settled on PEGylated and fluorinated areas. The spores prefer to settle on the fluorinated strips up to a dimension of 5 µm. Images are shown at a microscope magnification of 10× except the 5 µm image, which is shown at a 20× magnification for clarity [87].

$\leq 2\,\mu m$, the spores were not able to sense the two different surface chemistries.

2.3.2 Hydration

High surface hydration is found to be a benefit if one aims to prevent protein and cell adhesion [84]. It is hypothesized that if the hydration energy between molecules is high enough, the water molecules within the interface of a substrate can not be displaced and glue proteins secreted by the organisms are not able to adhere irreversibly.

Polyethylene glycol (PEG) is one of the chemistries showing highest resistance towards biological matter. The highly and strongly hydrated ethylene glycol (EG) surfaces mimic the stable water environment and prevent any interactions between the surface and the adhesive [84]. They have been used as model surface to study their interaction with proteins, bacteria, and cells for several years [21, 88, 89]. In the marine fouling sector these substrates were also applied as model surfaces [90, 91]. To determine the minimal threshold of monomer EG units which are required to keep the surface resistant to protein adsorption or settlement of spores of *Ulva*, experiments were performed on SAMs [91, 92]. By lowering the number of EG units and therewith decrease the amount of hydration water in the SAMs, while keeping the wettability the same, it could be shown that proteins and *Ulva* spores do not adsorb on a surface if there is more than one EG unit present (Figure 2.10) [91]. With *in-situ* observations during the experiments of the immersed samples, it could be revealed that spore settlement was highest on the EG_6OH surface and rafts of settled spores were formed. The adhesion strength of these spores was so low that a minimal shear force was sufficient to remove the attached spores from the substrate. The spores started the settlement process by shedding their flagella and tried to attach to the substrate. However, the secreted adhesive was not able to irreversibly bind to the surface.

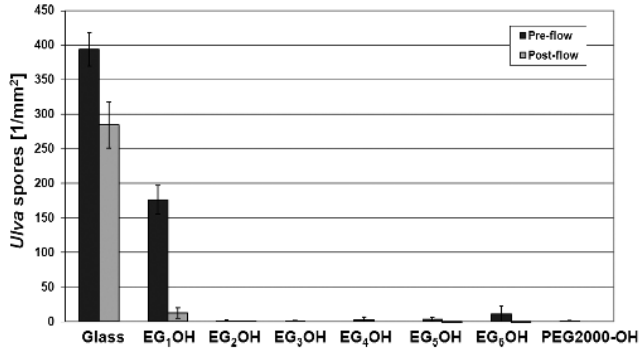

Figure 2.10: Density of attached zoospores of *Ulva* on short chain EG_YOH-SAMs with different chain lengths (y) and PEG2000-OH before (preflow) and after (postflow) exposure to a wall shear stress of 53 Pa [91].

If the number of EG units in the SAM is reduced to one, the adhesion of *Ulva* and proteins become irreversible. Since the binding energy of water is reduced, the adhesive-surface strength is stronger. As the spore adhesive consists of a hydrophilic and hygroscopic glycoprotein [93], less EG units makes it easier for the glue to displace the water from the interface, thus promoting strong adhesion to the underlying surface [84, 91].

2.3.3 Charge

During the movement of marine organism through the bulk water they experience different forces. When the settlement process starts and they approach the surface these forces change. Electrostatic interactions are one of these surface forces which could have an impact on the attachment of different model organisms [94].

The effect of surface charge can for example be best studied by using single component charged SAMs and mixed zwitterionic SAMs. Comparing the adsorption of fibrinogen to SAMs with different charges it could be shown that positively and negatively charged SAMs showed nearly a full monolayer of protein adsorption while only about 1 % of a monolayer adsorbed onto the mixed substrates [95]. For bioassays with *Ulva* spores the settlement was also high on all charged substrates. Comparing three surfaces with different net charges, the effect was relatively small but statistically significant. The spore density on the negatively charged surface was significantly lower than on the neutral and positively charged surfaces. An explanation could be that swimming spores have a zeta potential of -19.3 mV leading to an electrostatic repulsion of these negatively charged spores from the also negatively charged surfaces [94].

Another indication that electrostatic interactions may affect the settlement of zoospores of *Ulva* is given by experiments of Ista *et al.* [20]. Mixed SAMs consist-

ing of methyl and hydroxyl terminated alkanethiols were compared with mixed SAMs composed of methyl and carboxylic acid terminated alkanethiols. In both cases the wettability of the surfaces was systematically varied by the mixture ratio of the two components. Comparison of the settlement of spores of *Ulva* on the two types of mixed SAMs showed that for equivalent wettabilities, settlement on the carboxyl group containing SAMs tended to be lower than for the hydroxyl containing ones. The observed difference might be due to selective response to the carboxylic acid groups or due to electrostatic repulsion, but also a chemical response cannot be excluded. A contrary effect could be observed using larger organisms like cyprid larvae. Petrone *et al.* was able to investigate that the attachment was dependent on the surface charge with significantly higher attachment on the negative SAMs, an intermediate state for the neutral substrates, and lowest attachment on the positive monolayer [96].

2.3.4 Topography

Not only chemistry, but also hydration and charge of a surface (Sections 2.3.1, 2.3.2 and 2.3.3) have an influence on the biofouling process. Also the morphology has a high impact on the adhesion.

In contrast to man made structures, many marine organisms remain strikingly free of organisms, although they face the same fouling pressure as any other immersed hard substrate. This seems to be due to antifouling mechanisms, which can be of chemical, mechanical or physical nature [40]. In the natural environment there are many examples where animals use anti fouling strategies. The skin of sharks for example is covered with small scales (denticles) that can be flexed against each other due to the elasticity of the skin underneath. On closer examination, it was found that the surface of these denticles comprises a regular pattern of parallel ridges and grooves. This combination of microstructure and elastic properties leads to a reduction of attachment of microorganisms of about 70 % [97]. Another example is the self cleaning skin of pilot whales, which consists of nanostructured pores filled with a special gel. As soon as fouling organisms adhere to the skin, they are rinsed out together with the gel. Therefore the formation of a biofilm as well as the settlement of organisms is prevented [98]. This leads to the hypothesis that by using nanostructured surfaces also the attachment of marine organisms on ships could be avoided.

An interesting approach was pursued by Liedert *et al.* [99]. They used shark skin to investigate which impact its microstructure had to the adhesion of parasites. With this knowledge they invented a coating that prohibits the attachment of barnacle larvae. The background for this development is the so called 'attachment point theory'. This theory proposes that the amount of adhered organisms is dependent on the number of potential attachment points. While the attachment

is increased when there is an optimal number of 'potential settling points' [100] it is reduced when there are just few (sub-optimal) points of attachment [19]. The number of available attachment points is dependent on the size of the settling organisms and the wavelength of the microtexture [101].

In further studies this theory could be validated by Callow *et al.* by analyzing the attachment of *Ulva* zoospores to polydimethylsiloxane elastomer (PDMS) surfaces with defined microtopographies [102]. The topographic features were based on 5 µm deep valleys with valley floors and ridges varying between 5 µm and 20 µm. Significantly higher numbers of spores attached to the substrate valleys compared to the surrounding flat PDMS and this number could be correlated with the spatial frequency of the valleys. Most of the spores attached to the sector with 5 µm wide valleys, which lie in the range of the size of the spore body (Figure 2.11). On this surface spores formed tightly packed rows and only a single spore adhered on top of the ridge (Figure 2.11a). The 10 µm valley accommodated mostly 2 spores per valley width (Figure 2.11b) while settlement in the 20 µm valleys was lower (not shown). This study concluded, that spores are able to 'select' the best place to settle and that they prefer to settle on topographies with sizes in the same range of their body.

Based on this hypothesis some more studies were performed using structures with a width of 2 µm. Cao *et al.* used layer-by-layer spray-coating deposition of polyelectrolytes to prepare a series of coatings with varying structure sizes [24]. They showed that settlement of *Ulva* zoospores was strongly influenced by the feature size present on the surfaces. The lowest number of adhered spores was observed for a structure size on the order of 2 µm.

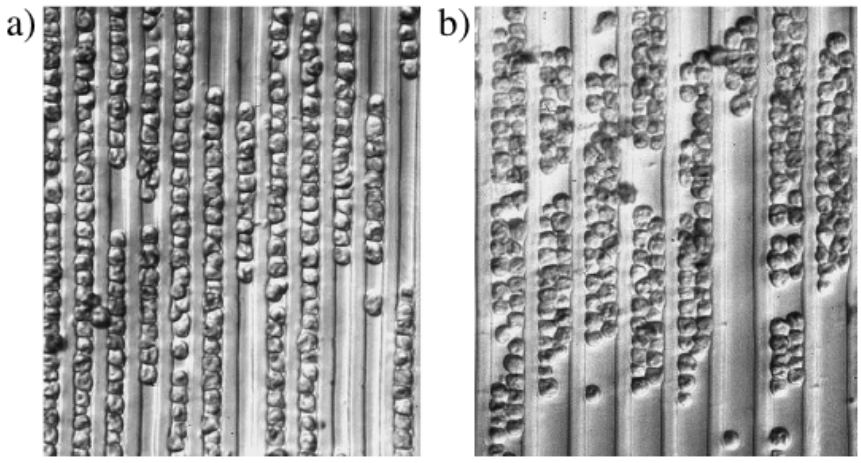

Figure 2.11: Light micrographs of spores settled in a) 5 µm and b) 10 µm wide valleys. Both features were 5 µm deep and separated by 5 µm wide ridges. Note that very few spores attached to the ridges [102].

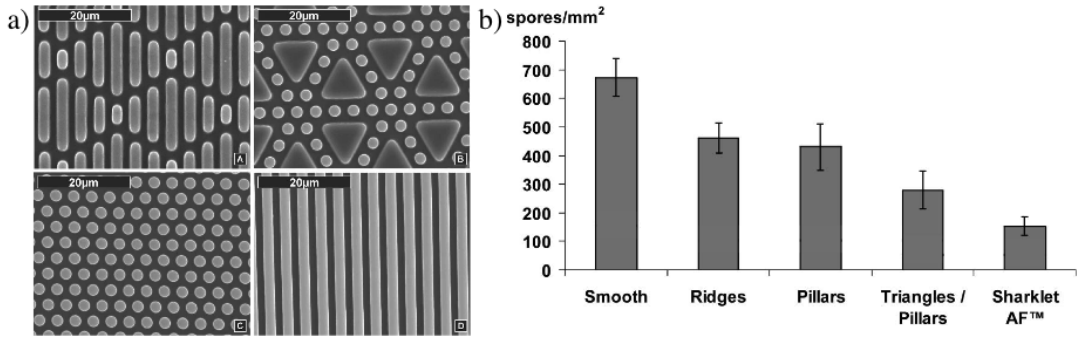

Figure 2.12: a) SEM images of PDMS engineered topographies, b) Results of *Ulva* spore settlement [103].

But not only the size, also the shape of the topography plays a major role. Brennan *et al.* mimicked the shark skin effect by preparation of PDMS elastomer structures with four different designs, patterned by photo lithography (Figure 2.12a) [33, 103]. These structures include the biomimiked skin of sharks with 2 µm wide ridges of various lengths, 10 µm equilateral triangles together with pillars (2 µm in diameter), pillars (2 µm in diameter) and 2 µm wide ridges. The distance between two features was 2 µm and the height was approximately 3 µm. *Ulva* settlement assays were performed and the results are shown in Figure 2.12b. With microtopographically patterned structures the settlement of spores can be effectively reduced compared to the flat PDMS substrate [33, 103]. Although the distance between the features and the height of the features were similar in all four patterns, the sharklet structure reduced the amount of settled *Ulva* spores notably. These results also suggest, that the settlement of spores is influenced quite strongly by the feature size, roughness and the geometry of the surface. Since the biofouling process includes a very diverse range of marine organisms which differ in size, a topographical pattern having a single length scale will likely not perform as a general antifouling surface. Surface structures having multiple length scales should be more promising in the design of an effective antifouling surface [31].

2.4 Lithography methods

The ability to generate small structures is central to modern science and technology. There are many opportunities that might be realized by making new types of small structures or by downsizing existing structures. Therefore modern lithography techniques are used to modify structures of surfaces. The structuring of surfaces can be accomplished by diverse methods. Table 2.1 gives an overview over most important ways of structuring surfaces. In most of these techniques

so-called resists, irradiation sensitive films, are used, since they change their chemistry upon irradiation. If the irradiated area of the resist is easily removable from the substrate through etching or the use of solvents, this unirradiated area is a positive resist. If the irradiated area is not removable or less removable, the unirradiated area is a negative resist. Different types of optical lithography with UV light [116] and X-ray lithography exist [115] but these methods usually require a huge technical effort. The advantage is that these are fast methods by which high resolutions and good aspect ratios can be achieved.

A higher resolution can only be achieved by using dip-pen lithography [118], nanographting [121] or scanning tunneling microscopy (STM) lithography [122]. However, these methods are much slower and not applicable to structure big areas. Other printing or stamping techniques which utilize self assembly processes are inkjet printing [108], nanoimprint lithography [106] and microcontact printing [105]. For the latter, a conformal contact between the stamp and the surface of the substrate is essential to transfer the 'ink' to the surface. By backfilling the non-patterned areas with a different alkanethiol, binary-component SAMs are formed. This printing has the advantage of simplicity and convenience. Once a stamp is available, multiple copies of the pattern can be produced and it is, with

Table 2.1: Overview of different lithography methods.

Method	**Resolution**	**Area**	**Ref.**
Microcontact printing (μCP)	$\approx 100\,\mathrm{nm}$	$> 1\,\mathrm{cm}^2$	[104, 105]
Nanoimprint lithography (NIL)	$\approx 10\,\mathrm{nm}$	$> 1\,\mathrm{cm}^2$	[106, 107]
Inkjet printing (IP)	$\approx 30\,\mu\mathrm{m}$	$> 1\,\mathrm{cm}^2$	[108]
Magnetolithography (ML)	$\approx 10\,\mathrm{nm}$	$> 1\,\mathrm{cm}^2$	[109, 110]
Lithography with electrons, ions, photons	$\approx 10\,\mathrm{nm}$	$> 1\,\mathrm{cm}^2$	
Electron beam lithography (EBL)			[111, 112]
Focused ion beam lithography (FIB)			[113, 114]
Optical lithography (UV, X-ray)			[115, 116]
AFM/STM-based lithography	$\approx 1\,\mathrm{nm}$	$\mathrm{nm}^2 - \mathrm{cm}^2$	[117]
Dip-pen lithography			[118, 119]
Nanographting			[120, 121]
STM lithography			[122]

this method, possible to structure larger areas [123]. However, the roughness and the dimensions of the elastomeric stamps limits the resolution of the resulting patterns [124]. Also, the mechanism of the patterning has an influence since after the transfer the alkanethiols can spread from the contact region of the stamp into noncontact areas, like ink spreads on a piece of paper [125].

Higher efficiency can be achieved by linking so-called bottom up techniques like self assembly with top down techniques like e-beam lithography. There are two different methods available to structure surfaces via e-beam. Proximity printing is a parallel technique, while direct writing with a focused e-beam is a serial one. Proximity printing has the advantage that large areas are accessible by a broad e-beam which irradiates the substrate covered by a mask with a constant irradiation dose. Here the resolution is limited to $\sim 100\,\mathrm{nm}$ due to the accuracy of the used masks.

With direct e-beam writing, a better resolution down to a few nm is possible. The drawback is that this serial mode is limited in speed [126]. The important parameter for both methods is the choice of the right electron energy. Figure 2.13 shows the often referred to as 'universal' curve for the penetration depth of electrons in some metals which depends on the electron energy [127]. The lowest penetration depth of $\sim 50\,\mathrm{nm}$ could be observed in the range of $50\,\mathrm{eV}$ to $100\,\mathrm{eV}$ independent of the material of the substrate. Elastic and inelastic scattering processes lead to a generation of secondary electrons which are scattered in all directions (proximity effect). This leads to a broadening of the primarily irradiated area. Hence the higher the energy of the electrons is, the higher the penetration depth is and thereby the lateral scattering. On the other hand beams of higher electron energies are better focusable since the electrons interact less with each other leading to a smaller spot size. As a consequence, a compromise between focusability and the proximity effect has to be made in e-beam lithography.

2.4.1 Chemical lithography

The interaction of electrons with SAMs leads to various effects. Terminal nitro functional groups in 4'-nitro-1,1'-biphenyl-4-thiol SAMs can be converted into amino groups [126, 128], aliphatic SAMs can be destroyed and backfilled with amino SAMS [129–131] and SAMs with mostly deactivated tail groups like 11-amino-1-undecanethiol hydrochloride (AUDT) get activated [131, 132]. These new amino groups open up many possibilities to couple molecules to the surface in a high spatial resolution. Proteins and with this also cells that couple to the proteins, can be immobilized on the substrate [133, 134] or start sites for surface initiated polymerizations [135, 136]. A number of different surface-initiated polymerization methods are available reaching from free radical polymerization (thermally or photochemically initiated) [135] over reversible addition

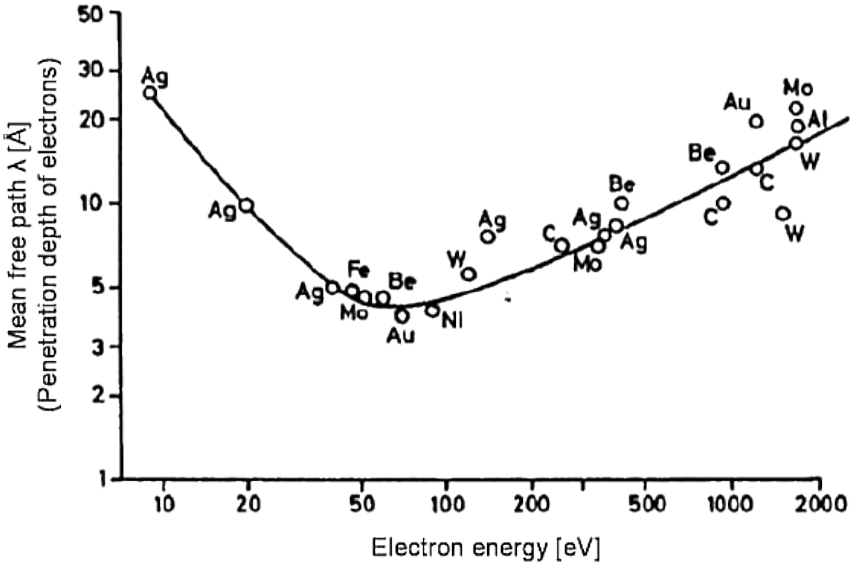

Figure 2.13: Penetration depth of electrons in dependence of primary electron energy and the irradiated material [127].

fragmentation chain transfer (RAFT) [137] to atom transfer radical polymerization (ATRP) [138–142].

To perform successful polymerizations it is important to have an equilibrium between inactive and active species. The radicals (active species) are generated with a rate constant k_a via a reversible redox process which is catalyzed by the abstraction of a (pseudo) halogen atom from an inactive species. The present of this radical together with a unsaturated C−C double bond leads to a radical chain polymerization with the rate constant k_p. Recombination and combination reactions between two radicals can occur which stop the polymerization process. Pre requisites for a sharp molecular weight distribution are a fast starting reaction and a fast propagation of chain growth [143]. This requirement is fulfilled by numerous radical polymerization reactions like ATRP, RAFT, and reverse ATRP.

In the framework of this thesis surface-initiated atom transfer radical polymerization (SI-ATRP) was applied in combination with chemical lithography. Hence, the SI-ATRP reaction is described briefly [139]. Figure 2.14 shows the reaction scheme of the copper-catalyzed ATRP reaction. In the first reaction step the initiator (e.g. 2-bromoisobutyryl bromide, BIBB) is coupled to the surface. By adding the Cu(I) complex a radical is formed by dispensing the bromide molecule. This radical can then react with the monomers to form long polymer chains until an abortion reaction takes place, e.g. by recombination of the chain with other radicals. The radical concentration is, according to the requirements of a controlled polymerization, low and the equilibrium is far on the side of the inactive species.

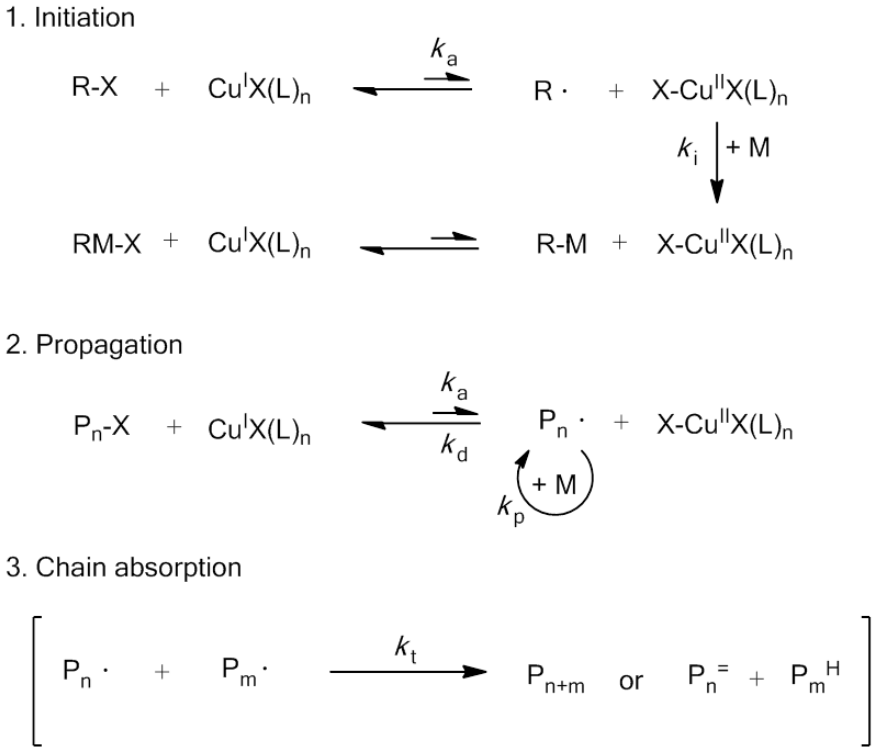

Figure 2.14: Mechanism of copper-catalyzed ATRP (after [139]). In the initiation step a radical is formed by the abstraction of a (pseudo) halogenid atom. In the propagation step the formed radical reacts with a monomer and polymer chains are formed until an abortion reaction takes place.

2.5 Analytical techniques

In this section the analytical methods are described which were used in the course of this thesis to verify the quality of the prepared surfaces and to analyze the conditioning films in order to relate the determined surface properties to the fouling behavior of studied organisms.

2.5.1 Ellipsometry

Spectral ellipsometry is a sensitive optical tool to characterize light reflection (or transmission) from a substrate. The key feature is the measurement of changes in the polarization state of light upon light reflection on a sample (or light transition by a sample). This change is represented as the amplitude ratio Ψ and the phase difference Δ. The measured response depends on optical properties and thickness of individual materials. Thus, ellipsometry is primarily used to determine film thickness and optical constants [144].

Light can be described as an electromagnetic wave and its electric field is always orthogonal to the propagation direction. Therefore, a wave traveling along the z-direction can be described by its x- and y- components. When the light has completely random orientation and phase, it is considered to be unpolarized. When two orthogonal light waves are in-phase, the resulting light will be linearly polarized (Figure 2.15a). The relative amplitudes determine the resulting orientation. If the orthogonal waves are 90° out-of-phase and equal in amplitude, the resultant light is circularly polarized (Figure 2.15b). The most common polarization is 'elliptical', one that combines orthogonal waves of arbitrary amplitude and phase (Figure 2.15c) [145]. This is where ellipsometry gets its name. The next question to be answered is what happens with polarized light moving through matter. Therefore a reflection plane has to be defined and the polarization of light is defined in terms of the spatial orientation of the electric field component E, which can be parallel (p-wave or transverse magnetic) or perpendicularly (s-wave or transverse electric) to the plane of incidence. Any intermediate orientation between s and p waves can be described by a linear combination of the base vectors E_p and E_s. After reflection and interaction with the substrate, the phase of the s- and p-polarized part is shifted so that it gets elliptically polarized [147]. The change in polarization can be expressed by the ratio of the reflection coefficient ρ, which can be described by the fundamental equation of ellipsometry [145]:

$$\rho = \left(\frac{r_\mathrm{p}}{r_\mathrm{s}}\right) = \tan(\Psi)\exp(\mathrm{i}\Delta), \tag{2.1}$$

where $\tan(\Psi)$ is the amplitude ratio upon reflection and Δ denotes the phase shift between the s- and p-polarized wave. In general the measured values of Ψ

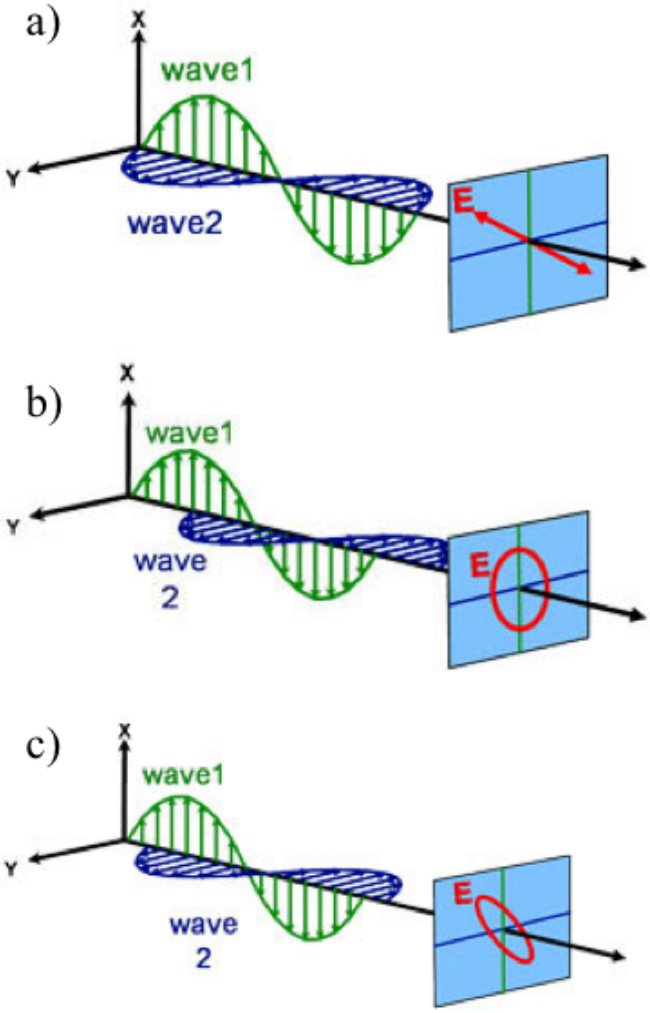

Figure 2.15: Orthogonal waves combined to demonstrate polarization: a) linear, b) circular and c) elliptical [146].

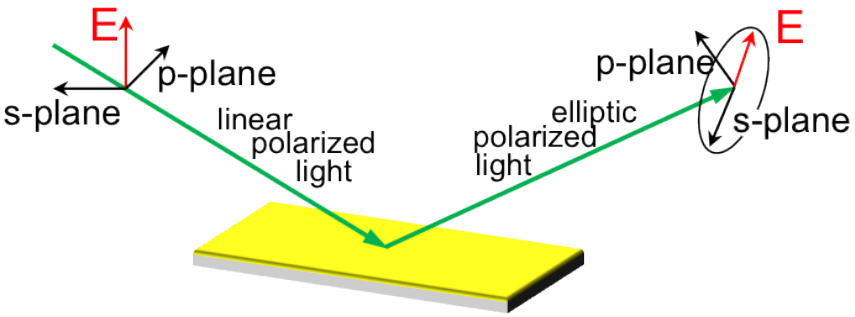

Figure 2.16: Operating mode of an ellipsometer (inspired by [145]).

and Δ cannot be converted directly into the optical constants of the sample. A regression analysis has to be performed, at which a layer model has to be established considering the optical constants and thickness parameters of all individual layers of the sample. By using an iterative procedure unknown optical constants and/or thickness parameters are varied and Ψ and Δ values are calculated using the Fresnel equation [148]

$$r_{\mathrm{p}} = \frac{n_1 \cos\Theta_0 - n_0 \cos\Theta_1}{n_0 \cos\Theta_1 + n_1 \cos\Theta_0}\,, r_{\mathrm{s}} = \frac{n_0 \cos\Theta_0 - n_1 \cos\Theta_1}{n_0 \cos\Theta_0 + n_1 \cos\Theta_1}. \tag{2.2}$$

The calculated Ψ and Δ values which match the experimental data best, provide the optical constants from which e.g. the film thickness can be modeled. It is possible to determine film thicknesses down to the nanometer regime but in the case of multilayers each layer has to be modeled individually. For different wavelengths the optical constants of a material vary and have to be described at all wavelengths probed with the ellipsometer. A table of optical constants can be used to predict the material's response at each wavelength, but it is not convenient to adjust unknown optical constants on a wavelength-by-wavelength basis. It is more advantageous to use all wavelengths simultaneously. A dispersion relationship often solves this problem by describing the optical constant shape versus wavelength. The adjustable parameters of the dispersion relationship allow the overall optical constant shape to match the experimental results. Compared to fitting individual n and k values at every wavelength, this greatly reduces the number of unknown 'free' parameters. For transparent materials ($k = 0$), the refractive index is often described using the Cauchy relationship [149]:

$$n(\lambda) = A + \frac{B}{\lambda^2} + \frac{C}{\lambda^4} \ldots, \tag{2.3}$$

where A, B and C are adjusted to match the refractive index of the material. One of the remarkable features of ellipsometry is the high precision of the measurement and high thickness sensitivity ($\sim 0.1\,\text{Å}$).

2.5.2 Contact angle goniometry

Contact angle goniometry is a technique to describe the wettability of solid surfaces by liquids [150]. It is very sensitive to the molecular structure of the underlying substrate and the contact angle (CA) Θ can vary from 0° to 114° dependent on the surface chemistry of the substrate [70]. It is defined as the angle between the tangent to the solid-liquid interface and the tangent to the liquid-gas interface (Figure 2.17) [151]. A small contact angle displays a high wettability and therefore a strong interaction of the liquid with the solid.

There are different models describing the CA closest to reality, also called apparent CA. More than 200 years ago, Young described the forces acting on a liquid droplet spreading on an ideal surface [152]. The Young CA Θ_Y

$$\Theta_Y = \frac{\gamma_{sl} - \gamma_{sg}}{\gamma_{lg}}, \tag{2.4}$$

where γ_{sl}, γ_{sg} and γ_{lg} are the solid-liquid, solid-gas and liquid-gas interfacial tensions respectively, describes the physico-chemical nature of the wetting system. However, equation 2.4 is a clear oversimplification of the real situation since it is only valid for atomically smooth and chemically homogeneous surfaces which do not change their characteristics due to interactions with the liquid.

On real surfaces that are rough or contaminated, the local CA varies from place to place on the surface. This means that the adhesion energy varies locally and the liquid has to overcome local energy barriers in order to wet the surface. One consequence of these barriers is the CA hysteresis. The extent of wetting, and therefore the observed CA, depends on whether the liquid is advancing or receding on the surface. The value of Θ classifies whether a substrate is hydrophilic

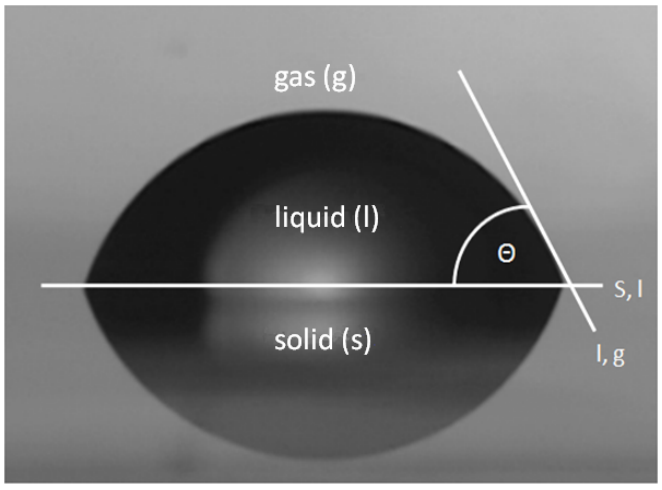

Figure 2.17: Schematic description of the contact angle.

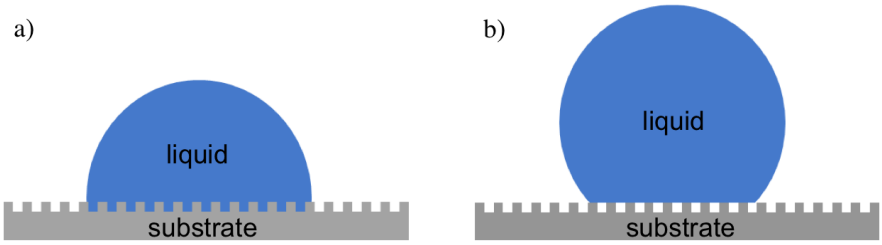

Figure 2.18: Scheme of the a) Wenzel and b) Cassie-Baxter principle. In the Wenzel model the surface roughness contributes to the contact angle. In the Cassie-Baxter model the droplet does not fully wet the substrate due to surface roughness (inspired by [31]).

($\Theta < 90°$) or hydrophobic ($\Theta > 90°$). Extremes of both categories are the superhydrophobic and superhydrophilic surfaces. The latter one is particularly interesting as it characterizes surfaces that are nearly completely non-wettable ($\Theta > 150°$) (Figure 2.18a) [153].

Not only the chemical composition influences the contact angle. Surface structure also has an impact on the wetting behavior and two different regimes can be described. In the Wenzel regime the liquid wets the surface, but the measured CA differs from the 'true' one. The Wenzel CA Θ_W

$$\cos\Theta_W = r\cos\Theta_Y, \tag{2.5}$$

is determined by the surface roughness ratio r, which is defined as the ratio between actual and projected surface area ($r = 1$ for smooth surfaces, $r > 1$ for rough surfaces) and the Young contact angle Θ_Y of a flat surface from the same material. Equation 2.5 predicts that in this wettability regime the hydrophobicity is enhanced by roughness ($\Theta_W > \Theta_Y$) when Θ_Y is larger than 90°. On the other hand, hydrophilicity is increased by roughness when Θ_Y is smaller than 90° [31]. When the surface is made of small pillars, which can not be filled by the liquid and thus stay filled with air, the wettability enters the Cassie-Baxter regime (Figure 2.18b) [154] and can be described by

$$\cos\Theta_C = \varphi(\cos\Theta_Y + 1) - 1. \tag{2.6}$$

Here the Cassie CA Θ_C is dependent on the surface contact fractions φ of the liquid droplet and the surface characteristic contact angle Θ_Y. However, since the pores are filled with air, which is hydrophobic, the CA always increases, relative to the behavior seen on a flat substrate with identical chemical composition. Hence, it has to be considered that surface morphology can have an effect on the wettability of the substrate.

2.5.3 Infrared reflection absorption spectroscopy

Infrared reflection absorption spectroscopy (IRRAS) is known to be a powerful tool to study the adsorption of molecules on surfaces [155]. It provides specific information about the chemical composition and the structure of thin layers as well as the orientation of the single molecules on the surfaces. In general, IR radiation, which lies in the range between the red edge of visible light ($\lambda \approx 0.7\,\mu m$) and the short radio waves ($\lambda \approx 1\,mm$ to $2\,mm$), can be divided into three regions, near IR ($0.7\,\mu m$ to $3\,\mu m$), mid IR ($3\,\mu m$ to $50\,\mu m$) and far IR light ($50\,\mu m$ to $1000\,\mu m$) [156].

If molecules interact with IR radiation, the energy is converted into energy of molecular vibration and rotation. When the radiation energy matches the energy of a specific molecular vibration, absorption occurs. Assuming that a molecule can also be described as a system of masses kept together by spring-like bonds, the frequency of the vibrational modes can be estimated by Hooke's law

$$\nu = \frac{1}{2\pi c}\sqrt{\frac{k}{\mu_{rm}}}, \tag{2.7}$$

where c is the speed of light, k is the force constant and μ_{rm} the reduced mass.

The general selection rule for IR-activity of a molecule states that its dipole moment μ has to change during a normal mode. Two different kinds of vibrations can be observed, stretching and deformation vibrations. Stretching vibrations can be described as a deflection of the atoms out of their idle state with periodically changing binding lengths (Figure 2.19a and b). If the symmetry of the molecule stays the same the vibrations are called symmetric. If the symmetry changes they are called asymmetric. During deformation vibrations the bond angle changes periodically, while the bonding distance is maintained (Figure 2.19c). Stretching vibrations appear at wavenumbers of $\nu = 1500\,cm^{-1}$, whereas deformation vibrations appear at smaller wavenumbers [157].

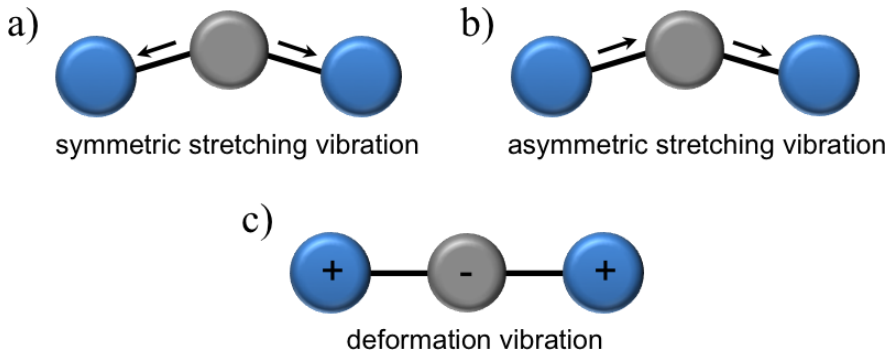

Figure 2.19: Different types of vibrations for molecules with 3 atoms. a) and b) main types of stretching vibrations, c) deformation vibrations.

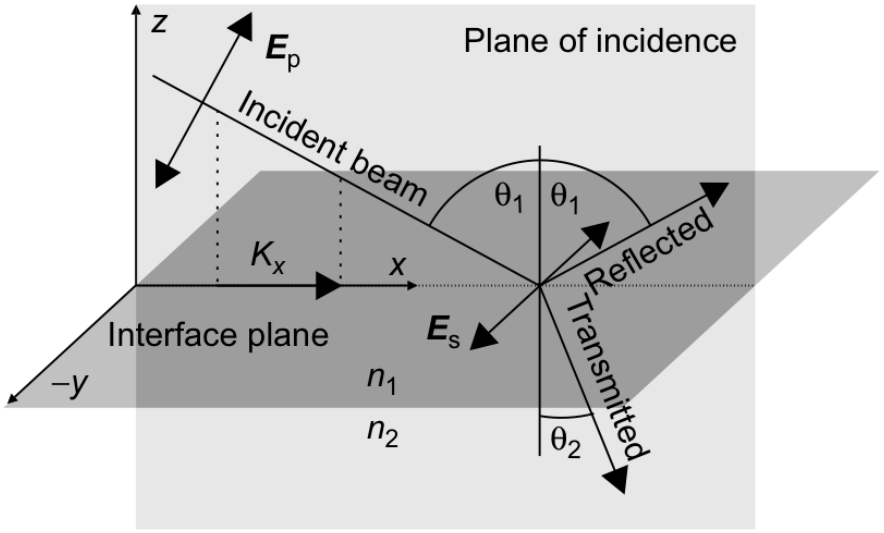

Figure 2.20: Beam geometry and polarization of IR radiation at the interface between two optically different media [155].

Regarding IR measurements on surfaces, the radiation consists of two components, a p-polarized part (E_p, parallel to the plane of incidence) and a s-polarized part (E_s, perpendicular to the plane of incidence) (Figure 2.20). At the contact point of the surface with the p-polarized radiation the vectors of the incoming light (E_p) and the vector of the reflected light ($E_{\mathrm{p}'}$) combine and form an amplitude that is almost twice as high. In contrast, for the s-polarized radiation, the incident and the emitted vector (E_s and $E_{\mathrm{s}'}$) undergo a phase shift of nearly 180° with respect to each other and the amplitude is zero [158, 159]. This means that only radiation with a p-component will interact with surfaces. This p-component can be split into two parts. One is parallel to the surface ($E_{\mathrm{p}\parallel}$) and one is perpendicular to it ($E_{\mathrm{p}\perp}$). When the incident light hits the surface a dipole moment is induced, which also can be oriented either parallel or perpendicular to the surface. If vibrations with a dipole moment parallel to the surface interact with the parallel part of the incoming light, a so called mirror charge is induced which compensates the other part and no vibrations can be detected. Only those vibrations are visible where the components of the dynamic dipole polarized in the direction normal to the surface will be enhanced by the electric field from the induced mirror charge. This is the so called 'surface selection rule' for IRRAS spectroscopy [158, 160].

2.5.4 X-ray photoelectron spectroscopy

X-ray photoelectron spectroscopy (XPS), also known as electron spectroscopy for chemical analysis (ESCA), is an analysis technique that utilizes the photoelectric effect to determine the chemical composition of surfaces. When a surface is irradiated by X-rays (Figure 2.21), the core level electrons of surface atoms can absorb the X-ray photon energy $h\nu$. If the binding energy E_B is overcome ($h\nu > E_\mathrm{B}$), electrons are emitted out of the surface with a defined kinetic energy E_kin. This process is described by Einstein's equation [161]

$$E_\mathrm{kin} = h\nu - E_\mathrm{B} - \psi. \tag{2.8}$$

In this equation, ψ is the work function of the instrument and $h\nu$ is the energy of the X-ray source. Mg K_α and Al K_α are the two commonly used sources because of their relatively high energies (Mg=1253.6 eV, Al=1486.6 eV) and narrow widths [161]. The kinetic energy E_kin of the emitted electrons is measured by an analyzer and therewith the binding energy E_B of the core level electrons can be determined, since it is an element specific constant.

The XP-spectrum of a material contains peaks of the elements (except H and He) present on the surface. The intensities of these peaks are related to the amount of each element, what allows to determine the concentration of each detected element. Typically, either elemental ratios or atomic percentages are calculated. Thus, it is only necessary to determine the relative relationships, not the absolute

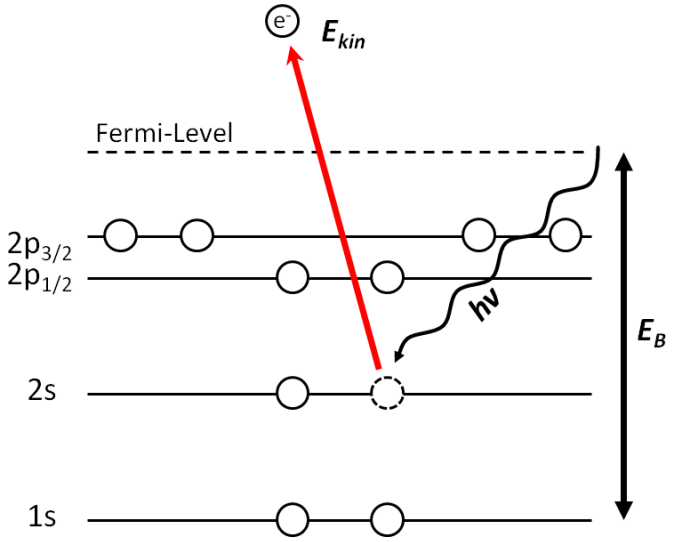

Figure 2.21: Scheme of the photoelectric effect. X-rays hit the inner shell electrons of a material followed by the emission of the electron (after [161]).

values of the quantities. The peak intensity ratio can be calculated with

$$\frac{N_\mathrm{A}}{N_\mathrm{B}} = \frac{I_\mathrm{A}}{I_\mathrm{B}} \cdot \frac{\sigma_\mathrm{B}}{\sigma_\mathrm{A}} \cdot \frac{\lambda_\mathrm{B}}{\lambda_\mathrm{A}}, \tag{2.9}$$

where N is the element ratio, I the peak area, σ the photoionization cross-section and λ the inelastic mean free path which can be obtained from literature or databases [161, 162].

Lambert-Beer's law describes the attenuation of an electromagnetic wave through a material. It is an empirical relationship between the adsorption of electromagnetic radiation and the properties of the material through which the radiation is traveling.

$$I(d) = I_0 \cdot \exp(-\epsilon c d) \tag{2.10}$$

Here $I(d)$ is the intensity of the radiation after transmission through a material, I_0 the intensity of the radiation before transmission, ϵ the adsorption constant of the material, c the concentration of the material, and d the thickness of the material [161]. When a thin film (thickness $< 10\,\mathrm{nm}$) is deposited on a substrate, the thickness of this film d can be calculated by the attenuation of the signal from the substrate caused by the overlayer. In this case, Lambert-Beer's law (equation 2.10) can be applied as:

$$I(d) = I_0 \cdot \exp\left(-\frac{d}{\lambda \cos\theta}\right) \tag{2.11}$$

where d is the thickness of the overlayer, λ is the attenuation length of photoelectrons with a certain kinetic energy (see Table 3.4 in section 3.8.4) and θ is the take-of angle.

2.5.5 Atomic force microscopy

Atomic force microscopy (AFM) is a frequently used technique to obtain 3D images of structured surfaces in the range of a few micrometer to single nanometers with a very high resolution. Therefore a sharp tip at the end of a cantilever is scanned over the substrate, which detects ultrasmall forces (less than 1 nN) present between the tip and the surface [163]. The topography of the substrate causes deflections of the cantilever and go along with changing interactions between the tip and the surface, such as van der Waals or electrostatic forces. A visible laser beam is reflected from the backside of the cantilever to a detector, also called position sensitive device (PSD), so that very small deflections of the substrate can be observed (Figure 2.22). The obtained linedeflection can be combined together to topographic images of the substrate.

The AFM can be operated in three different modes namely the contact, non-contact and tapping mode [164]. In the contact or static mode the tip is brought

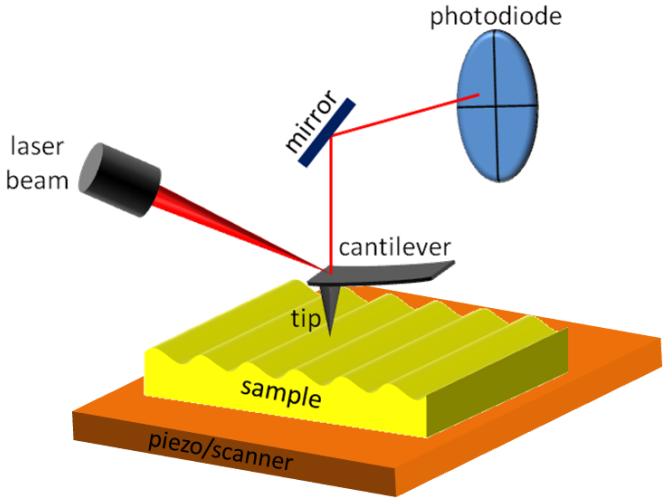

Figure 2.22: Scheme of an AFM microscope (after [166]). The tip is attached to a cantilever, and is scanned over a surface. The cantilever deflection due to tip-surface interactions is monitored by a photodiode sensitive to laser light reflected at the tip backside.

into direct physical contact with the sample [165]. The topographical information is detected and transferred to a piezoceramic element which adjusts the cantilever in a way that the force acting on the surface stays constant. This is called 'feedback loop' [163]. As the tip scans across the surface, varying topographic features cause deflections of the cantilever, which are measured and visualized as an image information. The disadvantage of this mode is that the constant force can deform soft biological samples or material can be wiped away or smeared over of the surface. To avoid these effects, the non-contact or dynamic mode can be used. In this mode the cantilever oscillates above the sample at its resonance frequency. When the tip gets closer to the surface, very weak van der Waals attractive forces change the oscillation amplitude of the tip. These changes can be detected and used to generate an image [164]. In this mode the tip-substrate interactions are very small and the lateral resolution is lower than in other operation modes. However, the greatest drawback is that it can only be used on dry samples. A small water layer disturbs the detachment of the tip from the sample because of the small oscillating amplitude [167].

In the tapping mode, the cantilever is driven to oscillate up and down near its resonance frequency [168]. When the tip gets closer to the surface, van der Waals forces, dipole-dipole interactions, electrostatic forces, etc. interact with the cantilever and with this change the amplitude and the phase of the oscillation. Mostly, this change in the amplitude is used to regulate the signal during the scan process. This means piezoceramics are used to control the height of the cantilever to keep the amplitude constant. Due to the fact that shear forces are

eliminated and vertical forces are reduced significantly, this mode is advantageous to investigate sensitive materials (e.g. biological surfaces) or unstable surface features (e.g. small particles) [169].

2.5.6 Scanning electron microscopy

Scanning electron microscopy (SEM) is a technique of major importance and is widely used throughout the scientific and technological communities [170]. This microscope is an instrument that achieves large magnifications by scanning the sample with a focused electron beam instead of light in a raster scan pattern. The electrons of the beam interact with the electrons in the sample and the intensity of reflected and secondary electrons produced by the incident beam can be detected and analyzed.

Detection limitations, e.g. the spatial resolution d of microscopic techniques, are closely linked to the wavelength λ of the incident beam via the lens specific numerical aperture NA

$$d = \frac{\lambda}{2 \cdot NA}. \tag{2.12}$$

This, in turn, is determined by the opening angle α of the lens and the refractive index of the medium n [171]

$$NA = n \cdot \sin \alpha. \tag{2.13}$$

Taking advantage of the de Broglie relation

$$\lambda = \frac{h}{p} = \frac{h}{\sqrt{2 m_\mathrm{e} E_\mathrm{e}}}, \tag{2.14}$$

where λ is the electron wavelength, h Planck's constant, p the electron momentum, E_e the electron energy and m_e the electron mass, electrons are used instead of photons, achieving shorter wavelengths and thereby better resolutions [166]. If, for example, electrons are accelerated with 100 eV, a wavelength of 0.122 nm is achieved, which is far below the wavelength of visible light applied in light microscopy.

Although the use of electrons theoretically has no limitations with respect to the resolution, the spherical aberration of the lenses limits it.

Essential components of all SEMs include an electron source ('gun'), electronic lenses, a measurement chamber and a detector for all signals of interest (Figure 2.23). A beam of electrons is produced by the electron gun, a cathode emitting electrons which are accelerated towards the anode. The emission can be excited either thermally (thermodynamic emission) or by applying high voltage (field emission). In conventional electron guns, the cathode, usually consisting

of tungsten (W) or lanthanum hexaboride (LaB_6), is heated until a stream of electrons is produced. The disadvantages of this system are the short lifetime of the filament and the high emission energy distribution [170].

The electron beam follows a vertical path through the microscope, which is kept under vacuum. The beam travels through electromagnetic fields and lenses, which focus the beam down toward the sample and correct symmetric defects of the beam with respect to the optical axis.

When primary electrons hit the surface of an object, interaction through elastic and inelastic scattering takes place. Secondary electrons (SE) and back-scattered electrons (BSE) with different energies are created, which are collected by various detectors. The penetration depth of the primary electrons depends on their energy, on the thickness and on the nature of the material.

Different detector designs are available to collect BSE or SE which generate different contrasts due to their interaction depth with the material.

The InLens detector is ring-shaped and situated above the sample in the column and detects secondary electrons that are emitted back into the column. With this

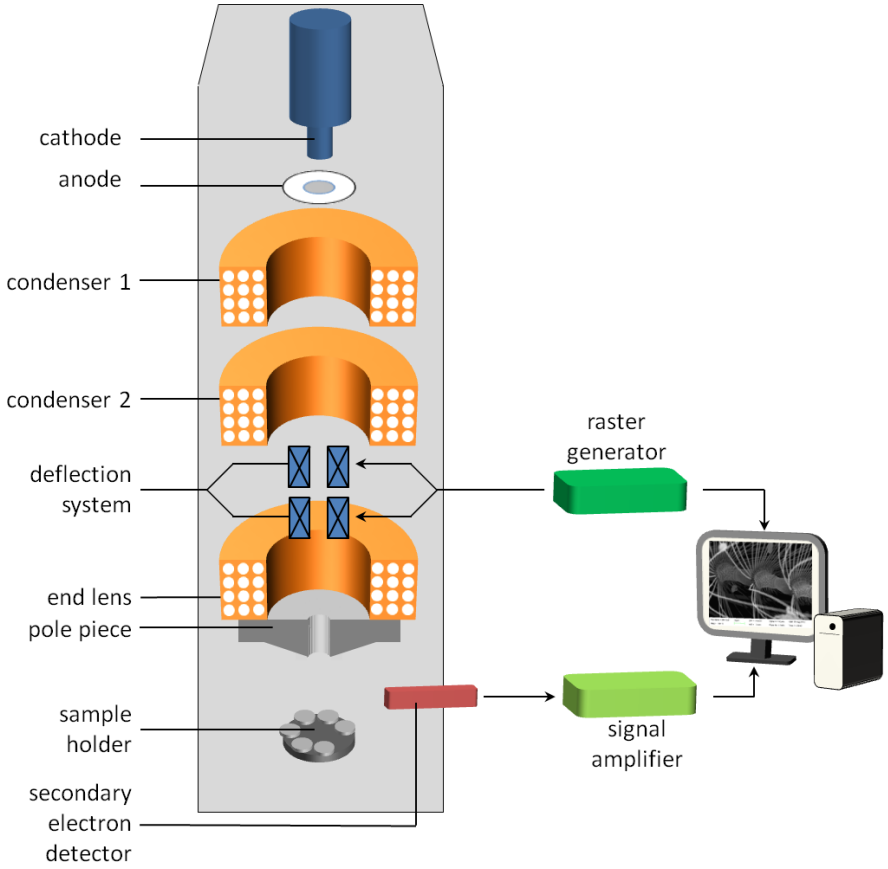

Figure 2.23: Scheme of an SEM microscope (after [172]).

detector it is possible do achieve high-resolution images (in the nm range) at small acceleration voltages of the beam due to the low working distance. This makes it possible to achieve images faster and more gentle than with other detectors. Since SE generally are low energy electrons, they only emerge from the outermost layer of the sample and carry information about the material contrast with them due to the different material-dependent attenuation lengths.

Another type of SE-detector is the SE2 detector which is able to achieve a topographic contrast and a high spatial resolution. Although the name is misleading this detector detects not only SE but also few BSE. In contrast to the InLens detector the picture information here originates from deeper penetration depths. The electrons are accelerated towards the detector, are collected by a positively biased collector grid and create a number of electrical impulses. The SE2 detector is mounted at the sideways above the sample with a tilt angle of 45° and provides a very naturally, 3D image.

BSE are electrons which are scattered elastically on atomic cores down to 10 nm under the sample surface. The BSE detector usually is a 4-quadrant-semiconductor and since it is situated in the measurement chamber, it is important to work with a high accelerating voltage (min. 5 keV) for obtaining a good signal intensity. Dependent on the circuit of the semiconductor crystals different topographic contrasts can be achieved, whereas deep areas seem to be darker. The property that heavy elements reflect the electrons more than lighter ones is used to draw conclusions from the chemical nature of the surface.

The SEM has some disadvantages. The samples have to be viewed in a vacuum (10^{-5} torr to 10^{-6} torr), as the air molecules would scatter the electrons. A second point is that for conventional SEM imaging the sample has to be electrically conductive, at least at the surface, and electrically grounded to prevent the accumulation of electrostatic charge at the surface. Therefore nonconductive substrates tend to charge when they are imaged by the electron beam, and especially in the secondary electron imaging mode, this causes scanning defaults and other image artifacts. They are therefore usually coated with an ultra thin coating of electrically conductive material like graphite or gold.

3 Materials and methods

In this section all experimental details regarding surface and media preparation as well as procedure of the biological assays with the different organisms are provided. Furthermore, an overview of the used analytical instruments will be given.

3.1 Preparation of self-assembled monolayers

Self assembled monolayers (SAMs) give access to surfaces with well defined and tunable properties [25, 26]. They have been extensively studied as protein resistant materials [173] and for developing anti-fouling surfaces [83, 174] (see also chapter 2.2). The most frequently used strategies to obtain highly ordered SAMs are self-assemblies of alkanethiols on gold.

All chemicals, such as ethanol, trimethylamine (NEt_3), 1-dodecanethiol (DDT), 11-mer-capto-1-undecanol (HUDT) and 11-amino-1-undecanethiol hydrochloride (AUDT) were purchased from Sigma Aldrich (Munich, Germany). 11-(tridecafluorooctyloxy)undecanethiol (FUDT) was purchased from ProChimia Surfaces Sp. z o.o. (Sopot, Poland). Hydroxy-PEG2000-thiol (PEG) was purchased from Rapp Polymere GmbH (Tübingen, Germany). Deionized water was purified with a MilliQ® plus system (Millipore, Schwalbach, Germany).

Gold substrates were purchased from Georg Albert (PVD-Beschichtungen, Germany). For SAM surfaces extra smooth float Nexterion B® glass slides (Schott, Germany) were coated with 30 or 100 nm gold (99.99 % purity) after applying a titanium adhesion promoter of 5 nm thickness. Evaporation was performed at a pressure of 2×10^{-7} torr and a deposition rate of $1\,\mathrm{nm\,s^{-1}}$. The resulting films had a grain size of 20 nm to 50 nm and predominantly possessed a (111) orientation. For the polymer brushes, Silicon (100) wafers (CrysTec, Germany) were coated using the same parameters, respectively. The gold coated surfaces used for the experiments were of extra smooth quality. The R_q roughness value was about 1 nm [175]. Gold substrates were kept in argon atmosphere at room temperature (RT) until they were used.

Prior to SAM synthesis the samples were cleaned under UV radiation for 1.5 h in order to remove organic adsorbents from the surface, then rinsed with absolute

ethanol, ultrasonicated for 3 min and dried in a nitrogen stream. For each substrate a reference measurement was performed by ellipsometry. The substrates were then immersed in 1 mM ethanolic solutions of the SAM molecules for 24 h. In the case of AUDT 3 vol % NEt_3 was added to remove the remaining HCl [176]. To produce PEG surfaces the substrates were kept in a 0.5 mM solution for 72 h. After the given immersion time in the dark at room temperature, the samples were removed from the thiol solution, rinsed with ethanol, treated in an ultrasonic bath for 3 min and then again rinsed with ethanol. Finally, the samples were dried in a flow of nitrogen and stored in an argon atmosphere until use.

3.2 Surface characterization

The prepared self-assembled monolayers, which varied in terms of protein resistance and wettability were characterized by various methods namely ellipsometry, contact angle goniometry, IRRAS and XPS. The obtained thicknesses and contact angles (CA) are summarized in Table 4.1.

The sessile drop CA varied between 27° and 112° and were in good agreement with literature values. And also the film thicknesses of the SAMs lay in the range of 1 nm to 2 nm according to literature [91, 177]. Only the PEG surfaces had a higher thickness of ∼3 nm originating from the much longer thiol molecules [178]. The film thickness of PEG indicates a coil-like chain conformation rather than upright standing brushes [179]. Furthermore, the chemical composition of the used SAMs was verified by IRRAS and XPS. Figure 3.1 and Figure 3.2 show overviews of the IRRAS spectra and the XPS peaks determined for the different chemistries.

Table 3.1: Thiol molecules used to form self-assembled monolayers, static water contact angle (error: ± 4°) and thickness as determined by spectral ellipsometry (error: ± 2 Å) and XPS (error: ± 3 Å).

Chemistry	**label**	**CA**	**thickness** [nm]	
		[°]	Ellips.	XPS
$SH-(CH_2)_2-(O-(CH_2)_2)_{44}-OH$	PEG	27	3.4	3.2
$SH-(CH_2)_{11}-OH$	HUDT	33	1.1	1.2
$SH-(CH_2)_{11}-NH_2$	AUDT	60	1.9	1.5
$SH-(CH_2)_{11}-CH_3$	DDT	104	1.2	1.1
$SH-(CH_2)_{11}-O-(CF_2)_5-CF_3$	FUDT	112	1.4	1.6

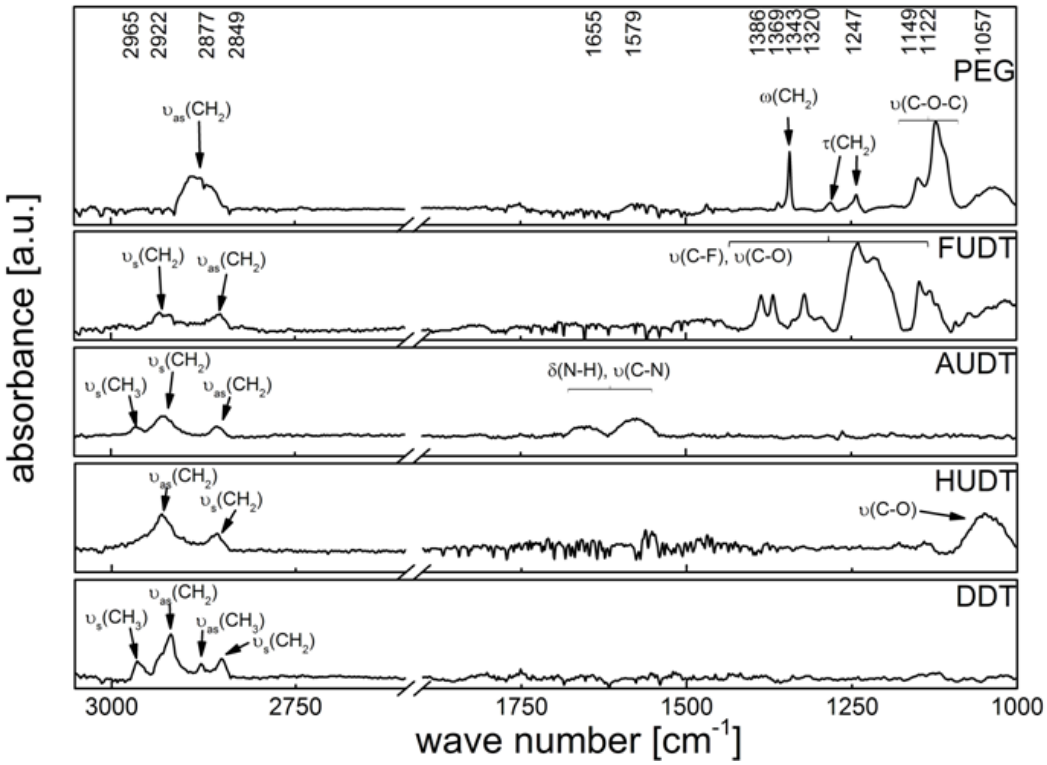

Figure 3.1: IRRAS of the different surfaces. Characteristic peaks for each chemistry are marked.

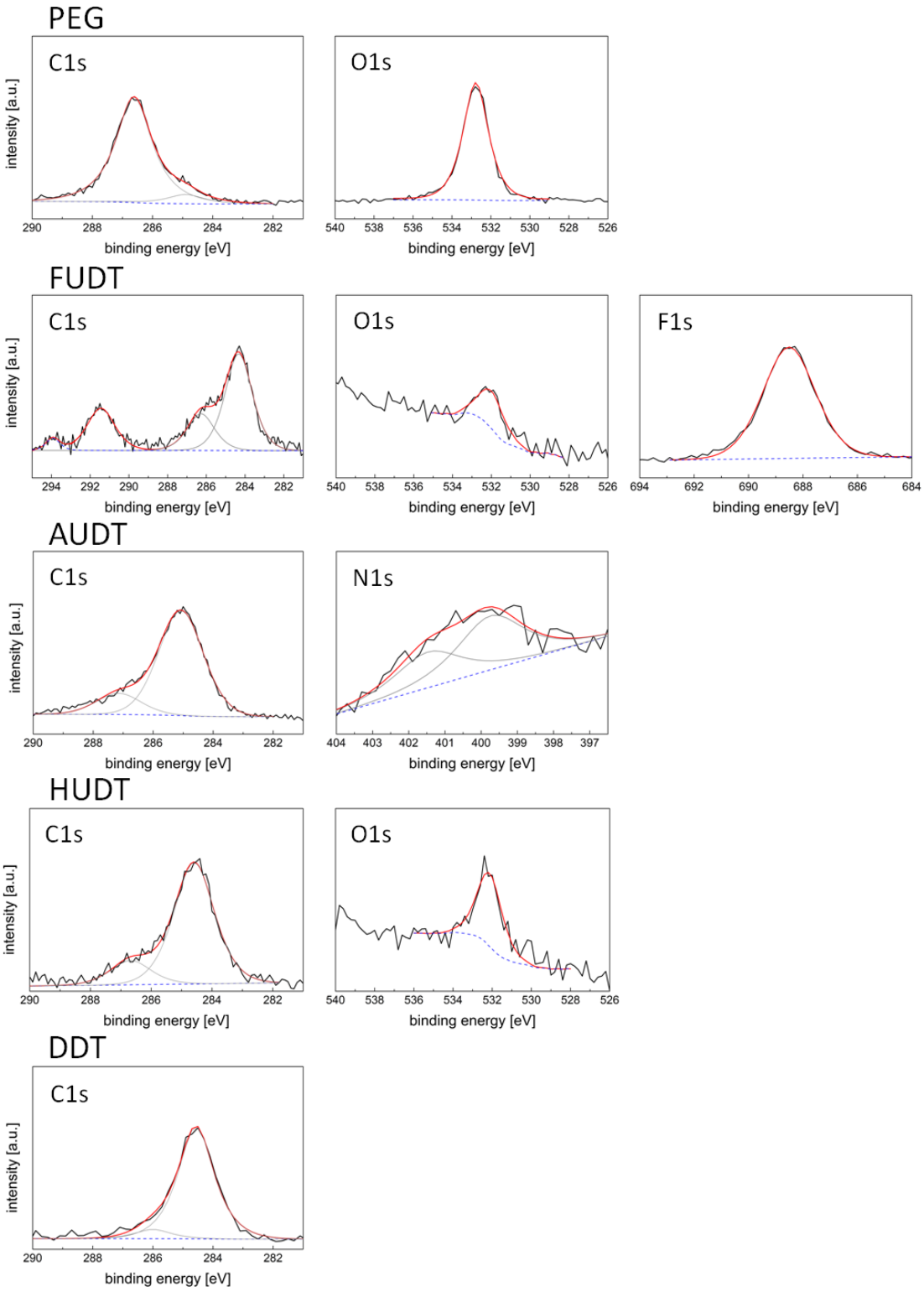

Figure 3.2: Photoelectron spectra of all five utilized surfaces. The typical peaks for each chemistry are shown.

The IR spectrum of the DDT surface shows the typical peaks in the range of $2965\,cm^{-1}$ to $2849\,cm^{-1}$ [27], which derive from symmetric and antisymmetric stretching vibrations of the CH_3 and CH_2 groups. While for the other surfaces these peaks are also present other peaks, specific for the surface chemistry, appear in the spectra. HUDT has an additional peak at $1050\,cm^{-1}$, AUDT in the range of $1579\,cm^{-1}$ to $1655\,cm^{-1}$ originating from C−O stretching and N−H bending, N−C stretching vibrations, respectively [156, 180]. The fluorinated surface shows significant bands in the range of $1386\,cm^{-1}$ to $1122\,cm^{-1}$ which correspond to C−F and C−O stretching vibrations [181]. The PEG spectra shows a sharp peak in the region of at $1343\,cm^{-1}$ originating from CH_2 wagging modes. The CH_2 twisting vibrations can be observed at $1247\,cm^{-1}$. The peaks in the range of $1149\,cm^{-1}$ to $1122\,cm^{-1}$ can be identified as C−O−C stretching modes [182–184].

In Figure 3.2 the characteristic XP spectra are illustrated for the different surfaces. The observed C1s peak of all alkyl SAMs has the typical shape according to literature [27] and consists of two sub-peaks at 285 eV and 286 eV, respectively. The peak at 285 eV derives from the alkyl carbon and the peak at 286 eV form carbon atoms bound to oxygen or nitrogen. For FUDT there are two additional peaks at 291 eV and 294 eV, originating from carbon atoms bound to fluor atoms. The surfaces also show additional peaks of oxygen or fluor, depending on the surface chemistry. The N1s spectra of the AUDT shows an expanded peak consisting of two individual nitrogen species. The signal at the lower energy of 399.5 eV derives from a free NH_2 group, while the signal at 401.3 eV originates from a nitrogen atom of an amine group to which probably water or carbon-dioxide from the surrounding environment is coordinated. Such double peaks appear often concerning amino SAMs [185, 186]. For the PEG SAM C1s and O1s peaks can be observed. Compared to the other SAMs here there is one pronounced C1s peak present, which indicates that the PEG molecules do not exhibit an alkyl spacer like the other samples do and nearly every carbon atom has an oxygen as neighbor. The very small underlying peaks result from alkyl contaminations on the surface. Additionally, the element ratios for each surface chemistry were calculated. For HUDT the C1s/O1s ratio was found to be 11.4/1 and for AUDT a 12.1/1 ratio was obtained for C1s/N1s. This perfectly fits with the stoichiometric ratios of the samples. The C1s/O1s and the C1s/F1s ratios for FUDT were obtained to be 14.5/1 and 1.2/1, which also lies in the range of the calculated ones. Finally, the PEG ratio was determined to be 2.1/1 for the C1s/O1s ratio, which also perfect fits with the calculated ratio of 2/1.

3.3 Preparation of liquids used for conditioning of surfaces

Tropic Marin® (TM) and Instant Ocean® (IO) were made up to the manufacturer's instructions, then filtered through a 0.22 µm Millipore filter. Seawater made from individual salts (Salt water; SW) was prepared freshly as described by Kester *et al.* (Table 3.2) [187]. All chemicals were of analytical grade and the salt water was filtered through a 0.45 µm Millipore filter after preparation.

'Spore water' (SP) was made from a suspension of swimming spores (3 l) prepared as described in section 3.5.2. The spore suspension (1×10^6 spores ml^{-1}) was stirred for 1 h (to prevent spore settlement) before it was filtered through 10 cm glass fiber A filters (Whatman) using vacuum suction. Microscopic examination of the filtrate showed that no spores had passed through the filter. The SP was not passed through a 0.22 micron filter to avoid removal of macromolecular aggregates/colloids that might serve as a source of conditioning molecules. Although the SP was not sterile, bacteria were not detected after streaking aliquots onto marine agar and were not detected by epifluorescence microscopy (after staining with Syto 13) on slides that had been immersed in 'spore water' for 24 h. The filtrate was aliquoted into 50 ml Falcon tubes and fast frozen by plunging into liquid nitrogen. The tubes were stored at −80 °C.

Brain heart infusion broth (BHi broth) (Merck KGaA, Darmstadt, Germany) was prepared to the manufacturer's instructions. PBS-buffer was prepared freshly using distilled water and the salts listed in Table 3.3a. Afterwards the pH was adjusted to 7.4. Basal medium 2 (BM2) was prepared freshly using the salt listed in Table 3.3b. For culturing *P. aeruginosa* glucose (0.4 % (wt/vol)) was added.

Table 3.2: Salt mixture used to prepare 35.00 % self mixed salt water (artificial seawater according to Kester *et al.* [187].

Salt	[$g\,l^{-1}$]
NaCl	23.926
Na_2SO_4	4.008
KCl	0.677
$NaHCO_3$	0.196
KBr	0.098
H_3BO_3	0.026
NaF	0.003

Table 3.3: Salt mixtures used to prepare a) PBS-buffer and b) Basal medium 2.

a) PBS-buffer	$[g\,l^{-1}]$	**b) Basal medium 2**	$[g\,l^{-1}]$
NaCl	8.006	K_2HPO_4	6.966
KCl	0.199	KH_2PO_4	2.993
$Na_2HPO_4 \cdot 2\,H_2O$	1.804	$(NH_4)_2SO_4$	0.925
KH_2PO_4	0.239	$MgSO_4$	0.241
		$FeSO_4$	0.015

3.4 Surface conditioning

Conditioning film formation was evaluated on a given surface and a chosen type of media in a similar manner to established protein resistance assays [188, 189]. The SAM coated surfaces (see section 3.1) were cut into pieces of 25×25 mm^2. The samples were immersed in a 50 ml glass bottle in 5 ml of self-mixed salt water solution (see section 3.3) composed of salts at concentrations found in seawater [187] or in PBS buffer solution (see above) for 15 min to allow the surfaces to saturate with water which had the same salinity as the used medium. Then 20 ml of the medium to be tested was added. After different immersion times (ranging from 10 min to 48 h), the solution was diluted with 500 ml of MilliQ® water (MQ), rinsed with MQ and dried in a stream of nitrogen. The prepared samples were used directly for spectral ellipsometery, contact angle and IRRAS measurements.

3.5 Biological assays

In the next sections the different biological assays which were used in this thesis are explained in greater detail and the analytical strategies concerning the different microorganisms will be explained.

3.5.1 Bacteria assay

The bacteria assays were performed in collaboration with the group of Prof. Ursula Obst at the Institute of Functional Interfaces, Karlsruhe Institute of Technology, Germany. Thereby 30 µl of an overnight glycerin cultures of *P.aeruginosa* ATCC 27853 colonies were diluted in 40 ml 1:4 BHi medium or BM2 and incubated at 37° on a shaker at 150 rounds per minute (rpm). This culture was diluted 1:10 with the corresponding medium and incubated for another 3 h at

37° at 150 rpm until the bacterial cells reached the exponential phase. This suspension was again diluted with 1:10 of the corresponding medium and used to start the biofilm cultivation in a biofilm reactor (in-house construction). The test samples were placed inside the bioreactor and the bacterial solution was mixed constantly. After 1 h, 3 h, 6 h, 24 h and 48 h, the slides were removed from the reactor and washed twice in sterile PBS-buffer. Afterwards the colony-forming units (CFU) were determined. Therefore each surface was thoroughly scraped with a sterile cell scraper and a homogeneous bacterial suspension was prepared in 1 ml PBS-buffer. The number of cultivable adherent bacteria was quantified by means of the pour-plate method, i.e. plating serial dilutions of bacterial suspensions obtained on the triple scale. Centrimid-agar (Merck Eurolab, Darmstadt, Germany) was used as growth medium. After incubating the agar plates for 2 days at 20 °C, the bacterial colonies were counted and the number of bacteria per square cm was calculated.

3.5.2 Zoospore settlement assay

The *Ulva* spore settlement assays were performed in collaboration with the group of Prof. James A. Callow at the University of Birmingham, UK. Spores were collected and released following the established protocol [41]. The thesis of Schilp gives a detailed description of the whole process [179]. Fertile plants of *Ulva linza* were collected from the seashore at Llantwit Major, South Wales, U.K. (51°40 'N; 3°48 'W) a few days before spring tide, the period where *Ulva* usually is most fruitful in producing spores [57]. Plants, where already white spots in the thalli and some light brown areas next to them were visible, were chosen, which indicated a high release potential of spores. Excess water was squeezed from the material, which then was wrapped in absorbent paper and carried to the laboratory in a cool box filled with ice. Ripe tips were cut off the seaweed and transferred into glass tubes which contained 3 ml to 5 ml of TM artificial seawater. The beaker was moved very gently to aid spore release. In order to remove any debris like sandgrains and diatoms which could alter the measurements, the spore suspension was filtered through 3 layers of nylon mesh (100 µm, 50 µm and 20 µm). The beaker containing the spore suspension was plunged into ice to concentrate the spores at the bottom (zoospores swim towards the darker bottom of the beaker, because they are negative phototactic). Afterwards they were removed with a pipette. This procedure was repeated and then the spore suspension was kept on a magnetic stirrer to prevent settlement and the absorbance was adjusted to 0.15 at 660 nm (1×10^6 spores ml^{-1}) with filtered (0.22 µm) TM. The spore suspension was used in bioassays within 10 min.

Ten milliliter of spore suspension were pipetted into individual compartments of quadriperm dishes (Greiner-One), each containing one test surface. The dishes were incubated in darkness at room temperature for 45 min (standard assay) or

different periods as specified. At the end of the incubation period, the slides were washed to remove unattached motile spores by passing the slide 10 times through a beaker of TM. The slides were fixed for 10 min in 2.5 % glutaraldehyde in TM. Subsequently, the surfaces were washed in TM, then in 50 % TM and 50 % deionized water and finally pure deionized water and allowed to air dry. Spores were counted by autofluorescence of chlorophyll using a Kontron 3000 image analysis system attached to a Zeiss epifluorescence microscope [102]. Thirty counts were made on each of three replicate slides ($n = 90$) except for the kinetic experiment, where the spore count at each point is the mean of 30 counts from one slide.

3.5.3 Static immersion field tests

Static immersion field experiments were performed in collaboration with the group of Prof. Geoffrey Swain in summer 2012 at the 'raft' test site of the Florida Institute of Technology, Melbourne, Florida, USA. The site is located at the east coast of Florida about 5 km north of the Sebastian inlet, Florida (27°59 'N; 80°28 'W). Samples pre-incubated in filtered seawater for 24 h and non incubated samples were immersed in the ocean for 24 h. All samples were immersed in sets of two replicates each to ensure that all samples within a set have the same treatment and allow comparability. The experiments were carried out twice (day 1 (d1), day 2 (d2)) on two following days. The test samples were placed into microscope slide holders according to Figure 3.3 and fixed with rubber band. All samples had the same orientation and distance to each other and faced glass. The sequence was DDT, HUDT, AUDT, FUDT, PEG, DDT, HUDT, etc. In each slide holder two replicates were placed of each chemistry, conditioned and unconditioned. This layout provides that environmental factors like shear, solar irradiation and salinity, have the same influence on all samples. Subsequently, the samples were submerged into the water, approximately 0.5 m

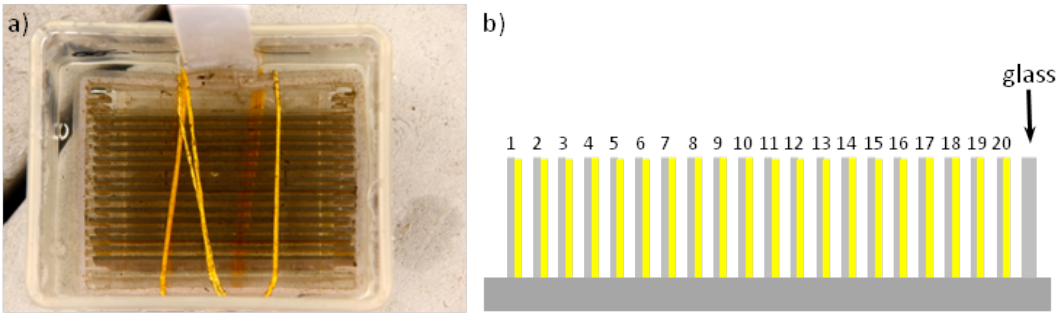

Figure 3.3: Experminetal layout of the field studies. a) Image of the samples in the microscope slide holder fixed with rubber band. b) All samples have the same orientation, same distance to each other and face glass.

below the water air interface. After 24 h the samples were removed from the water without passing through the water air interface using a bucket full of water and were there transferred into the fixation containers. All samples were fixed with 2.5 % formaldehyde solution for 1 h. Subsequently, the containers were flooded first with filtered seawater and the salt concentration was decreased by dilution with distilled water. After this treatment the samples were air-dried.

The samples were analyzed by phase contrast microscopy (TE-2000, Nikon) using a 15× phase contrast objective with a field of view (FOV) of 672 µm × 504 µm. For each sample 60 FOVs distributed across the whole surface were obtained.

During the evaluation of the samples several organisms were observed and most of the common ones were classified and counted. Mainly eleven diatom genus and one subclass of protozoa were found. The different diatoms were: *Navicula, Amphora, Bacillaria, Cylindrotheca, Mastogloia, Coscinodiscus, Plagiotropis, Licmophora, Brachysira, Triceratium* and *Progonoia* (Figure 3.4). The genera *Mastogloia, Coscinodiscus, Plagiotropis, Licmophora, Brachysira, Triceratium* and *Progonoia* were grouped together as 'others' since they were found on the substrate quite seldom. The found subclass of protozoa was *Peritrich ciliates* (Figure 3.4c).

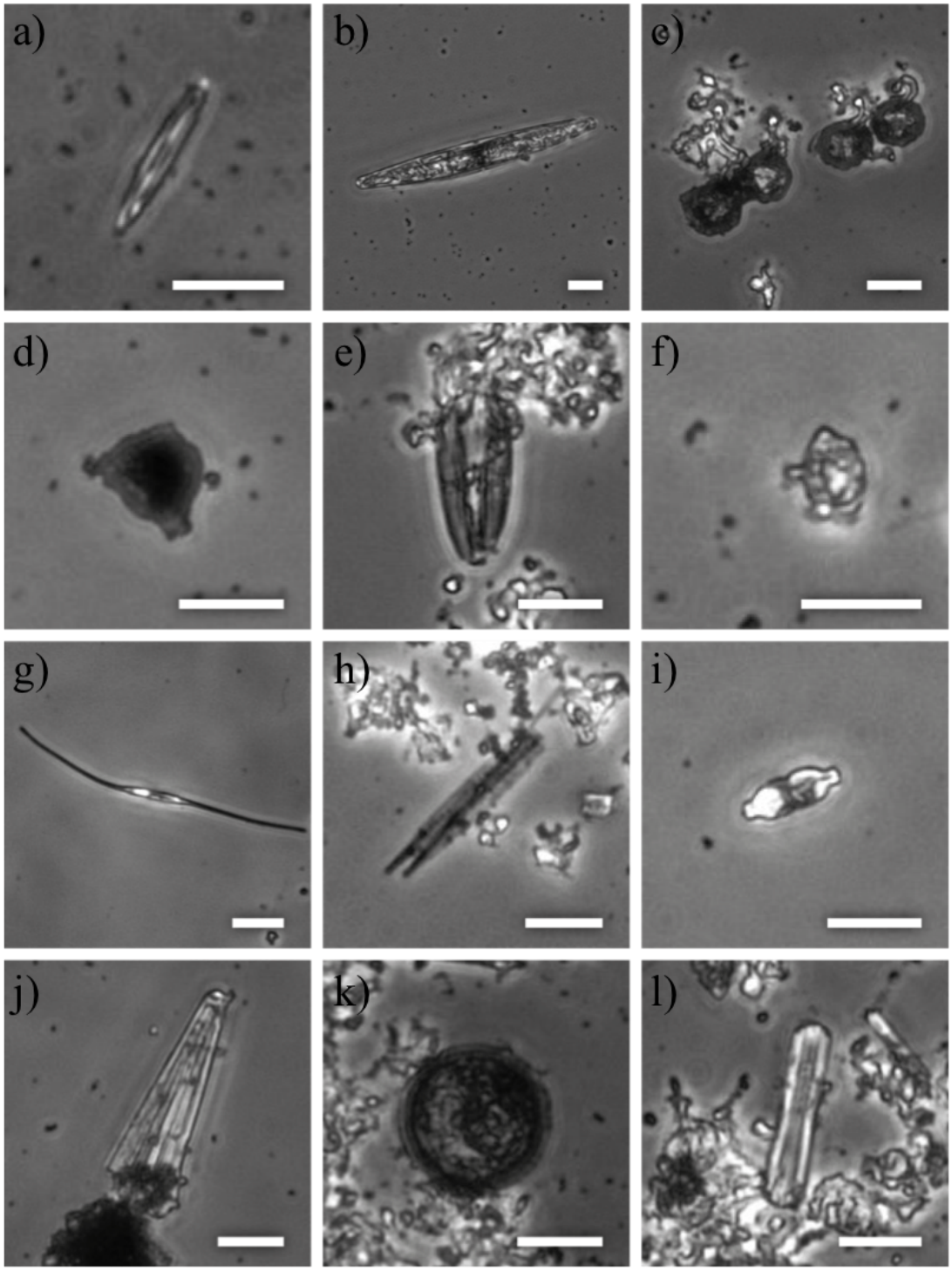

Figure 3.4: Most common observed organisms: a) *Navicula*, b) *Brachysira*, c) *Peritrich*, d) *Triceratium*, e) *Amphora*, f) *Mastogloia*, g) *Cylindrotheca*, h) *Bacillaria*, i) *Progonoi*, j) *Licmophora*, k) *Cocinodiscus*, l) *Plagiotropis*. Scale bars represent 20 µm. Pictures were acquired with a Nikon, TE2000 microscope.

Statistic analysis

Organism density was calculated as the mean number of settled organisms per cm^2 from 60 FOVs per sample ± standard error of the mean (SEM) ($n = 120$). Statistical differences between surfaces were evaluated using the two sited student's t-test with 95 % confidence limits. Two independent evaluations with varying FOV locations were performed on DDT surfaces (two conditioned (slide 1 + 2) and two unconditioned (slide 3 + 4)) in order to demonstrate that the results are reproducible. Figure 3.5 shows the obtained results for the different evaluations. It could be shown that the amount of counted organisms lies in the same range for both cases. Using student's t-test different p values were obtained, which give information about the significant differences or equalities of the samples. Comparing slide 1 and 2 provides a p value of 0.255, slide 3 and 4 a p value of 0.623. Both numbers are > 0.05, which means that these slides have no significant differences. On the other hand the p values of the comparison between conditioned and unconditioned slides lie in the range of 0.0003 to 0.0173 and are thus significantly different. This evaluation shows that the obtained results of evaluating 60 FOVs give a good summary of the slide and further analysis of the other samples was carried out the same way.

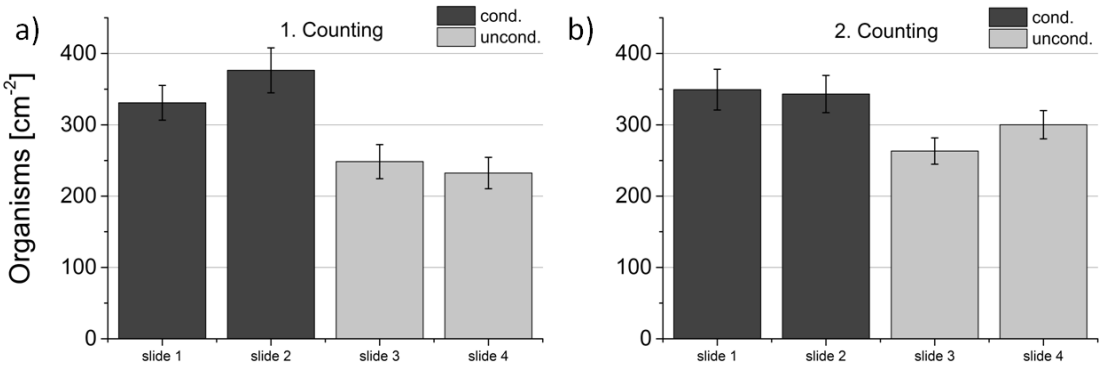

Figure 3.5: Statistic analysis of four different samples after a) the first and b) the second evaluation.

3.6 Electron beam activated lithography

Primary SAMs were formed by immersion of fresh gold substrates in a solution of AUDT in ethanol for 24 h at room temperature as described above. Electron irradiation was performed within the Karlsruhe Nano Micro Facility (KNMF) at the Karlsruhe Institute of Technology, using a VB6UHR EWF e-beam writer from Vistec Electron Beam (Jena, Germany) delivering electrons with a kinetic energy of 100 keV. The used dose was chosen at 15 000 µC/cm^2 with a beam current of 3.8 nA. After the electron beam activated lithography (EBAL) the substrates were treated following the protocol described in the next section.

3.7 Preparation of poly(*N*-isopropylacrylamide) polymer brushes

The polymerization procedure used for the preparation of polymer brushes was undertaken by modified protocols of Ahn *et al.*, He *et al.* and Schilp *et al.* [134, 141].

All chemicals, such as ethanol, methanol, dichloromethan (CH_2Cl_2), trimethylamine (NEt_3), bromo-isobutyryl bromide (BIBB), *N*-isopropylacrylamide (NIPAM) and *N,N,N',N",N"*-pentamethyldiethylenetriamine (PMDETA) were purchased from Sigma Aldrich (Munich, Germany).

Prior to use a 50 ml Schlenk flask was flame dried under vacuum (1×10^{-2} mbar) to remove moisture and oxygen, and then flushed with nitrogen after allowing it to cool down to room temperature. Under nitrogen counterflow, the fabricated patterns (see section 3.6) were added to the flask next to 5 ml dried CH_2Cl_2 and 50 µl dried NEt_3 (0.36 mM). The flask was placed in an ice bath to let the mixture cool down to 0 °C. After that, 250 µl of the surface initiator bromo-isobutyryl bromide (BIBB) (2.02 mM) were added dropwise under nitrogen counterflow. The mixture was kept for 1 h at 0 °C and then 6 h at room temperature. Finally, the substrates were rinsed with CH_2Cl_2, treated for 15 s with an ultrasonic bath, rinsed with ethanol, and then dried in a nitrogen flow. The samples were stored under argon until the next preparation step.

For the polymerization, all chemicals were added to the flask according to the nitrogen counterflow principle. First, 2.1 g of *N*-isopropylacrylamide (NIPAM) (18.36 mM) were conveyed to a 50 ml Schlenk flask I after which 4 ml of MilliQ® water and 1 ml of methanol were added. The mixture was degassed under vacuum until bubbling of the mixture ceased. The flask was then flushed with nitrogen and sealed. In a second, identical flask II, 2.5 mg CuBr were suspended in 1 ml methanol. The mixture was degassed under vacuum until it became cool, then it was flushed with nitrogen. Subsequently, 18 µl *N,N,N',N",N"*-

pentamethyldiethylenetriamine (PMDETA) (0.05 mM) were added, turning the color of the solution into pale green. After that the samples were added to flask II. The NIPAM mixture was pulled out of flask I with a syringe and then added to flask II through a syringe filter (pore size: 0.45 µm). The flask was sealed and the polymerization was allowed to continue at room temperature for 2 h. Thereafter, the samples were removed from the flask, rinsed with MQ water and methanol, and finally dried in a nitrogen flow. The sample were stored under argon.

3.8 Used analytical techniques

In this section, different methods are presented which were used in the course of this thesis to identify the quality of the prepared surfaces and to relate the determined surface properties to the fouling behavior of different organisms.

3.8.1 Spectral ellipsometry

To determine the thickness of the SAMs and the adsorbed protein layers, spectral ellipsometry measurements were performed with a M44 (JA Woollam Co., Inc.) operating in a wavelength range between 280 nm to 800 nm. As light source, a xenon lamp with a polychromatic spectrum was used. The organic film was modeled as a single Cauchy layer with fixed refractive index of 1.45 [92]. On each sample three measurements were performed at different positions and the reported value is the average of these three measurements. The error bars represent the standard error of the mean (SEM).

3.8.2 Contact angle goniometry

Sessile water drop contact angles were measured with a custom-built contact angle goniometer under ambient conditions. The reported values are the average of three measurements taken at different positions on the samples without the tip being in contact with the droplet. The error bars represent the SEM.

3.8.3 Infrared reflection absorption spectroscopy

IRRAS data for the SAMs were recorded at atmospheric pressure with a Bruker VERTEX 80 FTIR- spectrometer equipped with a liquid-nitrogen cooled narrow band MCT detector and a purge gas generator. All IRRAS data were recorded with a resolution of $2\,\mathrm{cm}^{-1}$ using the p-polarized part of the radiation at an incidence angle of 80° relative to the surface normal. SAMs of perdeuterated 1-hexadecanethiol on Au were used as reference in the IRRAS experiments.

3.8.4 X-ray photoelectron spectroscopy

XPS measurements were performed with a MAX 200 and a LHS 12 spectrometer (both Leybold-Heraeus GmbH, Germany) utilizing a non-monochromatic Mg K_α X-ray source. A concentric hemispherical electron-energy analyzer is used as detector. At the beginning of each measurement, a survey spectrum was recorded to verify the signal positions which are potentially shifted through charging of

the sample and furthermore to detect possible impurities on the surface. Subsequently, a detailed spectrum was recorded for quantification of each atomic species of interest.

For data evaluation SPECSLAB software was used to normalize the peaks of Au4$f_{7/2}$ signal to 84.00 eV. XPSPEAK software was used to determine signal intensity using the Shirley background subtraction method [190]. Because the position of the photoelectron peaks will shift by several eV when the tested surface is electrically isolated, the binding energy scale of the spectrum has to be calibrated by the position of a standard peak. Here the Au4$f_{7/2}$ peak serves as the standard and is set to 84 eV. The layer thicknesses are calculated according to Lambert Beer's law (equation 2.10) using the attenuated integral signal intensities (Table 3.4).

Table 3.4: Orbital cross section σ and inelastic mean free path of the photoelectrons λ [191, 192].

Orbitals	**O1s**	**N1s**	**C1s**	**F1s**	**Au4$f_{7/2}$**
σ	2.85	1.77	1.00	4.26	9.79
λ(Å)	15.9	18.7	21.4	12.3	26.1

3.8.5 Atomic force microscopy

AFM measurements were performed on a glass slide placed on the scanner of a MFP-3D BioAFM (Asylum, Mannheim) having a commercial Si_3N_4 cantilever of a normal spring constant of 0.6 N m^{-1} (μmash) in air. The microscope was operating in tapping-mode, where the tip was scanned back and forth at 90° along the horizontal line in a scan range of 20 µm. The AFM was used in a closed loop on all three axes. Topographic images were evaluated with the corresponding software IGOR.

3.8.6 Scanning electron microscopy

SEM images shown in this thesis were obtained with a LEO 1530 microscope from Zeiss (Oberkochen, Germany). Electron energies between 1 keV to 3 keV and the SE2 detector were used.

4 Results and discussion

Understanding to which extent surface chemistry and morphology influence the biofouling process will help in understanding how surface properties should be tuned to design antifouling or foul release coatings. In the first part of this thesis, the influence of the surface chemistry and the effect of a present conditioning film is evaluated. Laboratory experiments were done with the green alga *Ulva linza*. Additionally, in the second part, field tests at the east coast of Florida were performed and analyzed to also investigate the formation of a conditioning film in the 'real world' and its influence on the performance of model coatings. These field test are normally done over an extended time-period, however to quickly gain information, laboratory experiments with more mature biofilms are required. Therefore bacterial biofilms are most suitable and in the third part of this section artificial assays with the bacterium *Pseudomonas aeruginosa* were carried out. The influence of different culture media was examined towards the formation of a conditioning film and its influence on the settlement process. Since it is known that not only surface chemistry but also the topography plays a role in the adhesion process of organisms, the last part of this thesis deals with the influence of surface morphology on the settlement of the green alga *Ulva linza*.

4.1 Influence of surface conditioning on settlement behavior of *Ulva linza*

As described in section 2.3, it is well known that as soon as a surface is immersed into seawater, organic macromolecules from the surrounding water rapidly accumulate [44, 45]. This film is called conditioning film and it mainly consists of a mixture of glycoproteins, humic acids [49], proteins [43, 47], lipids, nucleic acids, polysaccharides, aromatic amino acids [44] and unspecified macromolecules [50]. For a detailed understanding of cell/larval settlement, adhesion and colonization, it is desirable to know the formation kinetics and chemical composition of the conditioning layer. As the natural environment is a complex community, laboratory assays are performed to study and interpret the influence of different surface properties on the settlement behavior of the most common fouling organisms.

In this part of the thesis, which was done in collaboration with the group of Prof. James Callow (University of Birmingham, UK), the influence of surface

conditioning on the settlement of *Ulva* zoospores is examined across a wide range of settlement times. Spores of this species have been extensively used in comparative assays of the antifouling performance of experimental coatings [3]. A suspension of spores is also supposed to contain molecules that may adsorb to test surfaces and therefore may subsequently influence the settlement of spores. These molecules originate from secretions by the spores themselves, but there will also be some residual molecules from the parent plants from which the spores were released. In the present work, 'spore water' (SP) composed of seawater in which spores released from plants had been swimming for 60 min, was used to precondition the substrates. Since a standard spore settlement assay is typically 45 min to 60 min long, SP contains the maximum amount of macromolecules available to condition a surface during the course of an assay. Conditioning by two types of commercial artificial seawater as well as self-prepared seawater was also evaluated. Spectral ellipsometry (SE), contact angle goniometry (CA), infrared reflection absorption spectroscopy (IRRAS) and x-ray photoelectron spectroscopy (XPS) were used to reveal the formation and chemical nature of the used surfaces and the conditioning layers. Another point to investigate was what influence the formed conditioning layer has to the subsequent settlement process of spores.

4.1.1 Preparation of conditioning films

Five chemically different surfaces were prepared and analyzed according to the protocol described in section 3.1 and 3.2, which varied in terms of protein resistance and wettability (Table 4.1).

First the deposition from different types of artificial seawater and seawater conditioned by spores (SP) was investigated on DDT surfaces. Two commercial sources of artificial seawater were used, Tropic Marin® (TM) and Instant Ocean® (IO), together with a non-commercial seawater equivalent ('salt water' (SW)), prepared

Table 4.1: Thiol molecules used to form self-assembled monolayers, static water contact angle (error: ± 4°) and thickness as determined by spectral ellipsometry (error: ± 2 Å).

Chemistry	**label**	**water CA** [°]	**thickness** [nm]
$SH-(CH_2)_2-(O-(CH_2)_2)_{44}-OH$	PEG	27	3.4
$SH-(CH_2)_{11}-OH$	HUDT	33	1.2
$SH-(CH_2)_{11}-NH_2$	AUDT	60	1.9
$SH-(CH_2)_{11}-CH_3$	DDT	104	1.1
$SH-(CH_2)_{11}-O-(CF_2)_5-CF_3$	FUDT	112	1.4

by mixing the main mineral salts present in natural seawater [187]. In order to compare the different seawaters, DDT SAMs were used as a non-protein resistant model surface with hydrophobic properties. The conditioning film was characterized after various incubation times by spectral ellipsometry.

It was found that the formation of a conditioning layer is most prominent for SP (Figure 4.1). The thickness of the formed protein layer is determined to be ~ 25 Å . This measurement is consistent with the values found in literature when proteins are deposited from different buffered protein solutions, e.g. ribonuclease A (RNase A), pyruvate kinase, fibrinogen and lysozyme [21, 92, 188]. Spectral ellipsometry showed that the formation of the conditioning film is insignificant (in terms of thickness) before 8 h. However, at longer timescales (48 h) a weak, but noticeable conditioning of the surfaces can be recognized for IO. As expected, SW, consisting only of mineral salts, showed no accumulation.

While hydrophobic surfaces, such as the DDT SAM, are known to readily adsorb a conditioning film [21, 92, 188], the question arose, to what extent spore conditioned water is able to condition other surface chemistries. The data collected in a second experiment are plotted in Figure 4.2 and show that a conditioning film is formed on all surfaces, except PEG which featured a decrease in film thickness. With the exception of PEG, the rate of film growth only changes slightly with the surface chemistry. Irrespective of whether surfaces are hydrophilic or hydrophobic, all seem to be conditioned rapidly by biomacromolecules. For PEG, the thickness values are negative, which could point towards a degradation of the surface over time. The time scale of the increase of thickness broadly matches the changes in the contact angle after conditioning (Figure 4.2b). The contact

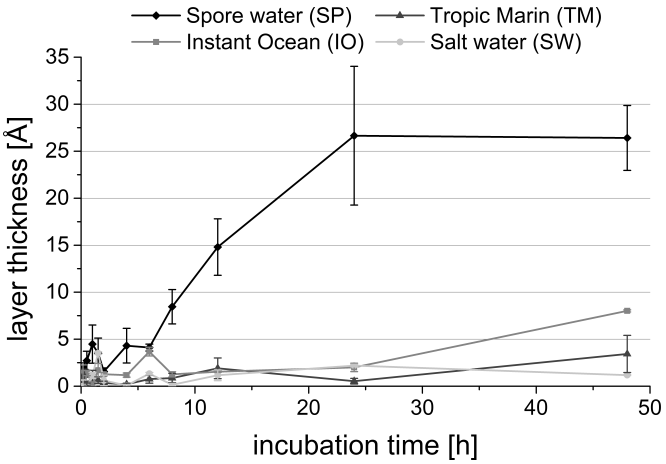

Figure 4.1: Thickness of the formed conditioning layer as a function of time exposed to 'spore water', Tropic Marin®, Instant Ocean® and salt water on a dodecanethiol (DDT) surface. Error bars are the standard error of the mean (SEM) (n = 3).

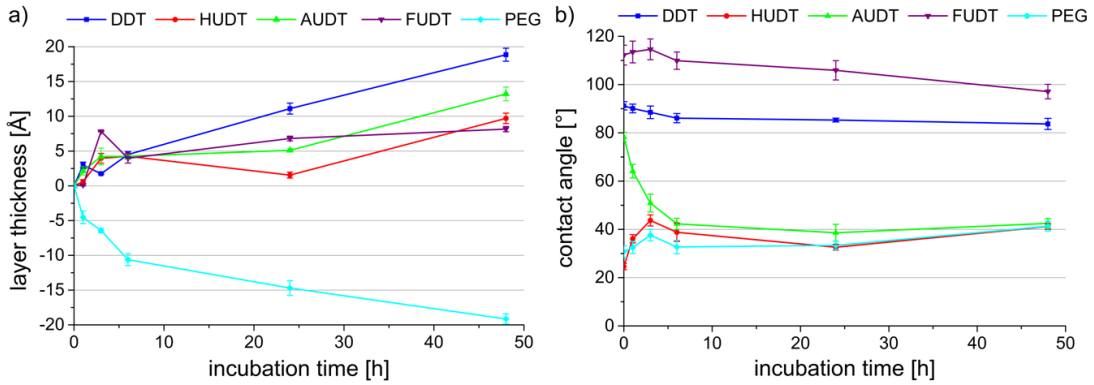

Figure 4.2: Conditioning of self-assembled monolayers with different chemical termination by 'spore water' (SP). Thickness of the conditioning layer (a) and contact angle (b) of the conditioned surfaces. Error bars are the standard error of the mean (SEM) (n = 3).

angle changes for all surfaces on a similar time scale of about 5 h to 10 h. Interestingly, the hydrophobic surfaces become more hydrophilic, while the hydrophilic HUDT surface becomes more hydrophobic. These data are in agreement with results reported by Pratt-Terpstra *et al.* [193]. They showed that the contact angle of surfaces with different hydrophobicities changed after being conditioned by bovine serum albumin (BSA). For a hydrophilic surface the contact angle increased from 26° to 59° and for a fluorinated hydrophobic surface, it decreased from 107° to 97° after conditioning with BSA.

In order to obtain more detailed information about the chemistry of the conditioning layers, infrared reflection absorption spectroscopy (IRRAS) was applied (Figure 4.3). In the range of 3000 cm^{-1} the symmetric and antisymmetric CH_2 vibrations of the methylene backbone of the aliphatic SAMs can be seen in all spectra [27]. While the intensities of the methylene vibrations increase just slightly for the different incubation times, the carbonyl (1745 cm^{-1}, C=O stretching vibration), amide I (1650 cm^{-1}, most likely C=O stretching vibrations of the peptide bond) and amide II (1540 cm^{-1}, N−H bending and C−N stretching vibrations) peaks [156, 180] increase during formation of the conditioning layer. This suggests that the conditioning layer contains macromolecules with amide groups, most likely proteins/glycoproteins. Figure 4.4 shows the carbonyl and amide bands in greater detail after incubation for 48 h in SP for all four surfaces. It can be seen that the peak shapes and relative intensities of the carbonyl, amide I and amide II peaks show slight differences. Especially on AUDT and HUDT the carbonyl and amide bands are very pronounced, indicating large amounts of protein or proteinaceous components on the hydrophilic surfaces. The two hydrophobic surfaces, DDT and FUDT, show completely different spectra, and in both cases the carbonyl and amide bands are comparably weak. As ellipsometric thicknesses

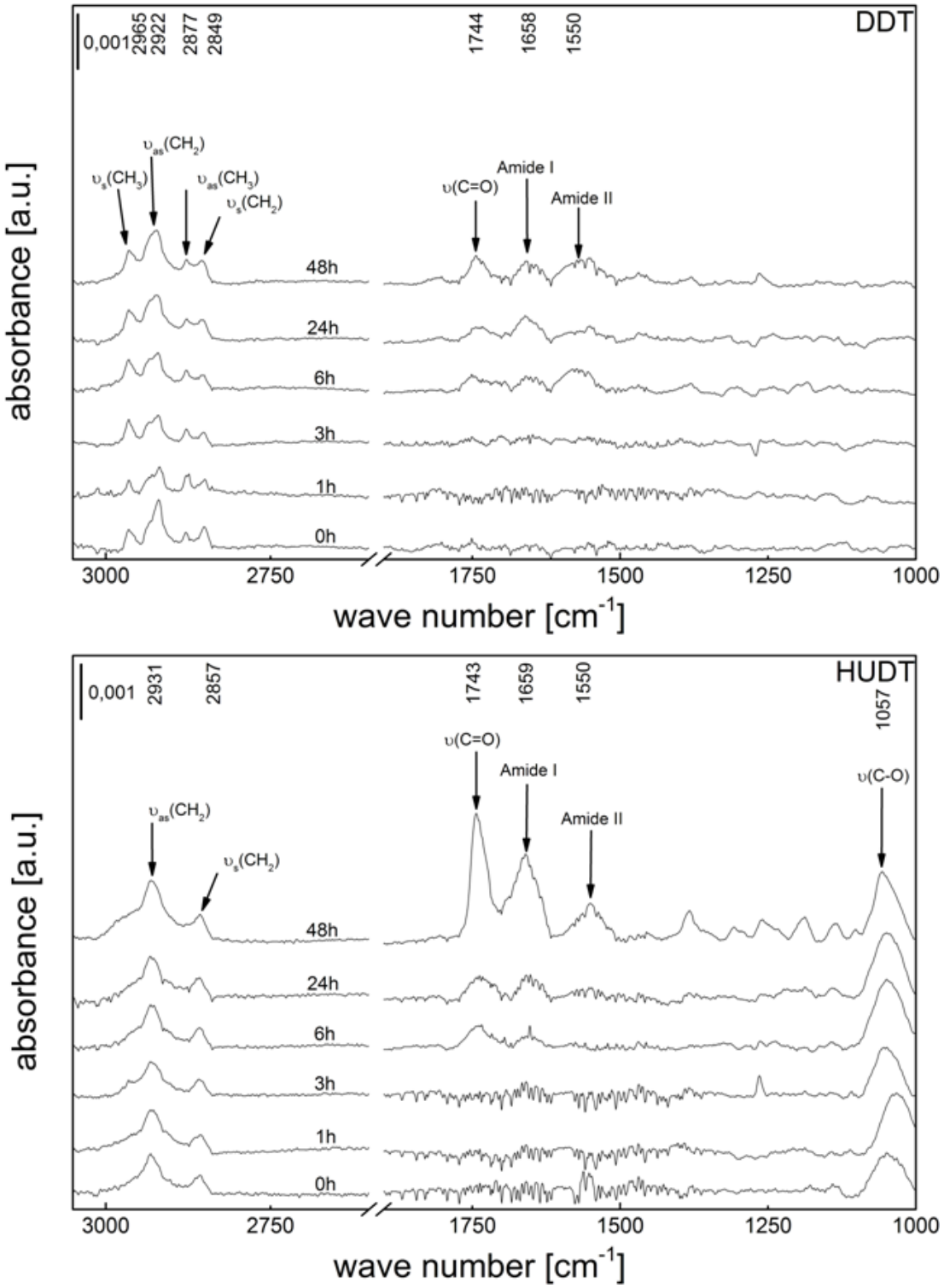
DDT
0,001
2965
2922
2877
2849
1744
1658
1550
$\upsilon_{as}(CH_2)$
$\upsilon_s(CH_3)$
$\upsilon_{as}(CH_3)$
$\upsilon_s(CH_2)$
υ(C=O)
Amide I
Amide II
48h
24h
6h
3h
1h
0h
absorbance [a.u.]
3000
2750
1750
1500
1250
1000
wave number [cm^{-1}]
HUDT
0,001
2931
2857
1743
1659
1550
1057
υ(C=O)
Amide I
Amide II
υ(C-O)
$\upsilon_{as}(CH_2)$
$\upsilon_s(CH_2)$
48h
24h
6h
3h
1h
0h
absorbance [a.u.]
3000
2750
1750
1500
1250
1000
wave number [cm^{-1}]

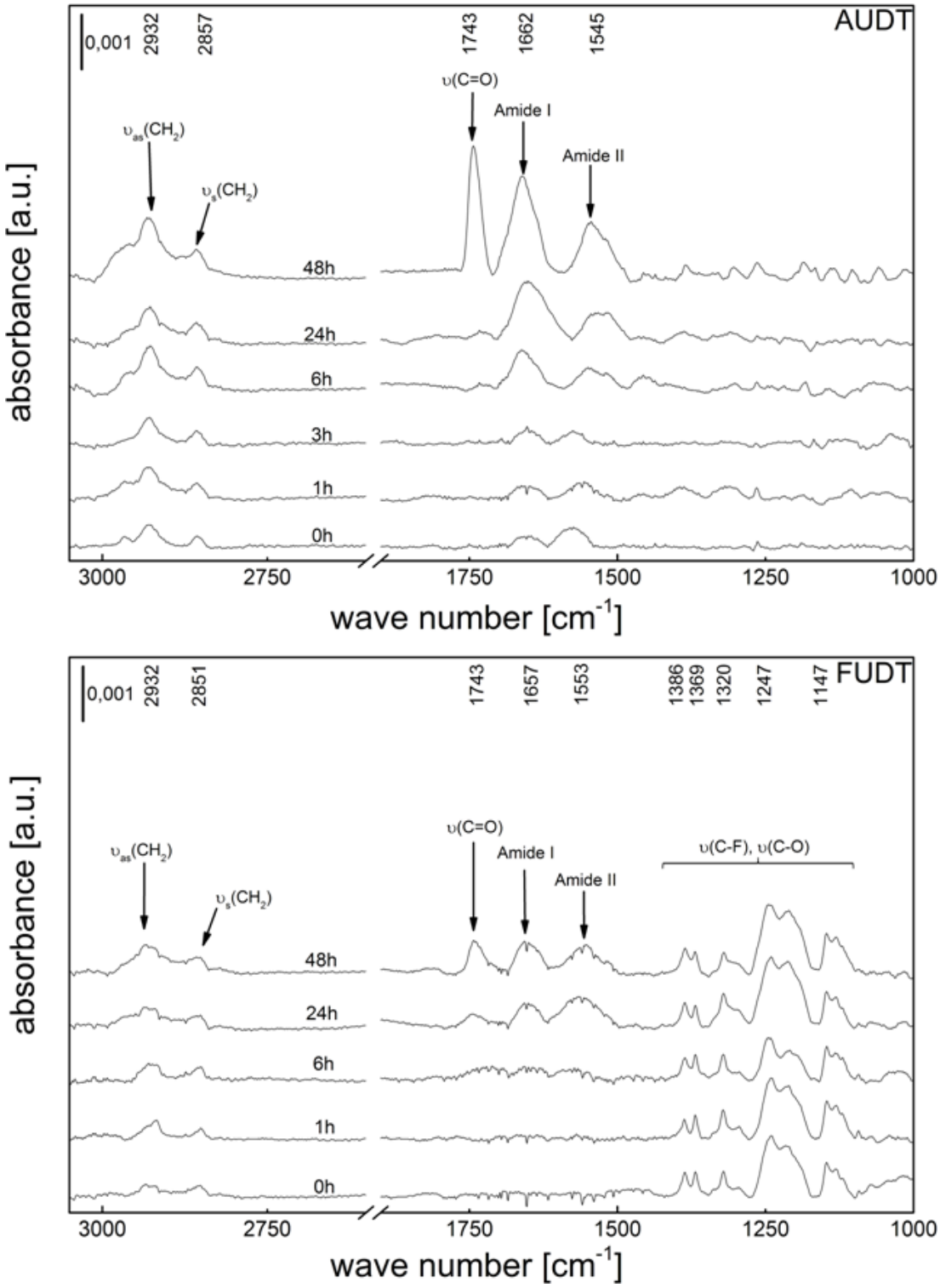

Figure 4.3: IR spectra of the different surfaces after several hours of incubation up to 48 h in SP. Depending on the surface chemistries the carbonyl (1745 cm^{-1}), amide I (1650 cm^{-1}) and amide II (1540 cm^{-1}) peaks grow by a factor of 5 for the hydrophobic and $\sim$ 10 for the hydrophilic surfaces during an incubation time of 48 h.

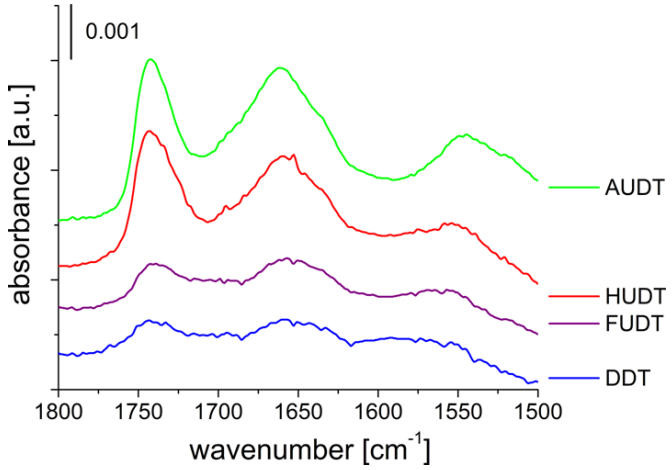

Figure 4.4: Carbonyl (1745 cm^{-1}), amide I (1650 cm^{-1}) and amide II (1540 cm^{-1}) intensity on all different surfaces after 48 h conditioned by 'spore water'.

are in a similar range for all four surfaces (DDT slightly higher), it may be concluded that the conditioning layers on hydrophobic surfaces have lower amounts of proteinaceous components compared to the hydrophilic surfaces. These absolute thicknesses are very similar to literature values of surfaces conditioned with natural seawater [51, 194].

If the development of the intensities of the alkyl, carbonyl and amide peaks is plotted against time it can be seen that while the development of the alkyl bands is weak but noticeable, the carbonyl and amide intensity increases rapidly (Figure 4.5). It should be remarked that the increase of the alkyl intensity is the same for all surface wettabilities indicating that the amount of alkyl containing compounds is the same. For the carbonyl and amide bands it seems to be different.

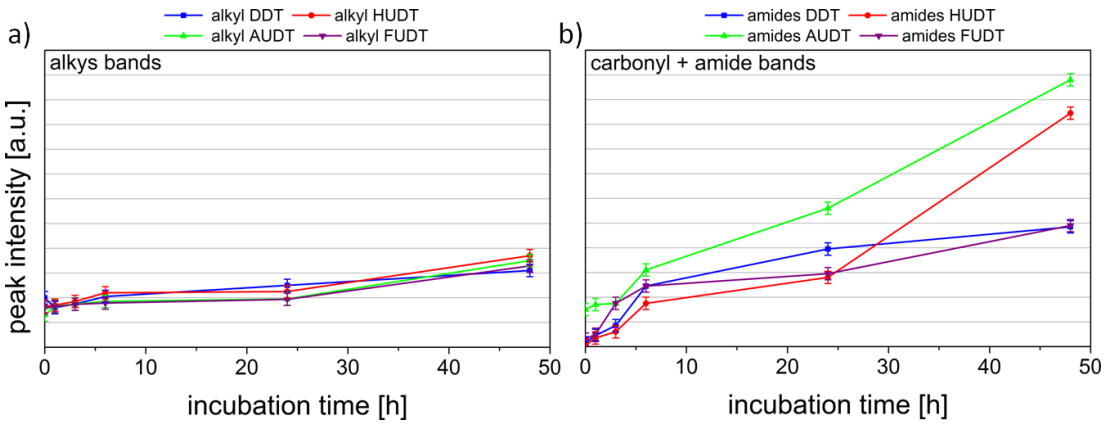

Figure 4.5: Intensity of the carbonyl, amide I and amide II bands on all chemically different surfaces plotted against incubation time in 'spore water'. Error bars are the reading error.

On the hydrophobic samples the growth is less intense then on the hydrophilic ones. Taking into account that the AUDT intensity starts at a higher level because of the present amino group, the hydrophobic surfaces end at a similar level as the hydrophilic ones do. This provides support for the statement that hydrophilic surfaces attract more proteinaceous components.

Figure 4.6 shows the IR and XPS spectra of the PEG surface. It can be noted that the molecule deteriorates in water over time. The IR peaks (Figure 4.6a) in the range of 1122 cm^{-1} to 1343 cm^{-1}, typical bands of the C−O−C stretching, CH_2 twisting and CH_2 wagging modes of the ethylene glycol units, respectively [182–184, 195], decrease with increasing incubation time in SP. The symmetric and asymmetric CH_2 stretching bands at 2888 cm^{-1} are also reduced. The XP spectra show the same trend. The C1s and O1s peaks lose their intensity over time (Figure 4.6b). As this does not happen for all other SAMs and is in agreement with spectral ellipsometry, it indicates that only the ethylene glycol coating deteriorates over time. As no amide peaks are visible either in the IR nor in the XP spectra, it can be concluded that the film does not appear to be completely degraded, and up to 48 h a certain resistance to conditioning is retained. The results in section 4.2.1 show that by enlarging the incubation time of the PEG surface to 1 week it was revealed that the PEG film completely disappears and only the peaks resulting from the conditioning film are detectable on the surface.

4.1.2 Time dependence of *Ulva* spore settlement

After the detailed investigation of the formation and chemistry of the conditioning films, the question arose as to how settlement of spores of *Ulva linza* is influenced by the conditioning layers. To compare the results of conditioning from SP on the test surfaces with the settlement of zoospores, spore settlement on the pristine surfaces up to $\sim$ 36 h was investigated. Figure 4.7a gives an expanded view of the first 2 h of settlement. The general trend for settlement is consistent with previous findings by Callow *et al.* [41] and Cooper *et al.* [196], but the rates of zoospore settlement are different for the five different surfaces. The grey area in Figure 4.7a represents the time used for standard settlement assays with spores [59]. Figure 4.7b shows settlement over 36 h. While the number of settled spores increases for about 5 h to 10 h, the settlement on the different surfaces (except for PEG) saturated at approximately the same value after $\sim$ 20 h, independent of the surface chemistry. However, at these longer incubation times the values for spore settlement must be considered with caution since by 22 h many spores had started to germinate and some spores had settled on top of previously settled spores. These effects reduce the accuracy of the image analysis macro in discriminating individual spores and this probably explains the apparent decline in spore density between 24 h to 36 h.

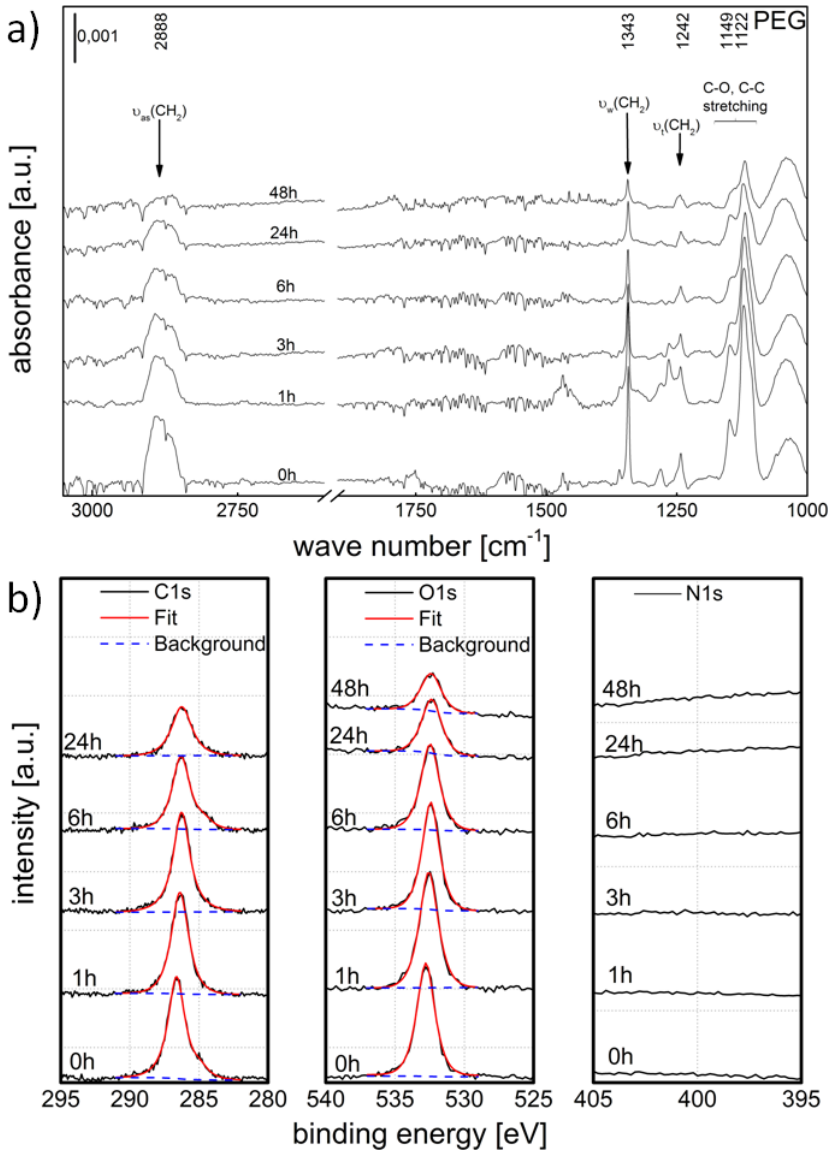

Figure 4.6: a) IR and b) XP spectra of the PEG surfaces after varying incubation times up to 48 h in SP. In both spectra it can be noted that the typical bands from the PEG molecules decrease over incubation time. However, no carbonyl (1745 cm^{-1}), amide I (1650 cm^{-1}) and amide II (1540 cm^{-1}) bands appear in the IR and also in the XPS no nitrogen can be found.

For PEG, the settlement of spores started after about 8 h, i.e. when the surface deterioration had advanced to the point where the surfaces were no longer inhibitory to settlement. With these exceptions, the kinetics of spore settlement occurred on a similar timescale as surface conditioning. These data rationalize the standard practice of using only 45 min to 60 min in the settlement bioassay for spores of *Ulva linza* when the intention is to compare the settlement rates on different types of antifouling coatings.

The observed saturation of spore settlement leads to the question whether this saturation is due to a full coverage of the surface or due to a depletion of the spore suspension. Table 4.2 shows the quantification of spores on the different surfaces after a long settlement time (36 h). For the coverage calculation, the projected area of a single spore was calculated to be approximately 1.96×10^{-5} mm^2 assuming the diameter of a hydrated spore to be 5 µm. However, it should be noted that this figure does not include the halo of adhesive that is secreted on settlement. The secreted adhesive spreads more on hydrophilic surfaces giving a mean diameter of the cell plus adhesive of about 8 µm for a CH_3- terminated SAM and 15 µm for a hydrophilic OH- terminated SAM [22]. For a settlement assay, 10 mL spore solution are used with 1.00×10^6 spores ml^{-1}. Assuming that all spores settled on the test surfaces, they could cover an area of 196 mm^2 (based on a diameter of 5 µm). Comparing this number to the area of the surface (1875 mm^2), which is available for settlement, (dimensions of the slides are 75 mm×25 mm) shows that the supply of spores could cover at most 10.4 % of the surface. Saturation in the kinetic curves is observed at about 5×10^6 spores, which means that only about 30 % to 50 % of the total spore population settled and the coverage of the surface was between 3.1 % and 6.1 %. Thus, in this case,

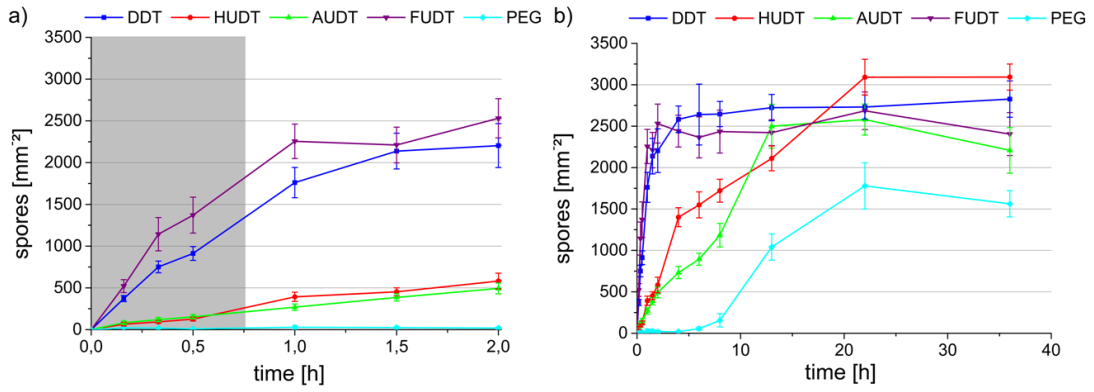

Figure 4.7: Kinetics of settlement of zoospores of *Ulva linza* on chemically different surfaces over a total duration of 36 h. a) Initial time up to 2 h, the area in grey represents the usual time for a spore assay. b) Settlement of spores up to a total settlement time of 36 h. Each point is from 30 counts on one slide, error bars show 2× SE.

Table 4.2: Number of settled spores, the percentage of settled spores and surface coverage after 36 h.

Chemistry	**number of adhered spores on whole surface area after** 36 h	**Coverage**
PEG	$2.98 \pm 0.29 \times 10^6$ spores	$3.1 \pm 0.3\,\%$
HUDT	$5.79 \pm 0.29 \times 10^6$ spores	$6.1 \pm 0.3\,\%$
AUDT	$4.14 \pm 0.52 \times 10^6$ spores	$4.3 \pm 0.5\,\%$
DDT	$5.30 \pm 0.41 \times 10^6$ spores	$5.5 \pm 0.4\,\%$
FUDT	$4.51 \pm 0.48 \times 10^6$ spores	$4.7 \pm 0.5\,\%$
Theoretical maximum coverage if all spores settled	1×10^7 spores	10.4 %

the full coverage of the surface, as observed in typical Langmuir kinetics [197], is not observed. A possible explanation for the decrease in the settlement rate may lie in the reduced amount of unattached spores in solution which can potentially settle on the surface [41].

Performing a kinetic analysis of spore settlement on glass surfaces by Callow *et al.* [41] a reduced competence of the zoospore population to settle with time was suggested, i.e. within a population of 'wild' spores there is a range of propensity for settlement so that over time the population of spores in the assay becomes biased towards those with a reduced propensity to settle. Indeed, it was observed that even after 48 h a few spores were still swimming in the assay dishes. The analytical data shown earlier suggests that surface conditioning might influence settlement over long settlement times.

Another effect, which is an unavoidable artifact of the assay design, may also be operating. Settlement assays are conducted on coated glass slides immersed in the spore suspension in individual compartments of polystyrene 'quadriperm' dishes. The slide (75 mm×25 mm) only partially covers the polystyrene surface (80 mm×28 mm) so spores are able to settle on the uncovered base of the dish and the sidewalls. Since polystyrene is attractive for spore settlement, during long assay periods the spore suspension becomes progressively depleted with spores, especially as they are attracted to settle in the angle between the bottom and side walls of the dish. Callow *et al.* [41] used Scatchard analysis to demonstrate that at high levels of spore settlement negative cooperative effects may be detected, i.e. the settlement of spores is inhibited by previously settled spores in a concentration-dependent manner. The basis for negative cooperativity may lie in the secretion of chemical anti-settlement cues as an adaptive mechanism to limit competition for resources between settled spores.

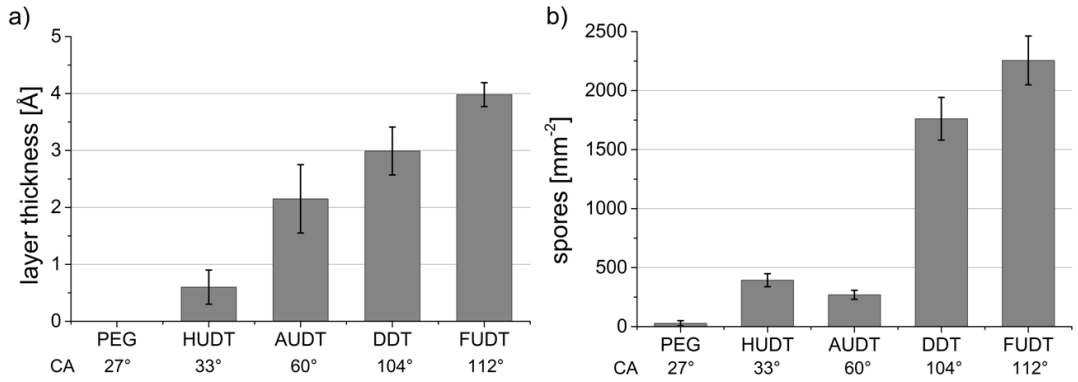

Figure 4.8: a) Layer thickness after one hour incubation of different SAMs in 'spore water' b) Spore density after one hour incubation of the five different self-assembled monolayers in spore suspension. Error bars represent a) the SEM of the mean value of three measurements on one sample and b) the SD of the mean value of 30 counts on one slide.

An alternative explanation is a possible impact the conditioning of surfaces has to the outcome of kinetic experiments. Since it is known that the formation of such a film starts immediately after immersion and after about 24 h it is fully established, proteinaceous compounds can be expected to alter the settlement density of spores. But this point has to be evaluated in detail, which will be accomplished in the following section 4.1.3.

Figure 4.8 compares the thickness of the conditioning layers and the number of spores on the differently terminated surfaces after 1 h, a time point at which the accumulation rate is high and thus allows a comparison of the accumulation of the conditioning film as well as the settlement density on the different SAMs. The thickness of the conditioning film (Figure 4.8a) greatly increases with increasing water contact angle, which is consistent with the published literature [48]. Figure 4.8b shows the spore density on pristine surfaces after a 1 h assay, i.e. without preincubation. It shows that the rate of spore settlement also broadly scales with the wettability of the surfaces, which is in line with previous findings [21, 83, 198].

4.1.3 Influence of surface conditioning to *Ulva* settlement

The fact that conditioning and colonization by spores occurs on a similar timescale and that both vary on the surface chemistry raises the question to what extent the increased conditioning of the surface changes the density of spores that settle. Therefore the density of settled spores in a 45 min assay was investigated as a function of different lengths of surface pre-conditioning. DDT was used as a hydrophobic, non-protein-resistant test surface. This surface was pre-immersed in SP or filtered TM (0.22 mm) for different durations (30 min, 60 min, 13 h or

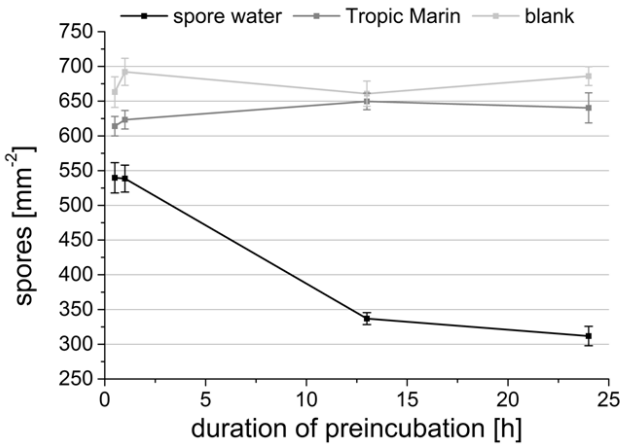

Figure 4.9: Settlement density of spores on DDT SAMs after varying durations of pre-incubation in either 'spore water' (SP) and Tropic Marin (TM). Separate blanks were also included in the assay at each of the time points. Error bars are 2× standard error of the mean (SEM) (n = 90).

24 h). After the different lengths of conditioning, a conventional 45 min spore settlement assay was carried out on all surfaces simultaneously in order to investigate if the pre-immersion caused any differences in the density of settled spores. Pristine samples as well as samples pre-incubated in seawater (TM) were included as controls. The results (Figure 4.9) show that preincubation with TM reduces the settlement of zoospores by $\sim$ 10 % at short time intervals (30 min, 60 min), compared with the pristine, non-preconditioned control. This effect is reduced at longer time periods. Pre-incubation in SP for $<$ 60 min causes a small ($\sim$ 11 %) reduction in spore settlement density compared with TM, and approximately a 17 % reduction compared with pristine controls. Interestingly, even after 1 h, although the conditioning film is not fully developed at this stage and is still very thin ($<$ 1 nm), changes in the settlement density can be observed. The contact angles also change on a similar timescale. Preincubation in SP for $>$ 1 h causes a more substantial decrease in the number of settled zoospores ($\sim$ 50 % compared with the controls).

Epifluorescence micrographs (Figure 4.10) reveal that on pristine samples and at short incubation times, spores settled in small groups on the surface. This pattern is typically observed on hydrophobic surfaces. After preconditioning in SP for 13 h and 24 h, a clear trend can be observed towards fewer spores settling, mainly as individuals on the surface.

IRRAS revealed that conditioning layers on the different surface chemistries show slight differences in their chemical nature (Figure 4.3 and Figure 4.4). Also, the water contact angles of the initial surface chemistry change and converge towards more similar values for the different surfaces. Thus, the question arose whether

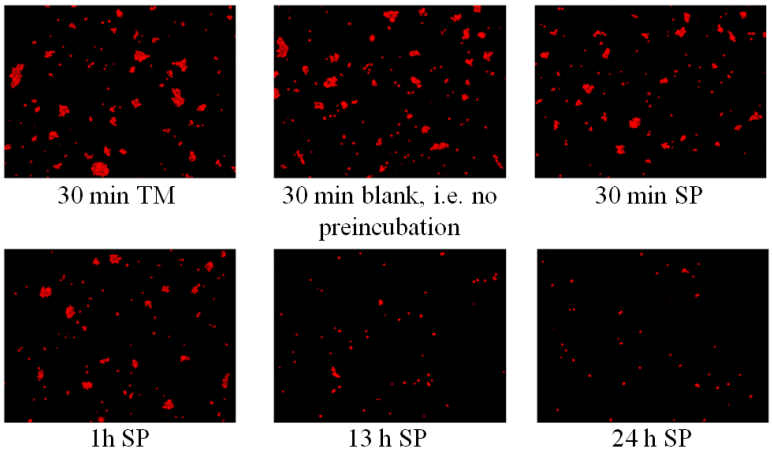

Figure 4.10: Epifluorescence micrographs of settled *Ulva* spores on DDT SAMs after varying durations of preincubation. TM and blank samples at the different time points are visually similar to the 30 min samples (top row). Image width is 450 µm.

the conditioning layers formed on different surfaces affected spore settlement in a different way. Figure 4.11 shows the change in spore density on the different surface chemistries after preincubation in SP for 16 h. For both hydrophobic surfaces (DDT and FUDT), incubation in SP led to a decrease in spore settlement density compared to the controls. For the hydrophilic HUDT surface, the pristine surface is populated with only ~ 100 spores mm^{-2} and settlement density increases with increasing length of preincubation. Figure 4.11 also shows that spore settlement density nearly reaches the same value after conditioning for both the different

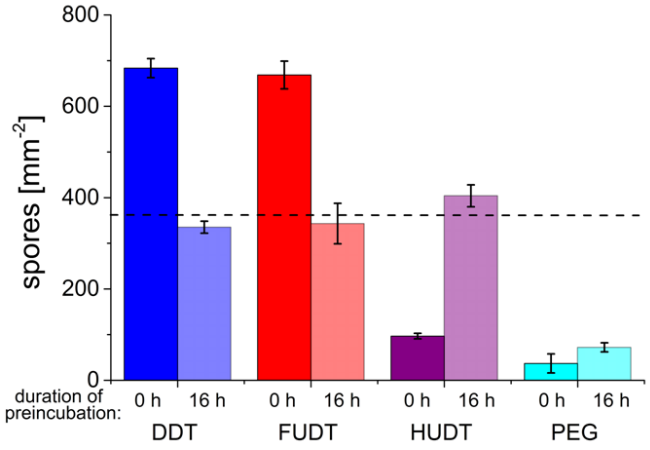

Figure 4.11: Settlement density of *Ulva* spores on SAMs without and with preincubation in 'spore water' for 16 h. Error bars are the standard error of the mean (SEM) (n = 90).

hydrophobic and hydrophilic surface chemistries. PEG is an exception, where the spore density stays almost as low as it is without preincubation.

4.1.4 Conclusion

Standard spore settlement assays are extensively used in the laboratory to explore the influence of physico-chemical surface properties on settlement, and to evaluate potential antifouling coatings. The linear kinetics at typical settlement periods of 45 min are suitable for comparing spore settlement rates and thus the 'attractiveness' of different surfaces. The assay time of 45 min furthermore minimizes complications due to saturation and conditioning. In this part of the thesis, the influence of such a conditioning film on the spore settlement process was investigated using 'spore water' (SP) (commercial seawater in which spores were allowed to swim for 1 h before being filtered out). A protein film was formed on different surfaces independent of the surface chemistry and analyzed using multiple surface analytical techniques like ellipsometry, contact angle goniometry, IR and XP spectroscopy. The time dependence of the film formation and the appearance of carbonyl, amide I and amide II bands could be observed. Furthermore it was shown that the PEG surfaces deteriorate with advancing incubation time. An interesting point to be noted is that although the surfaces deteriorate, some PEG molecules are left on the surface which keep it protein resistant.

After the investigation of the formation of the conditioning films and their chemistry, the influence of the formed conditioning layers on the settlement of *Ulva* spores was analysed. To compare the results of conditioning from SP on the test surfaces with the settlement of zoospores, spore settlement on the pristine surfaces up to 36 h was investigated. It was found that settlement on the different surfaces (except for PEG) saturated after about 20 h —independent of the surface chemistry. Comparing the thickness of the conditioning layers and the number of settled spores on the chemically different surfaces after 1 h showed that both processes occurred over a similar timescale.

The next question to be answered was to what extent the increased conditioning of the surface changes the density of spores that settle. The obtained data show that the settlement density of spores on the test surfaces preincubated in SP was one the one hand reduced for the hydrophobic surfaces but on the other hand increased for the hydrophilic ones, for preincubation times in the range of 24 h to 48 h. The maximum effect on the spore settlement of preconditioned test surfaces with SP for 30 min to 60 min followed by a 45 min settlement period was up to 17 %. However, this is a worst-case estimate of the potential effect since in a standard bioassay, test surfaces are not preconditioned, i.e. both spores and conditioning molecules are presented to the test surface at the same time. While for a standard spore assay of 45 min the effect of conditioning is likely to be

rather slight, this work also suggests that care must be taken for any laboratory study on longer time scales as surface conditioning can contribute to the outcome of the assay. Furthermore, it should be noted that filter-sterilized commercial ASW contains macromolecules that will condition the surface if assays are of long duration. Surface conditioning can be reduced by the use of self-made ASW.

4.2 Surface Conditioning and its implication for fouling in the field

As described in the previous section, laboratory assays with single organisms are widely used for a rapid screening of different antifouling coatings. However, to test the real performance of these coatings in a natural environment with mixed species, not only laboratory but also field tests are necessary.

In literature many studies of coatings immersed into the ocean for two or more months are published [61–63], but just few things are known about the composition of the early fouling communities on well defined model surfaces like SAMs. The conditioning of a surface, the adsorption of proteins and other macromolecules is one of the fastest steps in the fouling process. The main question in this part of the thesis was to investigate the time dependent conditioning of chemically different surfaces in natural seawater. Seasonal changes could affect the salinity, pH or temperature and with this also the dissolved organic carbon (DOC) concentration in the water. Since it is known that these seasonal changes could have an impact on the formation of conditioning films [199], it was also investigated whether there is a difference between the conditioning layers related to different times of the year. Until now the chemical nature of the adsorbed layer is still poorly characterized [43]. For a scientific understanding of the whole biofouling process in the field, it is certainly necessary to gain more information on the formation kinetics and chemical composition of conditioning layers, as well as their influence on the settlement and adhesion of microorganisms.

In the present study, which was done in collaboration with the group of Prof. Geoffrey Swain (Florida Institute of Technology, Melbourne, Florida, USA), natural seawater was collected from two static immersion test sites at two different times of the year (summer (June) and winter (December)). The two test sites were chosen since population and seasonal variations of organisms have extensively been studied over the last decades [61–63, 200]. The water was filtered and used to precondition chemically different substrates. Spectral ellipsometry (SE), water contact angle goniometry (CA) and infrared reflection adsorption spectroscopy (IRRAS) were used to investigate the formation and chemical nature of the conditioning layers. In the second part of this study, the extend to which surface conditioning affects the early fouling process was investigated. Therefore preconditioned as well as non-incubated samples were immersed during summer at one of the static immersion test sites (raft test site) for 24 h to be sure to have a full 'activity' circle of the organisms. The most dominant organisms observed on the surfaces were diatoms (*Navicula*, *Amphora*, *Cylindrotheca* and *Baccillaria*) and the protozoa *Peritrich ciliate*.

4.2.1 Preparation of conditioning films

The same five surfaces, which varied in terms of protein resistance and wettability, as in the previous section (section 4.1) were prepared and analyzed according to the protocol described in section 3.1 and 3.2.

In order to compare the different seawater types used for the conditioning of the surfaces and the influence of temperature, deposition from filtered seawater from two different static immersion test sites ('raft' test site of the FIT, located at the east coast of Florida about 5 km north of the Sebastian inlet, Florida (27°59 'N; 80°28 'W), 'cape' test site, located at the east coast of Florida at the Cape Canaveral Port (28°28 'N; 80°39 'W)) was investigated on the different samples. While these surfaces are known to readily adsorb a conditioning film (see section 4.1), the question arose, to what extent natural seawater is able to condition the surfaces and what influence the time of the year has. The conditioning films were characterized after various incubation times by spectral ellipsometry and contact angle measurements.

Figure 4.12 shows the obtained results. On all surfaces, independent of the chemistry, a conditioning film is built up, except for PEG, which shows a decrease in film thickness, which is in line with previous studies (section 4.1). Interestingly, the film thickness for the hydrophobic surfaces is in the same range of 10 Å to 17 Å in June (water temperature: 29 °C) and December (water temperature: 22 °C), while for both hydrophilic surfaces the film thickness is slightly higher in December (13 Å for HUDT, 18 Å for AUDT) than in June (8 Å for HUDT, 14 Å for AUDT). This could be an indication for differences in the composition of the films. The rate of film growth only changes slightly with the surface chemistry, irrespective of whether surfaces are hydrophilic or hydrophobic and all seem to be conditioned rapidly by biomacromolecules. The thickness of the formed protein layers is found to be independent of the water temperature with the exceptions of small variations concerning the hydrophilic SAMs. The layer thickness lies in the range of 10 Å to 20 Å for all different surfaces (PEG is an exception). This measurement is consistent with the thickness values obtained by using 'spore water' to condition surfaces described in section 4.1.

With spectral ellipsometry it could also be shown that the time scale of increase in the thickness of the conditioning layer broadly matches the changes in the CA after conditioning (Figure 4.12c, d). The CA changes for all surfaces on a similar time scale of about 5 h to 10 h. Interestingly, it decreases for the hydrophobic surfaces more in June than in December, and the samples become more hydrophilic. The change for the hydrophilic ones is in the same range independent of the time of the year and thus the water temperature.

To obtain more detailed information about the chemistry of the conditioning layers and the influence, the surface chemistry has on the composition of the

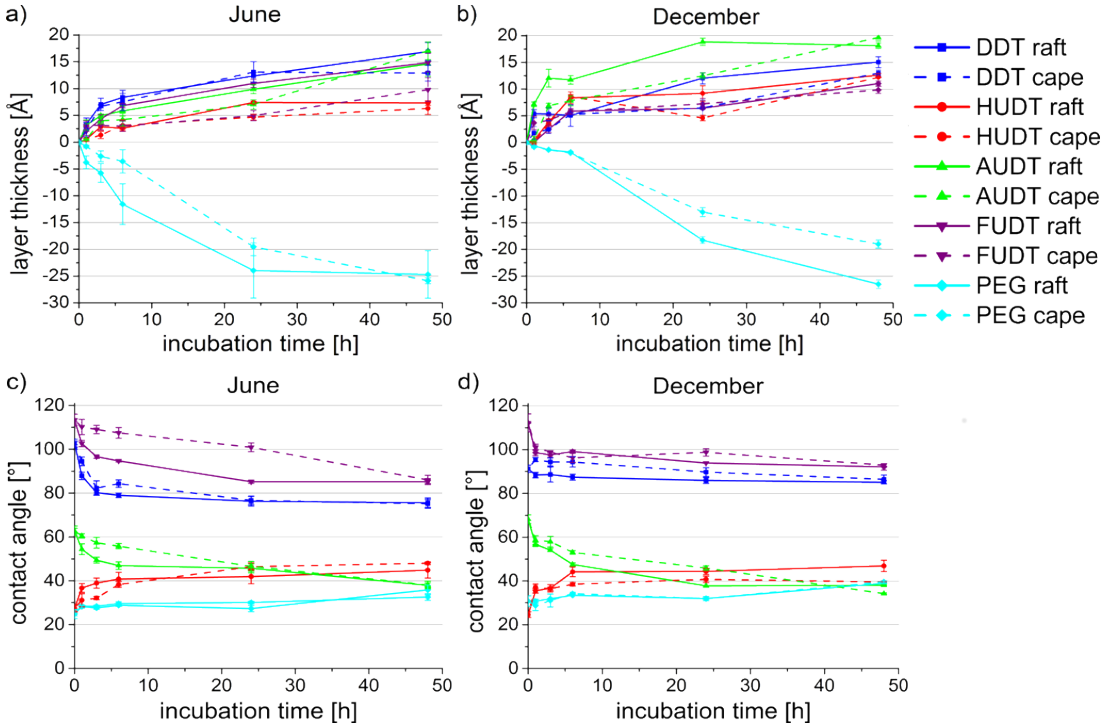

Figure 4.12: Conditioning of self-assembled monolayers with different chemical terminations by natural seawater from two test sides ('raft', 'cape'). Thickness of the conditioning layer (a, b) and contact angle (c, d) of the conditioned surfaces at two different times of the year. Error bars are the standard error of the mean (SEM) (n = 3).

film, infrared reflection absorption spectroscopy (IRRAS) was applied to samples conditioned with water from June (Figure 4.13 and 4.14). In the range of 3000 cm^{-1} the symmetric and antisymmetric CH_2 stretching vibrations of the methylene backbone of the aliphatic SAMs [27] can be seen in all spectra. While the intensities of the methylene vibrations do not increase much for the different incubation times, the carbonyl (1745 cm^{-1}, C=O stretching vibration), amide I (1650 cm^{-1}, most likely C=O stretching vibrations of the peptide bond) and amide II (1540 cm^{-1}, N−H bending and C−N stretching vibrations) peaks increase during the formation of the conditioning layers (peak assignment according to [156, 201]). This suggests that the films are comprised of macromolecules containing carbonyl and amide groups, i.e. most likely proteins, glycoproteins, lipids and polysaccharides [43, 44, 49].

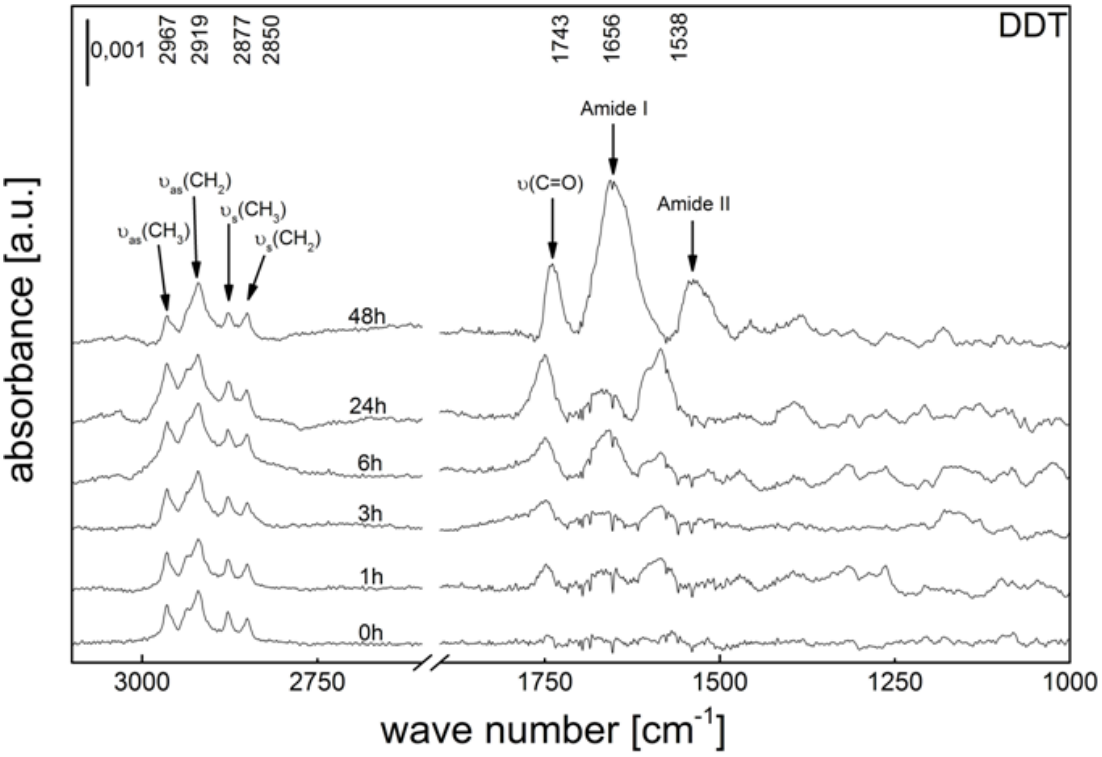
DDT
0,001
2967
2919
2877
2850
1743
1656
1538
Amide I
υ(C=O)
Amide II
υas(CH2)
υs(CH3)
υas(CH3)
υs(CH2)
48h
24h
6h
3h
1h
0h
absorbance [a.u.]
3000
2750
1750
1500
1250
1000
wave number [cm-1]

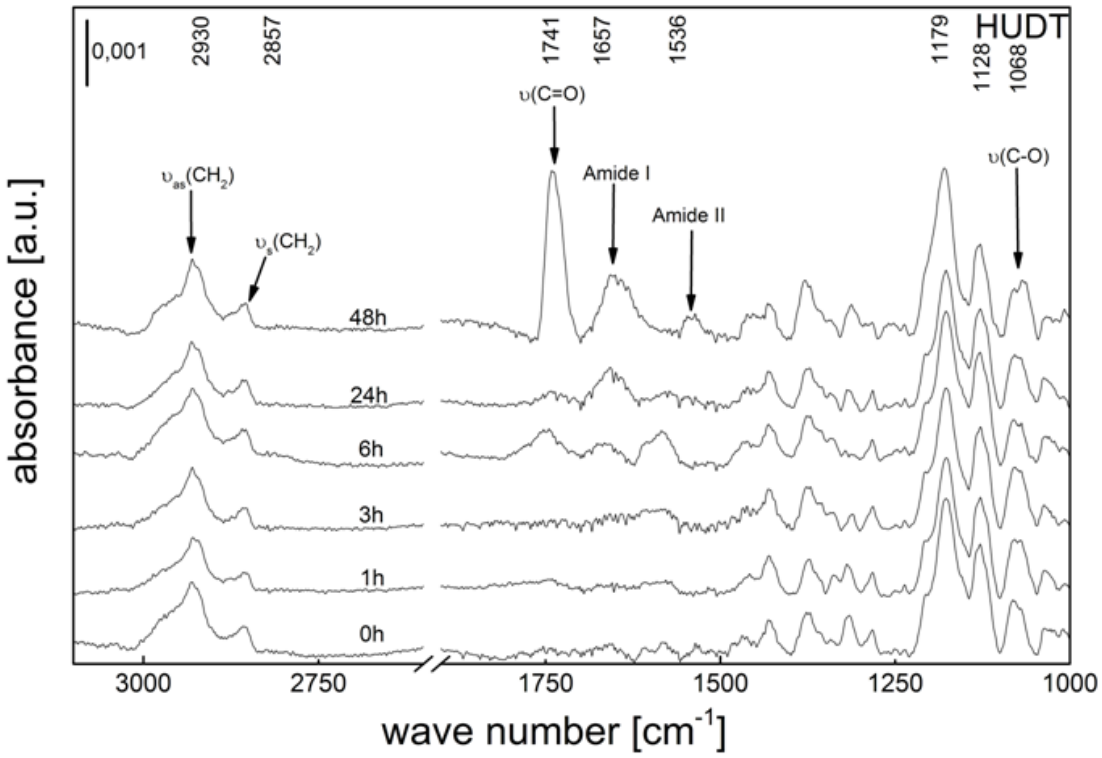
HUDT
0,001
2930
2857
1741
1657
1536
1179
1128
1068
υ(C=O)
Amide I
Amide II
υ(C-O)
υas(CH2)
υs(CH2)
48h
24h
6h
3h
1h
0h
absorbance [a.u.]
3000
2750
1750
1500
1250
1000
wave number [cm-1]

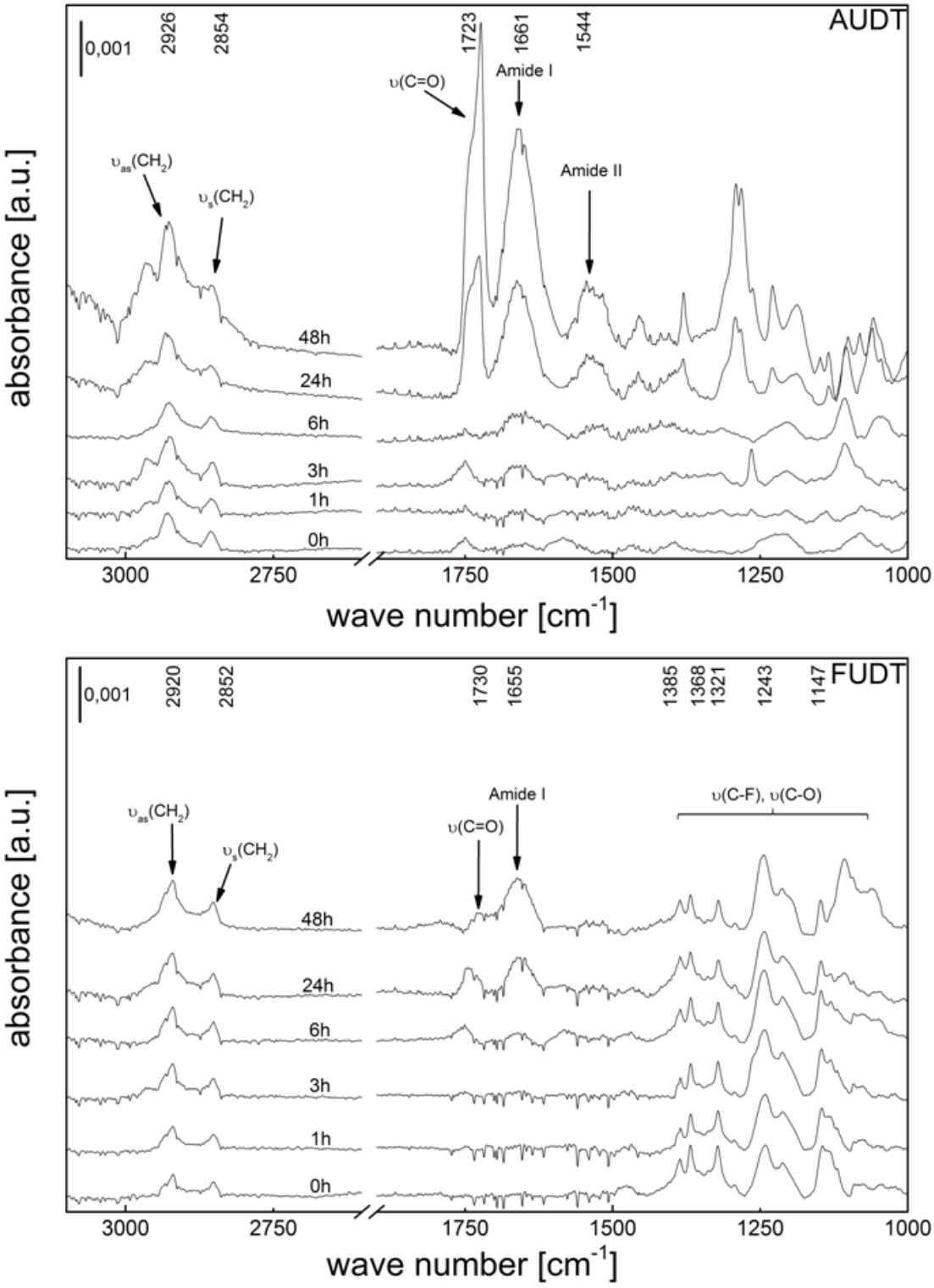

Figure 4.13: IR spectra of the different surfaces after several hours of incubation up to 48 h in 'raft water'. On all chemistries carbonyl, amide I and amide II peaks are growing within 48 h.

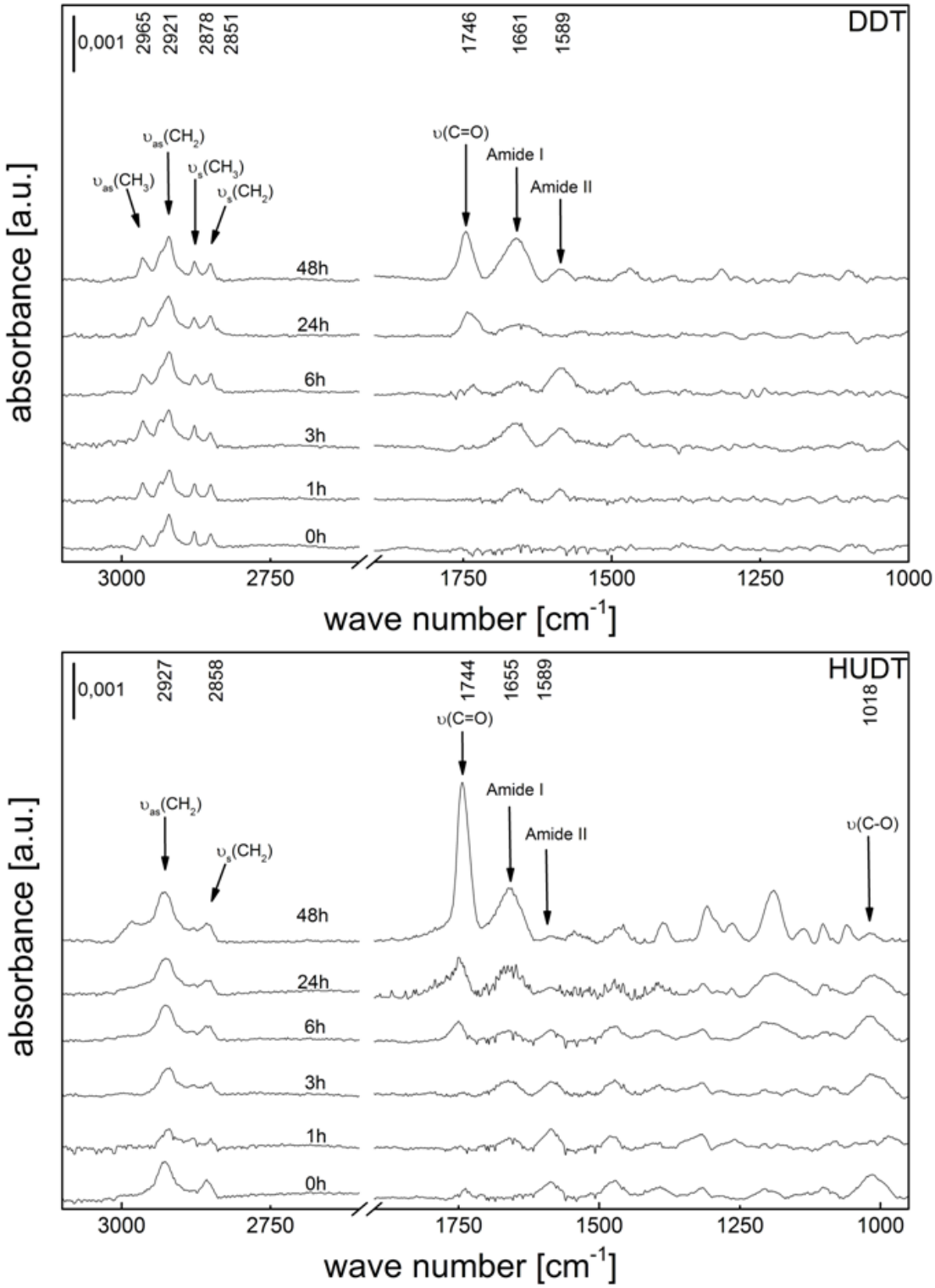
DDT
0,001
2965
2921
2878
2851
1746
1661
1589
υas(CH2)
υas(CH3)
υs(CH3)
υs(CH2)
υ(C=O)
Amide I
Amide II
48h
24h
6h
3h
1h
0h
absorbance [a.u.]
3000
2750
1750
1500
1250
1000
wave number [cm-1]
HUDT
0,001
2927
2858
1744
1655
1589
1018
υ(C=O)
Amide I
Amide II
υ(C-O)
υas(CH2)
υs(CH2)
48h
24h
6h
3h
1h
0h
absorbance [a.u.]
3000
2750
1750
1500
1250
1000
wave number [cm-1]

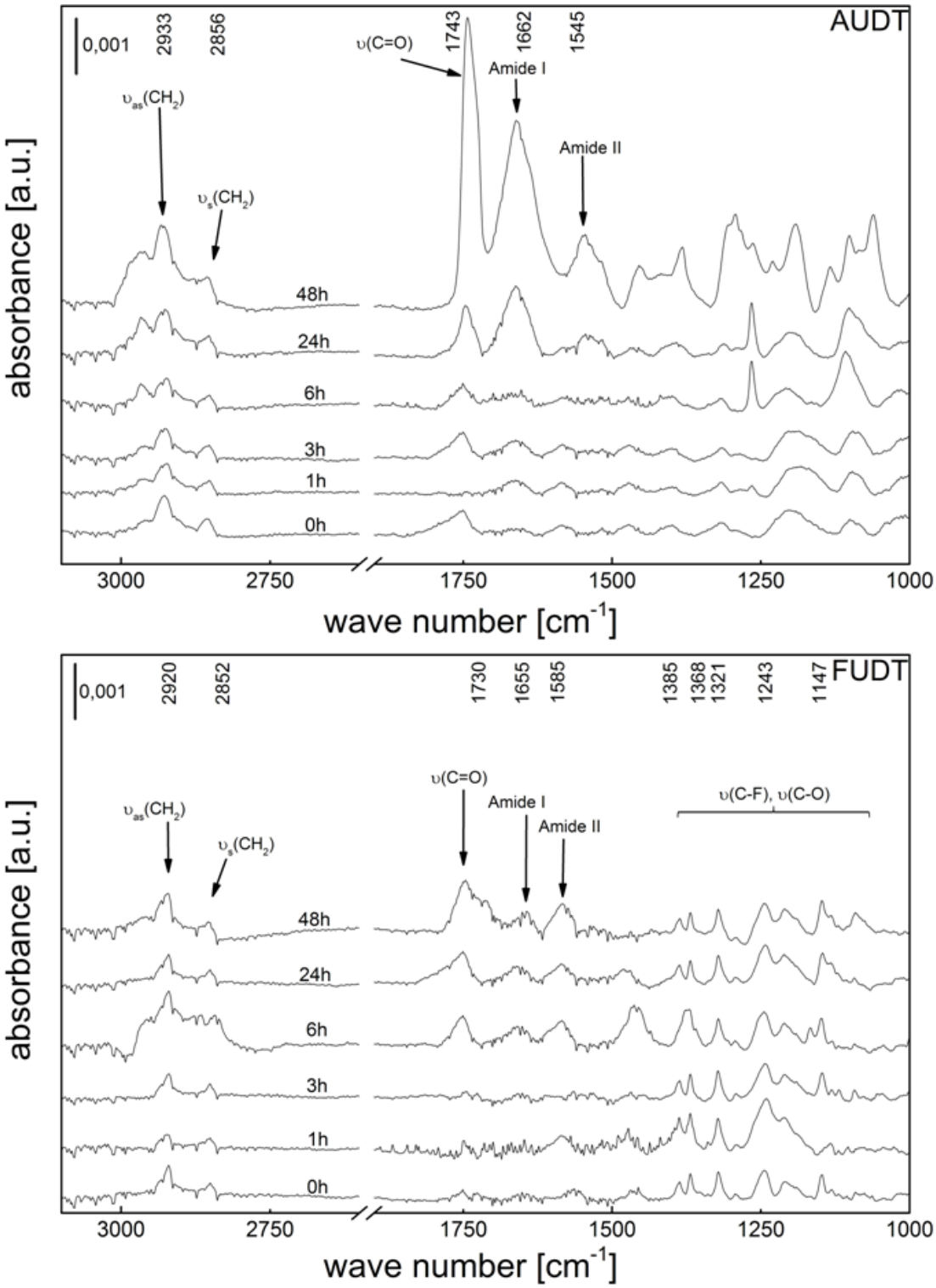

Figure 4.14: IR spectra of the different surfaces after several hours of incubation up to 48 h in 'cape water'. On all chemistries carbonyl, amide I and amide II peaks are growing with different intensities within 48 h.

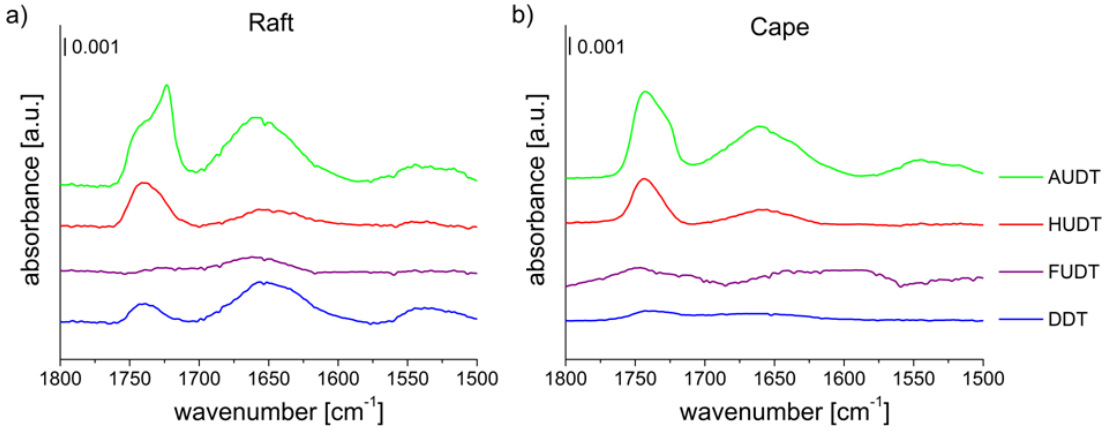

Figure 4.15: Carbonyl (1745 cm^{-1}), amide I (1650 cm^{-1}) and amide II (1540 cm^{-1}) intensity on all different surfaces after 48 h conditioned by a) 'raft water' and b) 'cape water'.

Figure 4.15 shows the carbonyl and amide bands after 48 h incubation time in 'raft water' (RW) and 'cape water' (CW) for all four surfaces in greater detail. It can be seen that the shapes and relative intensities of the carbonyl, amide I and amide II peaks show slight differences. Especially on the hydrophilic AUDT and HUDT samples, the carbonyl and amide I bands (1745 cm^{-1} to 1650 cm^{-1}) are very pronounced indicating large amounts of proteins or proteinaceous components. An interesting point to note is that the shape of the carbonyl bands at 1740 cm^{-1} differs between AUDT samples immersed at the raft and the cape test site. The peaks seem to be a summation of at least two components which reflect differences in the degrees of the hydration of, and hydrogen bonding to carbonyl groups [202–204]. Since the peak intensities of both films are nearly the same but the shape shows variations, it may be concluded that they have a similar amount of proteins attached to the surface but their compositions are different. In contrast, the two hydrophobic surfaces, DDT and FUDT, show different spectra and in both cases the carbonyl and amide bands were comparably weak. Here the DDT film formed with 'raft water' seems to be an exception. This observation is in line with the ellipsometric measurements where the thickness for the raft sample was slightly higher than for the cape sample.

If the development of the intensities of the alkyl, carbonyl and amide bands are plotted against time it can be seen that the rate of adsorption of molecules were different for different chemistries (Figure 4.16). While the intensity of the alkyl bands increases just slightly over time on all surfaces, the intensity of the carbonyl, amide I and amide II bands increases differently. As expected, the intensity of the carbonyl and amide peaks on the hydrophobic samples stays quite low. Therefore it may be concluded that the conditioning layers on hydrophobic surfaces have lower amounts of proteinaceous components. In contrast, it can be noted that

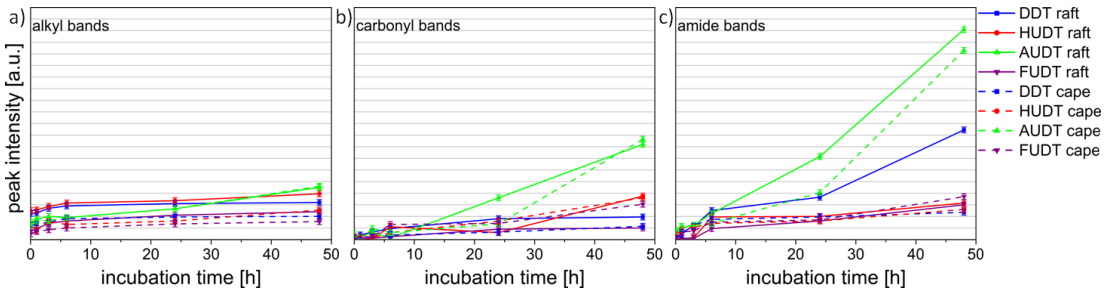

Figure 4.16: Intensity of the carbonyl, amide I and amide II bands on all chemically different surfaces plotted against incubation time in 'raft water' and 'cape water'. Error bars are the reading error.

the increase of the peak intensities is drastic for hydrophilic AUDT samples. It is surprising that the intensity of the carbonyl and amide bands of the HUDT surfaces are not as high as on the AUDT, as it was expected based on the results of studies with 'spore water'. It seems that the components in natural seawater are different from those in 'spore water' and that the HUDT surface is not as attractive to them when comparing to those formed in 'spore water'.

In agreement with the ellipsometry data, it can also be noted that PEG surfaces deteriorate over time (Figure 4.17). The peaks in the range of 1122 cm^{-1} to 1343 cm^{-1}, typical bands of the C−O−C stretching, CH_2 twisting and CH_2 wagging modes of the ethylene glycol units [182–184], decrease with increasing incubation time. Also the symmetric and asymmetric CH_2 stretching bands at 2888 cm^{-1} are reduced. No amide peaks grow in the first 48 h, since the film does not appear to be completely degraded and a certain resistance against accumulation of molecules is retained. By enlarging the incubation time to 1 week it could be revealed that the PEG film completely disappears, since no peaks originating from the PEG monolayer could be observed, and only the peaks resulting from the conditioning film are detectable on the surface.

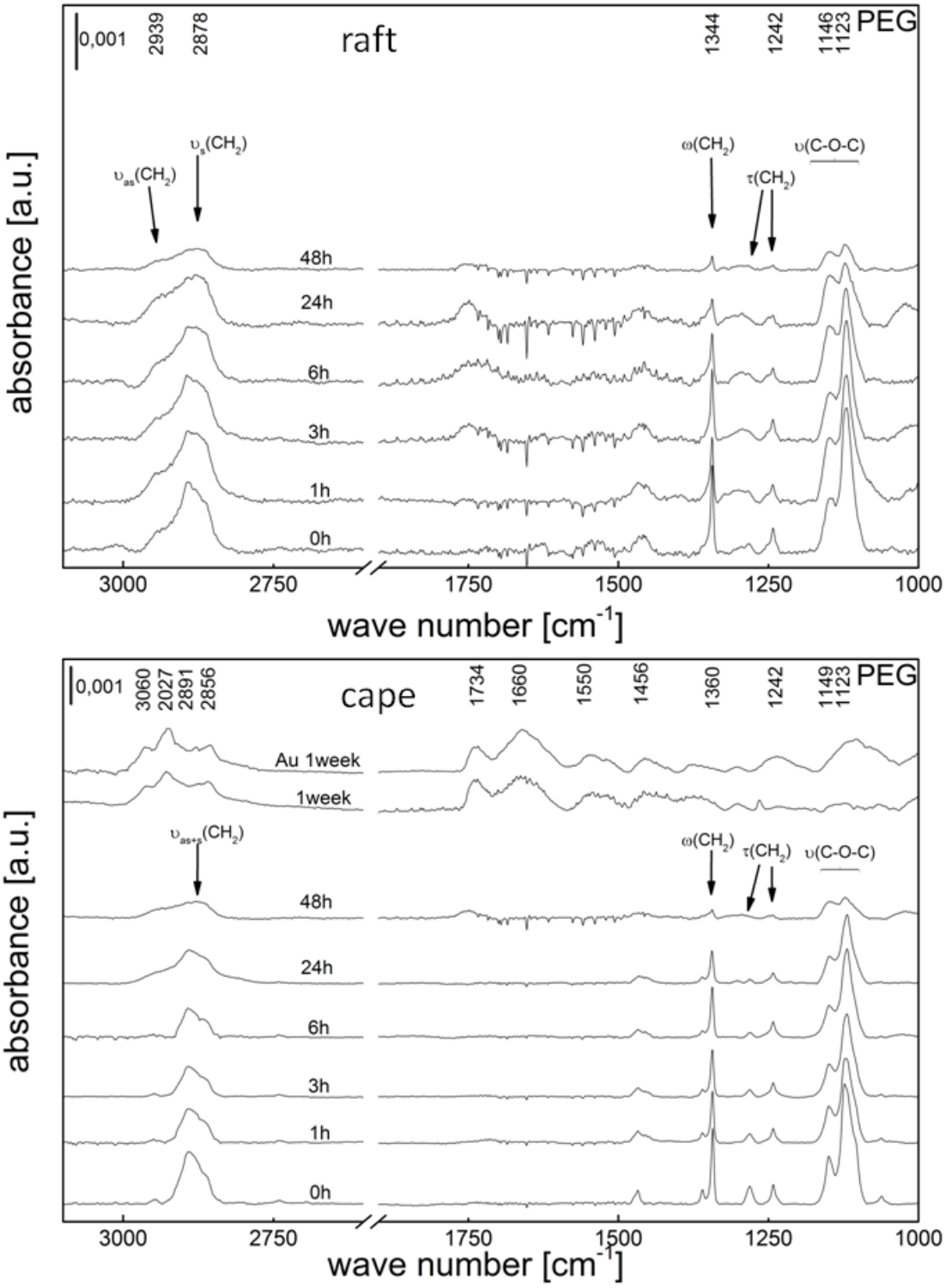

Figure 4.17: IR spectra of the PEG surfaces after several hours of incubation up to 48 h in 'raft water' and 'cape water'. In 'cape water' samples were incubated additionally for 1 week and a pure Au slide was added as a referenz.

4.2.2 Field tests

IRRAS revealed that conditioning layers on the different surface chemistries showed variations in their chemical nature. Also, the water contact angles changed and converged towards more similar values for the different surfaces. Thus, the question arose how settlement of marine organisms is influenced by the conditioning layers. Therefore surfaces were pre-immersed in RW for 24 h. After conditioning the incubated surfaces and surfaces without preconditioning were immersed into the ocean at the raft static immersion test site simultaneously on two following days with similar environmental conditions. It was investigated if pre-conditioning causes any differences in the density of settled organisms.

Figure 4.18 shows the distribution of the settled organisms on non-incubated (0 h) and preconditioned (24 h) surfaces with different end group chemistries. It can be noted that the most frequently species on all surfaces (30 % to 40 %) is represented by *Navicula*. The amount of the other organisms (*Bacillaria*, *Amphora*, *Peritrich ciliates* and *Cylindrotheca*) varies between 6 % and 17 % but the distribution is similar on all samples. Except for HUDT where the amount of *Peritrich ciliates* is slightly smaller. It was also shown that no difference could be detected between unconditioned and preconditioned samples.

In Figure 4.19 the change in the density of settled organisms on the different surface chemistries before and after 24 h preincubation is shown. It can be noted that the amount of organisms on the pristine samples on the first day (d1) is nearly the same for all surface chemistries. On the second day (d2), the hydrophobic

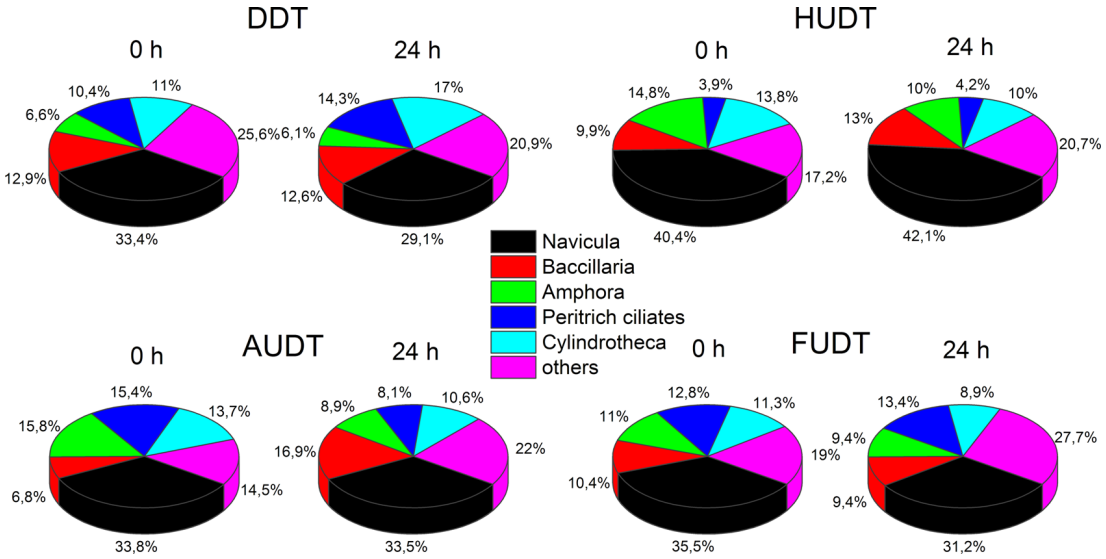

Figure 4.18: Distribution of the organisms being present on incubated and non-incubated samples immersed at the raft test site for 24 h. It can be noted, that the distribution is similar for all surface chemisties.

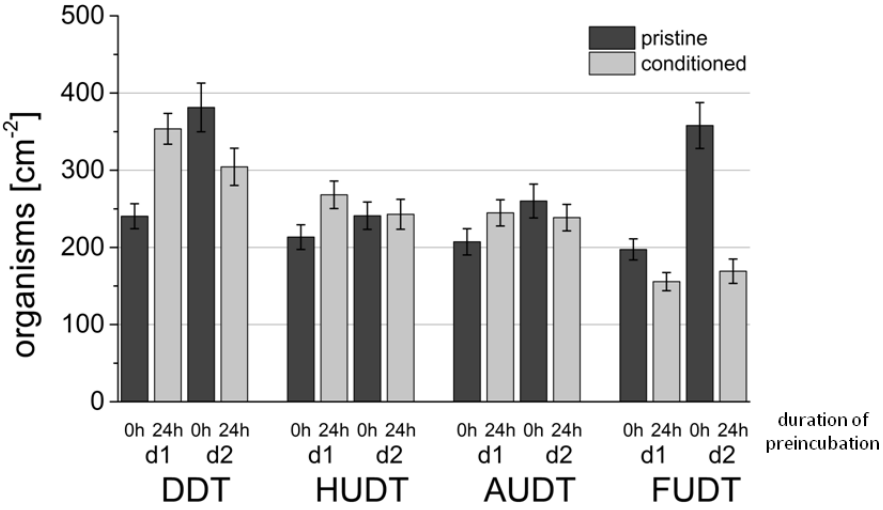

Figure 4.19: Settlement density of marine organisms on different SAMs after an immersion time of 24 h in the ocean, with and without pre-incubation in 'raft water' for 24 h. Error bars are the standard error of the mean (SEM) (n = 120).

DDT and FUDT samples show a higher settlement density, which fulfills the expectations as this trend is well-known from laboratory bioassays [21, 83, 85]. Since the distribution of the organisms is similar on all samples all species are influenced by the surface wettability the same way. Concerning preconditioned surfaces it can be observed that while on the hydrophilic HUDT and AUDT samples the settlement density is nearly the same, the hydrophobic DDT surfaces seem to be more attractive than the FUDT SAMs. This may be due to the fact that the accumulated conditioning films have different compositions. As shown in section 4.2.1 the conditioning films on hydrophilic surfaces accumulate more proteinaceous compounds. Concerning the film formation with 'raft water', also the hydrophobic DDT SAMs showed a higher intensity of proteins while only for the FUDT samples the protein intensity was weak. Since the conditioning films seem to mask the original chemistry the organisms are not able to sense the underlying physico-chemical properties and only the varying components of the conditioning films can be detected. This could in turn be interpreted so that samples with a higher concentration of proteinaceous compounds are more attractive for marine organisms.

4.2.3 Conclusion

Laboratory assays with single organisms are extensively used for rapid screening of antifouling coatings. To test the performance of such coatings, not only laboratory but also field tests are necessary. In the last decades, several studies

about coatings being immersed into the ocean for month or even years have been done. However, few things are known about the composition of the first fouling communities in field experiments on well defined model surfaces like SAMs. As the adsorption of proteins and other macromolecules is one of the fastest steps in the process of biofouling and until now the chemical nature of the adsorbed layer is still poorly characterized, it is, for scientific understanding of the whole biofouling process in the field, necessary to derive additional information about the formation kinetics and the chemical composition of such films. Since seasonal variations can affect the salinity, pH or temperature and thus the dissolved organic carbon (DOC) concentration in the water, these factors could have an impact on the formation process.

Therefore it was investigated to what extent a conditioning film is formed on chemically different surfaces in the field and if there is a difference between the conditioning layers relating to the different times of the year. A protein film was formed on different surfaces independent of the surface chemistry and analyzed using ellipsometry, contact angle goniometry and IR spectroscopy. The time dependence of the film formation and the appearance of carbonyl, amide I and amide II bands could be observed. It was also shown that on the hydrophilic samples, the carbonyl and amide I bands are very pronounced indicating large amounts of proteins or proteinaceous components. Furthermore it was shown that the PEG surfaces deteriorated with longer incubation time and after an immersion time of 1 week, only bands originating from the conditioning film could be detected on the sample.

After the detailed investigation of the formation and chemistry of the conditioning films, it was explored as to what extend the increased conditioning of a surface affected the density of settled organisms. Therefore pre-conditioned as well as non-incubated samples were immersed at a static immersion test site for 24 h. The obtained data showed that the distribution of the organisms was similar for all samples independent of the chemistry and incubation time. The most dominant organisms observed on the surfaces were diatoms (*Navicula*, *Amphora*, *Cylindrotheca* and *Baccillaria*) and the protozoa *Peritrich ciliate*. It was shown that the amount of organisms on the pristine samples on the first experimental day was nearly the same for all surface chemistries, while on the second day the hydrophobic samples showed a higher settlement density. Concerning preconditioned surfaces and taking into account that the components of the formed conditioning films vary on chemically different surfaces, it was observed that samples with a higher concentration of proteinaceous compounds are more attractive for marine organisms.

4.3 Influence of surface conditioning on bacterial adhesion

As described in the previous section 4.2, field test are necessary to gain knowledge of the performance of antifouling coatings in the 'real world'. But these experiments need a lot of time to achieve reproducible results since the factors which influence the settlement process depend on the environmental factors like weather, humidity or temperature. To make the screening of potentially coatings more efficient artificial experiments in the laboratory are needed with more matured biofilms cultivated in nutrient-rich media. Therefore microbial biofilms represent a well known bacterial mode of growth in which the microorganisms benefit from metabolic exchange, genetic flexibility, and protection (see section 2.1.2). Bacterial biofilm communities feature different properties and survival strategies that go beyond possibilities a single bacteria has [205]. Bacteria can form biofilms on all kinds of natural and synthetic surfaces. Therefore, bacterial biofilms represent a major problem especially in environmental biology, medical fields, food industry, and biotechnology.

The bacterial adhesion process includes an initial physico-chemical interaction phase in which surface wettability is believed to play an important role [194, 206, 207]. In this section the formation of a conditioning layer and the determination of the settlement kinetics of *P. aeruginosa* bacteria on surfaces with different wetting properties are examined in collaboration with the group of Prof. Ursula Obst (Institute of Functional Interfaces, Karlsruhe Institute of Technology, Germany). For both experiments hydrophobic DDT and hydrophilic HUDT SAMs were chosen, two surfaces exhibiting significantly different wettabilities. The rationale behind the study was to determine a) if there is a difference in the formation of a conditioning layer by using different media and b) if the settlement coverage of *P. aeruginosa* is influenced by the surface chemistry and the formed conditioning layer.

4.3.1 Preparation of conditioning films

Two chemically different surfaces were prepared and analyzed according to the protocol described in section 3.1 and 3.2, which varied in terms of protein resistance and wettability (Table 4.3).

The conditioning film adsorption experiments are described in detail in the materials and methods section 3.4. Each sample was immersed in 20 ml medium solution for different time periods. Two different medium types were used. The protein-rich BHi medium and the BM2 medium, which contains just a small amount (0.4 % (wt/vol)) of glucose. After rinsing and drying, the thickness of

Table 4.3: Thiol molecules used to form self-assembled monolayers, static water contact angle (error: ± 4°) and thickness of the used SAMs as determined by spectral ellipsometry (error: ± 2 Å).

Chemistry	**label**	**water CA** [°]	**thickness** [nm]
$SH-(CH_2)_{11}-CH_3$	DDT	104	1.1
$SH-(CH_2)_{11}-OH$	HUDT	33	1.2

the adsorbed conditioning layer was determined by spectral ellipsometry. Additionally the change of the contact angles depending on the incubation time were measured.

In order to compare the different media, DDT and HUDT SAMs were used as model surfaces with hydrophobic and hydrophilic properties. Figure 4.20 shows the obtained results. For BHi medium the formation of a conditioning layer was most prominent on the hydrophobic SAM. The thickness of the formed protein layer was determined to be about 25 Å. Although a conditioning film was also formed on the hydrophilic samples, this film was slightly thinner with just about 10 Å. These measurements are in line with the values found in the previous sections (section 4.1.1 and section 4.2.1) for the conditioning of DDT and HUDT surfaces with 'spore water' and natural seawater. Performing the same experiment with the BM2 medium it could be shown that the adsorption was lower for the DDT sample and was about 10 Å, while for the hydrophilic HUDT surface nearly no accumulation could be detected.

The time scale of the increase in film thickness broadly matched the changes in contact angle after conditioning. The contact angle changed for both surfaces on a similar time scale of about 5 h to 10 h. Interestingly, for the hydrophobic surfaces the change in CA corresponds to the layer thickness of the formed conditioning film. With BHi the layer was much more prominent and the CA changed from about 100° to 70°, becoming more hydrophilic, while for BM2 it only decreased from about 100° to 85°. The hydrophilic surfaces changed their CA from about 20° to 38° and became more hydrophobic, independent of the used medium. These data are in agreement with the results obtained by 'spore water' and natural seawater conditioning in section 4.1.1 and section 4.2.1, where it could be shown that the CA of the hydrophobic DDT surface decreased from 95° to about 80°. For the hydrophilic HUDT surface the CA increased from 25° to about 40°.

These results are not surprising keeping in mind that the BHi medium consists of crushed beef heart, calf brains and glucose, while the BM2 medium mainly consists of different salts and a small amount of glucose (0.4 % (wt/vol)). With this ingredients the BHi medium is highly proteinaceous and according to this the

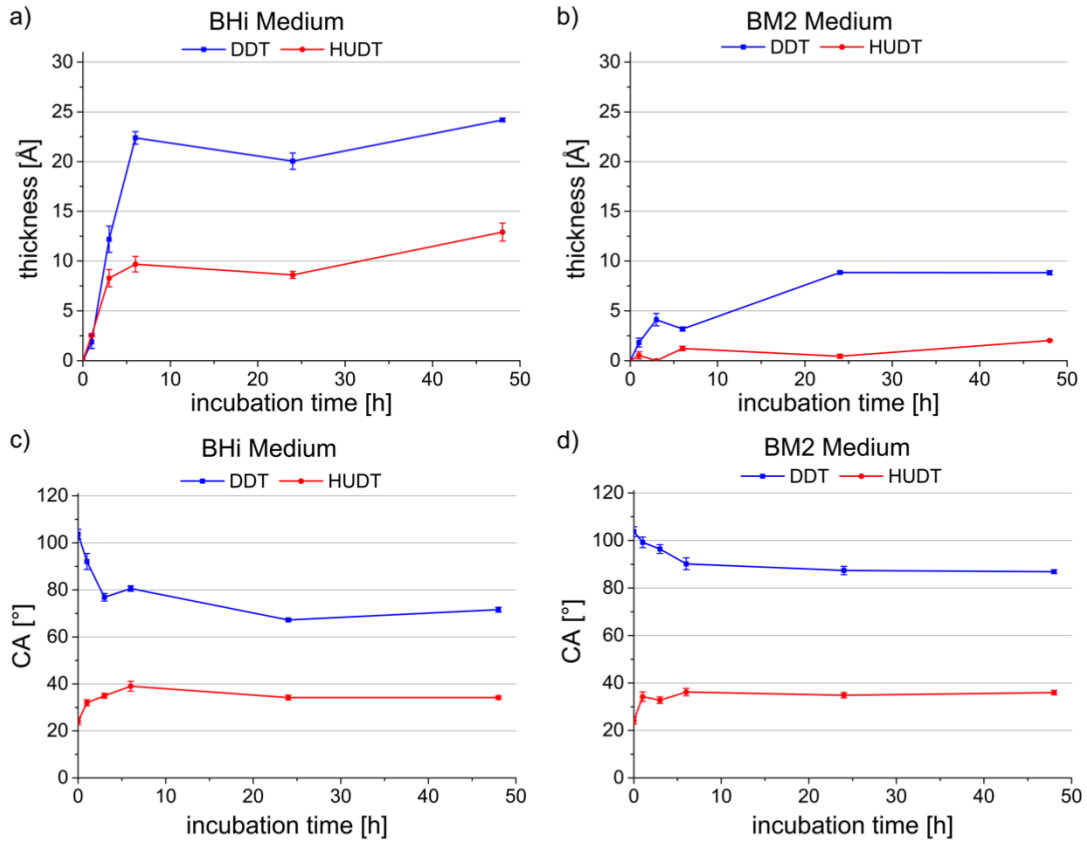

Figure 4.20: Characterization of the conditioning of self-assembled monolayers with different chemical termination by BHi and BM2 medium. a) and b) Thickness of the conditioning layer; c) and d) Contact angle of the conditioned surfaces. Error bars are the standard error of the mean (SEM) (n = 3).

formed films show a higher thickness. With BM2 only the added glucose is able to form a conditioning layer what explains the small amount of proteins on the surface, which is detectable in the thinner layer thickness and the less changing CA.

4.3.2 Bacterial adhesion assay

After investigating the formation of a conditioning film, the question arose to which extend the surface adhesion of bacteria is influenced by a protein layer. Therefore bacterial adhesion assays were performed in different media according to the protocol described in section 3.5.1. Samples were placed into an in-house built bio-reactor and the bacterial solution was added. After different incubation times the samples were removed according to the protocol and the colony forming

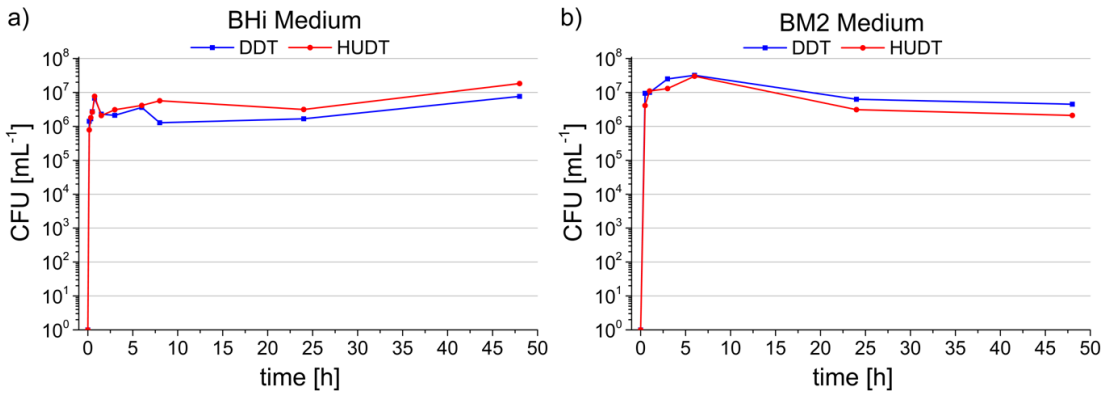

Figure 4.21: Kinetics of settlement of bacteria *P. aeruginosa* on chemically different surfaces over a total duration of 48 h. a) BHi and b) BH2 media were used for the bacteria assay.

units (CFUs) were determined. Figure 4.21 shows the results of these experiments. It was observed that after only 10 min settlement time in BHi medium the amount of organisms reached a level in the range of 10^6 to 10^7 CFU per mL. This amount did not change in the following 48 h. Since the concentration of the bacterial solution increased constantly because of the high proliferation rate of the bacteria in a nutritious environment, another experiment was performed using the less proteinaceous BM2 medium, in which the bacterial growth should be limited. However, also here the final amount of bacteria was reached very fast and did not change over time.

This observation can be explained considering another study in our group [208]. Here, a suspension of the bacterium *Cobetia marina* was injected in a fluidic channel system and the bacteria were allowed to adhere to underlying surfaces with varying end group chemistries. After the incubation phase, a flow was induced into the channel and increased stepwise, while the detachment of the cells was followed by a microscope. It could be revealed that the chemical termination of a surface did not influence the fraction of cells that adhere to it but the bacterial adhesion strength varied on chemically different samples.

In another study in our group a different fluidic system was used to determine the settlement kinetic of *P. aeruginosa* [209]. Therefore bacteria were incubated under flow for one hour and the attachment was followed by a microscope. The results show that at the beginning only few cells adhered to the surface but with longer incubation time the settlement density increases. An interesting observation was that although these experiments are performed in a different manner, the bacteria here do also not distinguish between surface chemistries and the adhesion follows similar kinetic curves for all chemically different surfaces.

The obtained results of *P. aeruginosa* assays performed within this thesis are in line with the observations of other studies in our group and it may be concluded,

that surface chemistry has no remarkable effect on the fraction of inoculated bacteria that adhere to a surface. With these findings the question, if a conditioning film could have an influence on the adhesion of bacteria, could be answered. Since it is known that the films formed by using different kinds of media differ from each other a difference in the bacterial reaction to the surface should be detectable. But as no differences could be observed in the bacterial assays, also the formed layers could not have an impact on the behavior of the bacteria.

4.3.3 Conclusion

Two different types of self-assembled monolayers based on alkanethiols with chemically different terminations were prepared on gold coated glass slides to examine the correlation between surface wettability, the formation of a conditioning layer by different media and the adhesion of the bacterium *P. aeruginosa*. It was demonstrated that the formation of a conditioning layer was dependent on the surface chemistry and the protein content in the medium. For the protein-rich BHi media the thickness of the formed layer was higher than that formed with BM2 medium which contains only 0.4 % (wt/vol) of glucose. Another observed trend was that the formed layer was thicker on the hydrophobic DDT SAMs than on the hydrophilic HUDT surfaces. This is in line with studies carried out with 'spore water' and natural seawater as described in section 4.1.1 and section 4.2.1 previously. An interesting observation was made with an adhesion study with *P. aeruginosa*. It was shown that the bacteria do not distinguish between different surface wettabilities. All samples were colonized the same way independent of the medium, surface chemistry and incubation time of the samples in the bioreactor. Other studies in our group verified this trend for *P. aeruginosa* and the salt water bacterium *Cobetia marina*.

Since the concentration of the bacterial solution increases constantly —caused by the high proliferation rate of the bacteria— current assays are not optimized for long term tests of antifouling coatings. At this stage, it is hard to extrapolate more from these experiments than the fact that all surfaces exhibit similar densities of CFUs. In order to tackle questions beyond settlement densities, the assay procedure has to be tuned.

4.4 Influence of surface morphology on *Ulva* settlement

Not only surface chemistry and conditioning can influence the settlement process, also surface roughness has a well documented effect on the retention of microorganisms [210]. With the discovery of animals that display microstructures on their skin, which show fouling resistance, the study of microtextured surfaces has gained more and more attention in the last decades [32, 101, 211, 212]. With the development of three-dimensional micro- and nanostructured surfaces many processes such as cellular response, biocompatibility or adhesion of proteins and microorganisms can be investigated systematically on the basis of well-defined morphologies. In the marine environment the topography of a substrate has been proven to have both, deterrent and attractive effects on the settlement of spores [24, 103, 213–215]. It influences the hydrodynamic properties of a surface and therewith e.g. the settlement process. Especially the influence of microstructured bioinspired surfaces on the settlement behavior of microorganisms has been investigated [216]. Topographies of appropriate height, size and shape significantly reduce the contact area between glue secreted from the organism and the surface topography which leads to a decrease in settlement compared to a smooth surface [33]. The skin of sharks has the unique property of reducing hydrodynamic shear by being structured with microscalar denticle structure [217]. This structure has been mimicked successfully (Sharklet AF^{TM}) to reduce attachment of spores of *Ulva* [103, 214, 215]. The microtopography of honeycomb-patterned films has also been found to have a strong effect on the settlement behavior of cells and spores [213, 218].

However, the focus of research did not lie on nanostructured surface morphologies so far, although sub-micrometer structures could be important for the development of effective antifouling surfaces. A lack of accessibility for the preparation of such structures with at least one dimension in the nanometer scale could be the reason for this. By using carbon nanotubes as filler for silicone coatings which yielded a nanorough surface, Beigbeder *et al.* gave a successful example for structured surfaces which reduced the adhesion strength of marine organisms like barnacles or algae. Another example to achieve nanostructured surfaces was given by Cao *et al.* who utilized layer-by-layer spray-coating deposition of polyelectrolytes [24]. They showed that the lowest level of settlement is observed for structures in the order of 2 µm.

With state-of-the-art lithography techniques such as electron beam activation lithography (EBAL), it is possible to prepare features on the nanoscale in order to mimic structures that exhibit the potential to prevent fouling in nature [126]. Functionalized self-assembled monolayers on gold serve as basis for the fabrication of these structured surfaces. The method in the course of this thesis is based on

a primary template comprised of AUDT SAMs with mostly deactivated amino groups. With e-beam lithography these groups are activated and both, the active and inactive species, serve suitable for surface-initiated polymerization (SIP). While on the inactive 'background' SIP gives a thin but homogeneous polymer brush layer, the activated groups promote the controlled growth of higher polymer brushes leading to 3D morphology patterns exclusively comprised of the same polymer material.

The skin of pilot whales, a subspecies of the dolphin family, is nanoporous and exhibits an average pore size of about 200 nm, which is below the size of most marine fouling organisms [32]. Within this thesis these structures have been mimicked, since they provide a nanorough surface which effectively reduces the attachment area of potential fouling organisms. Therefore EBAL was utilized and a subsequent polymerization forming poly(*N*-isopropylacrylamide) (PNIPAM) polymer brushes which serve as pore ridges was performed. Baum *et al.* reported that these pores exhibit a honeycomb-like shape [98]. A hexagonal honeycomb structure was chosen as a model surface to investigate the settlement behavior of algal spores of *Ulva*.

4.4.1 Preparation of nanostructured polymer surfaces

As a primary template, self-assembled monolayers of AUDT were prepared on a gold coated silicon wafer according to the general protocol described in section 3.1. The samples were then placed in a VB6UHR EWF e-beam (Karlsruhe Nano Micro Facility (KNMF), Karlsruhe Institute of Technology) writer and a beam current was applied to irradiate the substrate. In earlier studies carried out in our group the layout of the EBAL was chosen to consist of a single structure size on one sample [179]. With respect to the comparability of the different structure sizes, a new layout was developed with all different structure sizes on one single sample according to Figure 4.22. Another drawback of the earlier work was a restricted

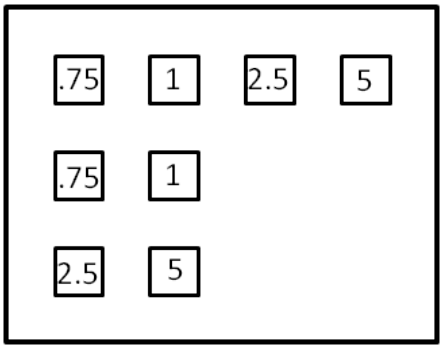

Figure 4.22: EBAL layout: each structure size is placed twice on one sample. The size of the gaps is indicated in the squares [µm].

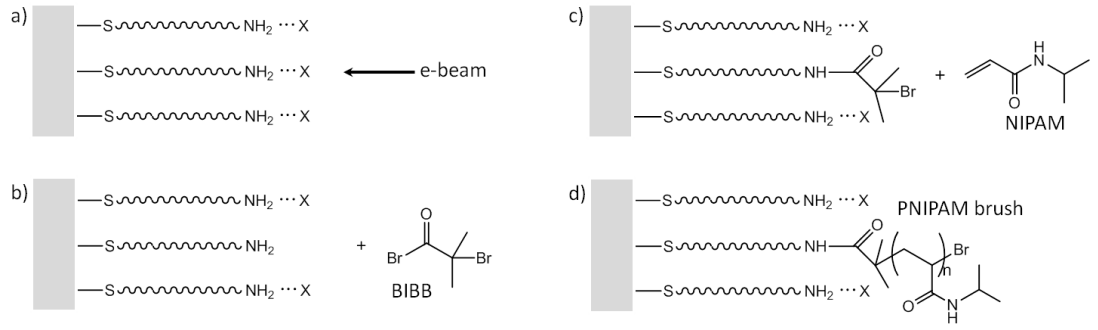

Figure 4.23: EBAL/SI-ATRP on an AUDT template: a) electron-beam induced activation of amino groups; b) selective anchoring of the surface initiator (BIBB) to the activated sites; c) start of polymerization; d) the resulting PNIPAM brush. Note that brush growth occurs on the non-activated areas as well, but the thickness is significantly smaller (after [132]).

area of $250 \times 250\,\mu m^2$ on which defined structures could be patterned. To achieve structures in the nanometer scale a very small e-beam focus is required. At the same time the beam has to be moved over the substrate which changes the focal distance due to the change of the beam path for every point. The more the beam has to be moved out of its central position, the more blurred are the structures. To obtain larger areas of well defined structures the decision to use an e-beam writer system where it is possible to move the whole substrate with respect to keep the electron beam constantly focussed on the sample surface was made. It was also decided to structure larger areas of $1000 \times 1000\,\mu m^2$ to achieve adequate statistics.

After the irradiation an ATR polymerization was performed. Figure 4.23 shows the procedure for the growth of PNIPAM brushes on an e-beam structured AUDT SAM. In step a), the area is activated where the electron beam hits the surface. Extensive brush growth will be observed here. However, brush growth also occurs where no activation took place, only to a much smaller extent [132]. Step b) shows the first part of the ATRP, i.e. the coupling of the initiator 2-Bromoisobutyryl bromide (BIBB). Steps c) and d) show how the polymerization starts and subsequently propagates.

4.4.2 Evaluation of honeycomb structures

Ulva spores have a diameter of about 5 µm at the widest point of the spore body [102]. Accordingly, four different honeycomb structures with varying diameters were prepared with a field size of $1000 \times 1000\,\mu m^2$. 5 µm structures were chosen to offer the organisms a structure in the size of their body, 2.5 µm were chosen to feature a size a little bit smaller than the spore body. 1 µm represents

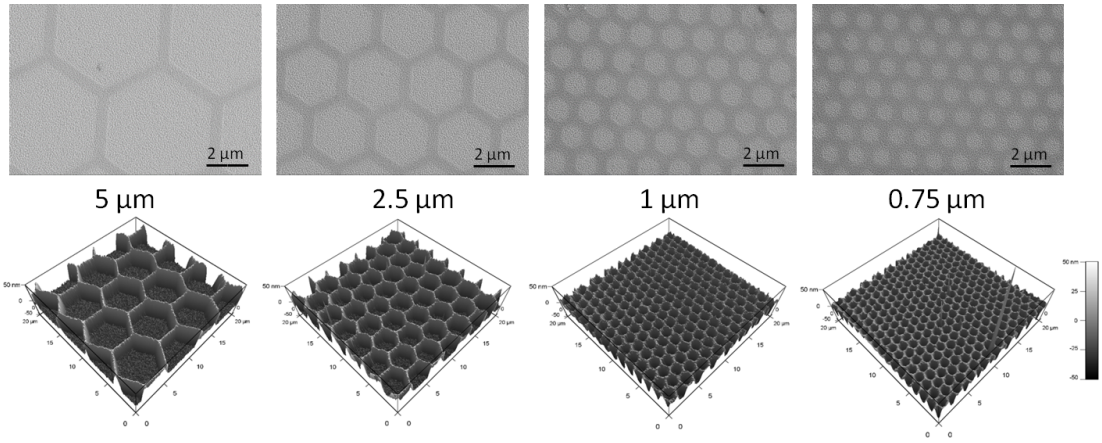

Figure 4.24: SEM and AFM images of the four evaluated PNIPAM honeycomb structures. Numbers underneath are diameters of the honeycombs.

a structure being much smaller than an *Ulva* spore and 0.75 µm is in the desired nanometer range. Figure 4.24 shows SEM and AFM images of the four tested structures. The heights of the elevated regions of which the honeycombs are constituted were measured by AFM. First, the dry ridge hight was measured, followed by *in-situ* measurement in saltwater. The results are summarized in Table 4.4. It shows the dry and the wet ridge height for the different structure sizes and the Wenzel roughness factor calculated using the wet ridge height. It is well known that PNIPAM-polymers swell as soon as they get in contact with water [141, 219]. Since the whole sample surface is comprised of PNIPAM polymers, the whole substrate swells during bioassays. While the unexposed surface areas exhibit a lower polymer density resulting in a mushroom conformation of the

Table 4.4: Ridge heights of the honeycomb structures obtained by AFM measurements and Wenzel roughness factors calculated with formula (4.1) using the wet ridge height.

Honeycomb diameter	**Dry ridge height** [nm]	**Wet ridge height** [nm]	r_{Wenzel}
5.00 µm	45	11[a]	1.007
2.50 µm	43	11	1.012
1.00 µm	40	10	1.017
0.75 µm	38	10	1.024

[a]Estimated ridge height according to AFM measurements performed on structure sizes of 0.75 µm, 1 µm and 2.5 µm.

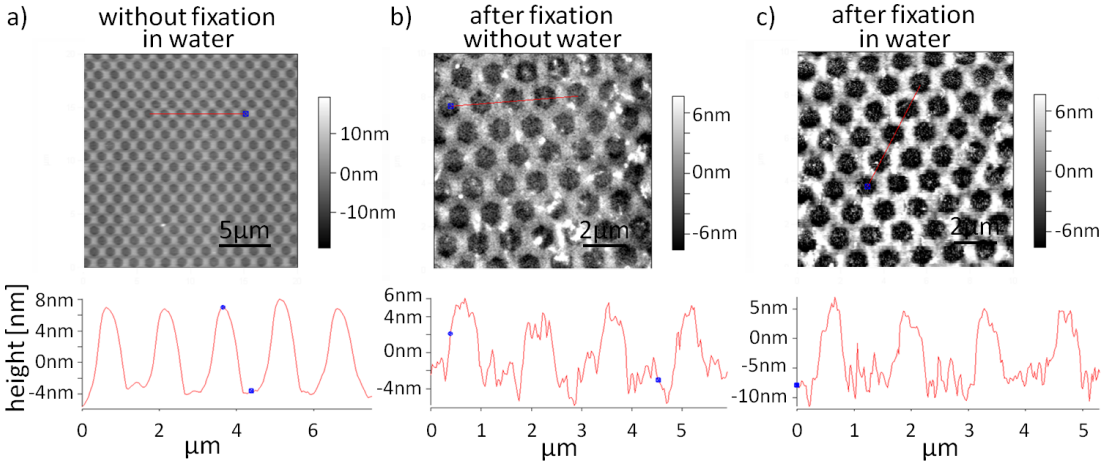

Figure 4.25: AFM images of a) surface after patterning in water, b) surface after fixation in air and c) surface after fixation in water. Below the images the height profiles are shown.

polymer brushes, the ridges of the structures have a more upright conformation going hand in hand with a higher packing density [131, 220–222]. Submerged in water the mushroom conformation is able to adsorb a comparably larger amount of liquid, which finally alters the conformation to the upright state. Due to this mechanism the brushes in between the elevated areas grew higher and so virtually reduced the height of the ridges by about 30 nm. This value corresponds to a total height of about 10 nm (see Figure 4.25a). These findings are in line with AFM studies performed on fixed samples after an *Ulva* spore assay. The samples were fixed in water with 2.5 % glutaraldehyde and using AFM it was observed that the ridge height was also in the range of 10 nm (see Figure 4.25b). An explanation for these findings could be that the water molecules within the polymers were exchanged by the glutaraldehyde molecules and during drying the glutaraldehyde polymerized and fixed the underlying polymers in their conformation. Even after immersing the samples in water the ridge height stayed in the same range of about 10 nm (see Figure 4.25c).

To correlate the surface topography with spore settlement, the Wenzel roughness of the honeycomb patterns was calculated using the variables introduced in Figure 4.26, where x and y represent the length and width of the extracted unit, respectively. m describes the width of the hexagonal pit, a is the side length of the hexagon and h the wet height of the microstructure. The Wenzel roughness factor r refers to the ratio of the actual surface area to the projected planar surface area [153].

$$r_{\text{Wenzel}} = \frac{S_{\text{actual}}}{S_{\text{geometric}}} = \frac{S_{\text{geometric}} + S_{\text{wall}}}{S_{\text{geometric}}} = \frac{xy + 18ah}{xy}. \tag{4.1}$$

The actual surface area includes the projected surface area and the area of the

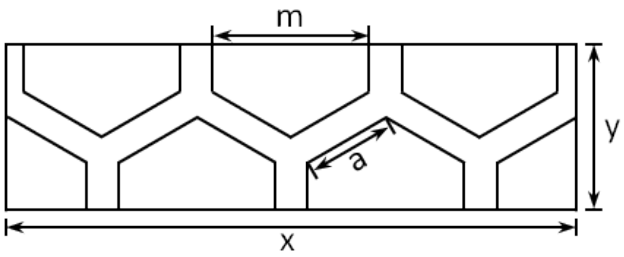

Figure 4.26: Schematic representation of the repeating units of the hexagonal structures (formula (4.1)).

side walls.

4.4.3 *Ulva* settlement assay

The samples were evaluated with respect to the settlement of *Ulva* spores. The density of spores on PNIPAM honeycombs of varying structure size and the smooth PNIPAM background is shown in Figure 4.27. The background counts were made on the same sample where the smooth, homogeneous PNIPAM layer was present on the surface. This is an important control as it serves as a basis for comparison between different substrates. The varying number of settled spores on the background, inhibits a direct comparison of data from different samples. In order to account for this deviation, the data from different samples have been normalized to the background and summarized, shown Figure 4.27. Even though

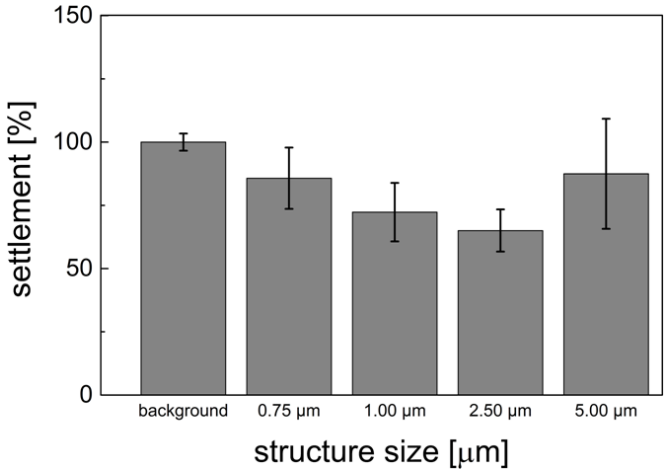

Figure 4.27: Density of *Ulva* spores on PNIPAM honeycomb structures of varying diameter and on smooth PNIPAM background. Error bars are the standard errror of the mean (SEM) (n = 8).

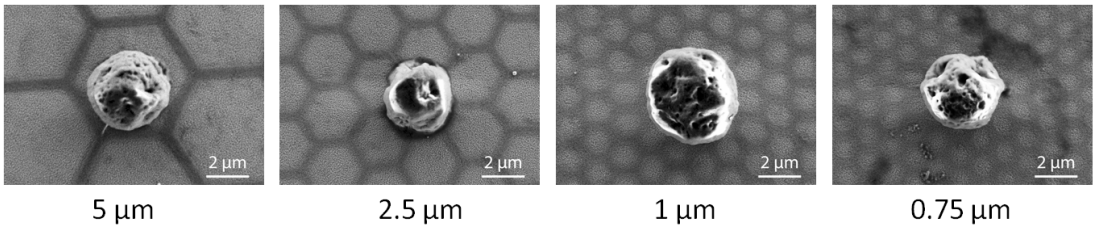

Figure 4.28: SEM images of Ulva spores and their position relative to the respective structure on the four evaluated honeycomb surfaces. Honeycomb diameters are indicated below each image.

the error bars overlap, the results are more meaningful than the ones obtained in earlier studies in our group [179]. Although the number of structured areas is limited, the writing fields are larger and therefore yield better statistics. Since the fluctuation between different surfaces is high, the new layout makes it possible to treat and evaluate all structure sizes the same way.

The results state that *Ulva* spore settlement is reduced on honeycombs of 0.75 µm, 1 µm and 2.5 µm size compared to the corresponding background spore density. This suggests that spores avoid settling on structures featuring these sizes compared to the smooth background. Settlement on the 5 µm structures seems to be as high as on the flat background. The differences are, however, not statistically significant (p value >0.05) as the results differ from sample to sample. Within the three structures that appear to reduce settlement, 1 µm and 2.5 µm show even better results than the 0.75 µm honeycomb structure. Spores avoid settling on these honeycombs when a smooth alternative —which is of the same chemical composition— is offered next to the structure. On the 5 µm structure size the settlement density is nearly the same as on the smooth PNIPAM. An explanation for this similarity could be the small ridge/depression area ratio so that the structuring only plays a minor role.

It appears that the ideal structure size to reduce *Ulva* settlement lies in the low micrometer regime and not in the nanometer range. To evaluate the positions the spores choose during the settlement process on the structured areas post analysis of the samples was performed by scanning electron microscopy after algae evaluation. Figure 4.28 gives an overview of the positions in which *Ulva* spores were situated on the honeycomb patterns. In the case of 0.75 µm and 1 µm diameter honeycombs the ratio between spore and structure is so big that no persuasive conclusion can be drawn from the positions. The situation is different for the 2.5 µm and 5 µm structures. 61 % of the spores present on the 2.5 µm honeycombs were located in the middle of a honeycomb although they are larger than the structure and just 39 % settled on the ridges. Also the 5 µm honeycombs, which are significantly larger in size than the spore body, reveal a similar trend. Here, also 62 % of the spores tend to settle inside the honeycomb pattern and

within this group of spores another 61 % seem to prefer to sit next to the ridge, in the so called 'kink site', rather than in the middle of a honeycomb where smooth PNIPAM is present. Only 38 % of all settled spores were sitting directly on top of a ridge. This observation is in line with other studies in our group where it was observed that spores preferentially settle at the 'kink site' [213]. The difference to a 'non-kink site' or step edge position is that there is one more attachment point available for binding. This is an indication for the ability of spores to detect edges and kinks on a surface. A similar observation was made with barnacle larvae, which showed a strongly increased settlement density on microstructures larger than their body size, which provide maximum anchoring sites [223].

According to recent studies, the length scale of the fouling organism is an important parameter when the effect of surface topography on the adhesion of *Ulva* spores is discussed [102, 103, 224]. Since the Wenzel roughness factor was introduced in 1934 [153], it has been applied in a number of different studies. The Brennan research group developed the dimensionless Engineered Roughness Indices (ERI)

$$ERI_{\mathrm{I}} = \frac{r \cdot df}{1 - \varphi_{\mathrm{s}}} \tag{4.2}$$

and

$$ERI_{\mathrm{II}} = \frac{r \cdot n}{1 - \varphi_{\mathrm{s}}} \tag{4.3}$$

to correlate surface topography and biofouling [103, 214, 215]. There, r is the Wenzel roughness index, df the degree of freedom, n the number of distinct features and $1 - \varphi_{\mathrm{s}}$ the depressed surface area. For fixed microstructures such as those described in their work [103, 196, 225], which consist of a feature spacing of 2 µm and a feature depth of 3 µm, spore settlement is inversely linear to the ERI_{I}. In their studies they used patterned surfaces with ERI_{I} values in the range of 5 to 9.5. In both ERI equations, (4.2) and (4.3), the Wenzel roughness ratio r is proportional to the ERI value. Both, ERI_{I} and ERI_{II}, take the depressed surface area fraction $(1 - \varphi_{\mathrm{s}})$ into account. In ERI_{I} the degree of freedom df to move across the surface is considered, while for ERI_{II} df is replaced by the number n of distinct features [214].

In the present study ERI_{I} values were calculated for the different structure sizes by using the above calculated Wenzel roughness factor. The degree of freedom df relates to the tortuosity of the surface and refers to the ability of *Ulva* spores to follow structures within features of the topographical surface. Since the structures form a continuous grid, spore movement in both the x and y coordinates is permitted and the degree of freedom is 2. The results are shown in Table 4.5.

Figure 4.29 shows the calculated ERI_{I} values plotted against the normalized spore settlement. A correlation can be observed regarding smaller structure sizes in the range of 0.75 µm to 2.5 µm between settlement and ERI_{I}.

Table 4.5: Calculated ERI_{I} with formula (4.2) using the Wenzel roughness factor obtained in Table 4.4.

Honeycomb diameter	r_{Wenzel}	$1-\varphi_{\mathrm{s}}$	ERI_{I}
5.00 µm	1.007	0.75	2.684
2.50 µm	1.012	0.63	3.211
1.00 µm	1.017	0.43	4.730
0.75 µm	1.024	0.35	5.852

For the hexagonally structured surfaces a trend of decreasing settlement with decreasing Wenzel roughness and ERI_{I} was revealed. This contradicts the general ERI model which anticipates lower settlement for an increasing Wenzel roughness that has been calculated on topographies of feature size and spacing above 2 µm [103]. It has to be noted though, that in the study of Schumacher *et al.* only ERI_{I} values higher than 6 were calculated and no data in the range of 2 to 6 is available. Hence, it is possible that there is a deviation from the estimated linear curve, as hinted by the results shown in Figure 4.29.

The 5 µm structures seem to be an exception, as the settlement density here is nearly as high as on the background. Earlier studies serve as an explanation for this observation. As an example the settlement of *Ulva* spores on structured PDMS surfaces with different length scales was compared to settlement on smooth PDMS surfaces. On the PDMS surfaces with 5 µm to 10 µm wide channels, the settlement is enhanced, because the spores fit perfectly into the pits [102]. In con-

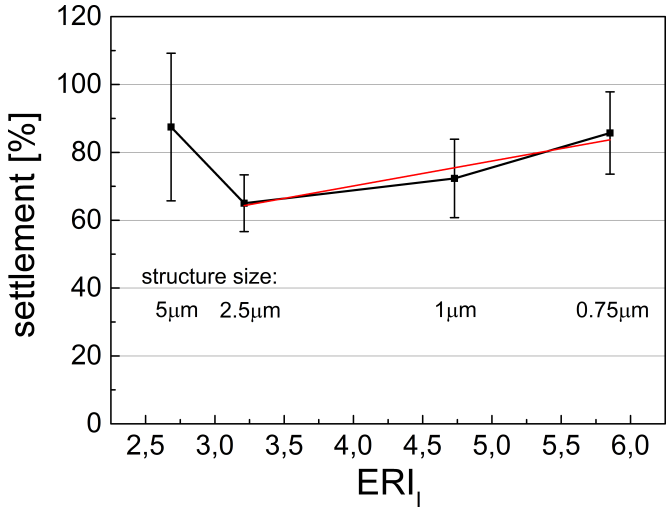

Figure 4.29: Correlation between *Ulva* spore settlement and ERI_{I} on surfaces with varying feature sizes.

trast, surfaces with only 2 µm structures and spacing (as shown in Figure 2.12), settlement is significantly reduced [103]. Both, the honeycomb structured areas with a size of about 1 µm to 2.5 µm, and the topographies evaluated by Schumacher *et al.* with a size of 2 µm seem to be the ideal spacing for effectively reducing *Ulva* settlement. This is probably due to the fact that the contact area between the organisms and the surface is minimized resulting in a weaker attachment [19]. By increasing the structure size above the size of the organism this effect changes. Here the organism is able to increase the attachment area by adhering between the features resulting in an enhancement of settlement.

Besides the size of the features discussed above, also the height can influence the settlement and adhesion behavior of *Ulva* spores [103]. It is assumed that the spores respond to different aspect ratios. Not only the ideal feature size of 2 µm but also the fact that if the features are high enough the organisms are not able to touch the ground can minimize the adhesion. However, the feature height of the structures presented in this thesis is about 45 nm dry polymer brush height. According to the swelling behavior after immersion in water [141, 219], which leads back to the hydration of the polar acid or amide side groups of the polymeric chain, it was detected that the average feature height in water is maximal 11 nm. Since *Ulva* spores have a body size of 5 µm one can imagine that the spore will not have any problems touching the surface between the structures. Thus, the argument given by Schumacher *et al.*, that if the *Ulva* spore is bridged between two topographical features, the surface has only an influence if the spore is not able to contact the floor between features [103], has to be rebuted for polymeric honeycomb structures with lower aspect ratios, since settlement is decreased.

4.4.4 Conclusion

In this section, e-beam lithography was shown as a suitable method to prepare well-defined three-dimensionally structured surfaces down to the nanometer scale. This method is based on electron irradiation of amino terminated self assembled monolayers. Through this irradiation deactivated amino groups are activated and serve as an anchoring site for surface-initiated polymerization. On the activated areas, strong PNIPAM brush growth can be observed in the subsequent polymerization process, while the non-irradiated areas show minimal brush growth leading to a thin and smooth PNIPAM background. Using this technique bioinspired honeycomb morphologies with varying structure sizes were prepared for investigating the impact of surface morphology on the settlement of the green alga *Ulva linza*. The sizes were chosen to be 5 µm, which lies in the range of the size of a spore body and 2.5 µm to feature a size a little bit smaller than the spore body. 1 µm represents a size being much smaller than an *Ulva* spore and 0.75 µm is in the desired nanometer range.

By evaluating the results of the *Ulva* settlement assay it was shown that structures smaller than the body size of a spore reduced settlement. With a feature size in the range of 0.75 µm to 2.5 µm, the contact area between the structures and the spores could be minimized, while for 5 µm structures (which exceed the size of a spore body) the settlement density was in the same range as that of the smooth surface.

A correlation between spore settlement density and surface roughness could be observed by calculating the Wenzel roughness factor. The presented results of the honeycomb surfaces revealed a trend of decreasing settlement with decreasing Wenzel roughness. This is in contrast to the general ERI model which predicts lower settlement for an increasing Wenzel roughness calculated on topographies based on feature size/spacing above 2 µm [103]. The 5 µm structures seemed to be an exception, as the settlement density here was nearly as high as on the background. The organism seemed to be able to increase the attachment area by adhering between the features, which results in an enhanced settlement. 62 % of the settled spores tend to sit inside the honeycomb pattern and within this group another 61 % seem to prefer to sit next to a ridge, in the so called 'kink site', rather than in the middle of a honeycomb where smooth PNIPAM is present. Only 38 % of all settled spores were sitting directly on top of a ridge.

5 Summary and outlook

Biofouling, the undesired growth of marine organisms on surfaces submerged in natural water, is a worldwide phenomenon that occurs in all intertidal zones. Suitable non-toxic coatings for the marine environment are required to prevent unwanted effects caused by adhering organisms.

This work describes the preparation and investigation of surfaces with well-defined properties to improve the understanding of the fouling behavior of microorganisms. The goal was to study how surface chemistry, conditioning and surface morphology influence the adhesion of foulers. The surface chemistry was systematically changed by using chemically different end group terminated self assembled monolayers (SAMs). To examine the influence of surface conditioning, various media were used and the influence of surface topography was evaluated by using nanostructured polymers based on poly(*N*-isopropylacrylamide) (PNIPAM).

Since a conditioning film is formed on a surface as soon as it is immersed in natural water, the influence of such a conditioning film on the settlement behavior of spores of the alga *Ulva linza* was investigated in the first part of this thesis. Therefore surfaces varying in terms of protein resistance and wettabillity were immersed in 'spore water' (SP) (commercial seawater in which spores were allowed to swim for 1 h before being removed) for 1 h to 48 h. Using surface analytical techniques, namely spectral ellipsometry, contact angle goniometry, IRRAS and XPS, it was found that a protein film was formed on all surfaces independent of the chemistry. After just 3 h to 6 h a notable conditioning film has been developed. IR measurements revealed the appearance of carbonyl, amide I and amide II bands, indicating that the formed layer mainly consisted of proteinaceous compounds and that the composition of this film differed in dependence of the hydrophobicity of the samples. While carbonyl, amide I and amide II bands were less pronounced on the hydrophobic samples, the intensity was high on the hydrophilic ones. Furthermore, it was shown that polyethylene glycol (PEG) surfaces deteriorated with increasing incubation time. It is important to note that although the surface thickness decreased, PEG molecules were retained and were clearly detectable on the sample surface.

Following the examination of the formation and the properties of the conditioning films, its implications on the settlement of *Ulva* spores were examined in collaboration with the group of Prof. James Callow at the University of Birmingham, UK. Therefore samples were pre-incubated in SP for 1 h to 24 h. Subsequently, a stan-

dard spore settlement assay was performed. It could be shown that preincubation for 24 h reduced the settlement density for hydrophobic surfaces and increased it for hydrophilic surfaces, resulting in an equalization of the number of settled spores. The maximum effect on spore settlement was a 50 % decrease/increase related to the total amount of settled spores on pristine surfaces. However, this is a worst-case scenario of the potential effect of a conditioning film, since in a standard 45 min bioassay, the test surfaces are not preconditioned, i.e. the test surfaces were exposed to both spores and conditioning molecules at the same time. While for such standard spore assays the effect of conditioning is likely to be neglectable, this work suggests that care must be taken for any laboratory study on longer time scales as surface conditioning can significantly affect the outcome of the assay.

In literature, many studies are published of coatings being immersed into the ocean for two or more months, but very little is known about the composition of the first fouling communities in field experiments on well defined model surfaces like SAMs. As the conditioning of a surface is one of the fastest steps in the fouling process, and since until now the chemical nature of such adsorbed layers is still poorly characterized, the main focus of the second part of this thesis was the investigation of the time dependent formation of conditioning films on chemically different surfaces using natural seawater. For this purpose water was collected at two static immersion test sites at the Florida Institute of Technology (collaboration with the group of Prof. Geoffrey Swain), filtered and used to precondition the same types of substrates used for the laboratory assays with *Ulva* spores. These results are in line with the findings obtained using 'spore water'. The layer thicknesses and changes of the contact angles of the conditioning films formed with natural seawater were all in the same range. Though, IR measurements showed differences in the composition of the films compared to both SP and each other. Furthermore, it became clear that the PEG surfaces were not stable in seawater but the protein resistance was maintained up to 48 h of incubation time. By increasing the immersion time up to 1 week, the PEG layer completely disassembled and only proteins from the seawater were present on the surface.

The effect of this conditioning film on the settlement of other marine organisms was studied. Therefore samples were pre-incubated in seawater for 24 h. Subsequently, preconditioned and pristine surfaces were immersed into the ocean for another 24 h. Afterwards the fouling communities on the samples were evaluated by light microscopy. The most dominant organisms observed on the surfaces were diatoms (*Navicula*, *Amphora*, *Cylindrotheca* and *Baccillaria*) and the protozoa *Peritrich ciliate*. It was found that the distribution of the organisms was nearly the same for all samples independent of the surface chemistry and conditioning. Interestingly it was observed that samples with a higher concentration of proteinaceous compounds are more attractive for marine organisms.

Microbial biofilms represent a well known bacterial mode of growth in which the microorganisms benefit from metabolic exchange and protection. The bacterial adhesion process includes an initial physico-chemical interaction phase in which surface wettability is considered to play an important role. In the third part of this thesis the formation of a conditioning layer and the determination of the settlement kinetics of *Pseudomonas aeruginosa* bacteria were examined. Therefore hydrophobic and hydrophilic surfaces were immersed in two kinds of media usually used for bacterial assays, protein rich BHi medium and less proteinaceous BM2 medium. It was found that the conditioning layers formed with BHi medium are thicker than those from BM2 medium and lie in the same range as for SP or natural seawater. Another point to be mentioned is that the hydrophobic samples were more attractive for proteins and thus the layer thickness was higher on these substrates than on the hydrophilic ones, which is also in line with previous findings.

Furthermore, it was investigated as to what extent a conditioning film influences the adhesion behavior of bacteria. These experiments were performed in collaboration with the group of Prof. Ursula Obst at the Institute of Functional Interfaces, Karlsruhe Institute of Technology, Germany. The two different media types were used to perform adhesion assays. It was observed that after an experiment time of 10 min the amount of organisms attached to the surface reached a maximum independent of the media type. In line with other studies in our group, it was found that the surface chemistry has no influence on the adhesion behavior of the bacteria. Although proteinaceous films were formed using BHi medium, the adhesion behavior of the bacteria was not affected.

In conclusion, it was demonstrated that conditioning films play a major role in laboratory assays for the tested SAMs. Conditioning also had a slight influence in field studies. Thus these films should be considered in the planning of long term laboratory and field studies. In the future, more experiments concerning the formation of conditioning films should be done with other surface chemistries such as ethylene glycol SAMs with decreasing wettability. Since it is known that these substrates are protein resistant, it would be interesting to investigate if a conditioning film is able to accumulate on these substrates. Furthermore, the focus of laboratory assays should not only lie in short term evaluation since it was shown that the whole biofouling process occurs on a much longer timescale. Another interesting point would be to identify the proteins which play a major role in the formation of the conditioning film.

Besides surface chemistry and conditioning, morphology is also an important surface property which could have an impact on the fouling process. The skin of sharks, for example, has the unique property of reducing the adhesion of foulers by being structured with microscalar denticle structures. To explore this morphological influence on *Ulva* spore settlement, e-beam activation lithography (EBAL) was performed in the last part of the thesis within the Karlsruhe Nano Micro Fa-

cility (KNMF) at the Karlsruhe Institute of Technology and subsequent surface-initiated polymerization was applied to prepare nanopatterned polymer surfaces. Therefore SAMs with amino groups were used to establish reactive sites on the surface via e-beam, from which polymer brushes can be grown. This method provides extensive growth of polymer brushes on the irradiated areas. Even more important is the consistent growth of a thin, homogeneous background brush on the non irradiated areas which allows the analysis of surface structures independent of surface chemistry. Inspired by the nanostructured skin of the pilot wale, a honeycomb topography was chosen. PNIPAM structures with varying honeycomb diameters ranging from 0.75 µm to 5 µm were prepared. The results showed that the size of the pattern had an effect on the settlement. Structures from 0.75 µm to 2.5 µm reduced *Ulva* spore settlement in comparison to the smooth background, due to the reduction of available contact areas between the spores and the sample. The calculated Wenzel roughness factor revealed a trend of decreasing settlement with decreasing Wenzel roughness. This is in contrast to general findings which predicted lower settlement for an increasing Wenzel roughness calculated on topographies based on feature size and spacing above 2 µm. The obtained results are noteworthy since polymer structures with a wet ridge height in the range of 0.01 µm still influenced the settlement behavior of spores with a body size of about 5 µm.

For future experiments it would be interesting to investigate the lowest sensing limit of the spores towards surface structures. Therefore the height of the polymer structures should be systematically varied and the influence of the wall thickness of the ridges should be evaluated in terms of varying structure diameters. This is interesting for structures larger than 5 µm, since within these sizes the ridge/background ratio is very low. Since EBAL allows the preparation of complex patterns, other structure features inspired by nature could be designed. Due to the fact that the population of biofouling organisms includes a diverse range of species with different sizes covering a range of several orders of magnitudes, one single topography pattern will not be sufficient to effectively reduce settlement in the natural environment.

List of abbreviations

μCP	Microcontact printing
AFM	Atomic force microscopy
AT-IR	Attenuated internal reflection infrared spectroscopy
ATRP	Atom transfer radical polymerization
AUDT	11-Amino-1-undecanethiol hydrochloride
BHi	Brain heart infusion
BIBB	2-Bromoisobutyryl bromide
BM2	Basal medium 2
BSA	Bovine serum albumin
BSE	Back-scattered electrons
CA	Contact angle
CFU	Colony-forming units
CH_2Cl_2	Dichloromethan
CW	Cape water
DDT	1-Dodecanethio
DOC	Dissolved organic carbon
EBAL	Electron beam activated lithography
EBL	Electron beam lithography
EG	Ethylene glycol
EPS	Extracellular polymeric substances
ERI	Engineered Roughness Index
ESCA	Electron spectroscopy for chemical analysis
FIB	Focused ion beam lithography
FOV	Field of view
FTIR	Fourier transform infrared spectroscopy
FUDT	11-(Tridecafluorooctyl-oxy)undecanethiol

HCl	Hydrochloric acid
HUDT	11-Mercapto-1-undecanol
IMO	International Maritime Organization
IO	Instant Ocean®
IP	Inkjet printing
IRRAS	Infrared reflection absorption spectroscopy
KNMF	Karlsruhe Nano Micro Facility (KNMF)
ML	Magnetolithography
MQ	MilliQ®
NEt_3	Trimethylamine
NIL	Nanoimprint lithography
NIPAM	N-Isopropylacrylamide
PBS	Phosphate buffered saline
PDMS	Polydimethylsiloxane elastomer
PEG	Polyethylene glycol
PMDETA	*N*,*N*,*N'*,*N"*,*N"*-pentamethyldiethylenetriamine
PNIPAM	Poly(*N*-isopropylacrylamide)
PSD	Position sensitive device
RAFT	Reversible addition fragmentation chain transfer
RNase A	Ribonuclease A
rpm	Rounds per minute
RT	Room temperature
RW	Raft water
SAM	Self assembled monolayer
SE	Secondary electrons
SEM	Scanning electron microscopy
SI-ATRP	Surface-initiated atom transfer radical polymerization
SIP	Surface-initiated polymerization
SP	Spore water
STM	Scanning tunneling microscopy
SW	Salt water
TBT	Tributyltin

TM	Tropic Marin®
UV	Ultraviolet
XPS	X-ray photoelecton spectroscopy

List of publications

Published articles

- I. Thome, M. E. Pettitt, M. E. Callow, J. A. Callow, M.Grunze, and A. Rosenhahn.
  Conditioning of surfaces by macromolecules and its implication for the settlement of zoospores of the green alga *Ulva linza*.
  Biofouling, 28(5):501-510, 2012.
- S. Maleschlijski, G. H. Sendra, A. Di Fino, L. Leal-Taixe, I. Thome, A. Terfort, N. Aldred, M. Grunze, A. S. Clare, B. Rosenhahn, and A. Rosenhahn.
  Three dimensional tracking of exploratory behavior of barnacle cyprids using stereoscopy.
  Biointerphases, 7(50):1-9, 2012.
- C. Christophis, K. Sekeroglu, G. Demirel, I. Thome, M. Grunze, M. C. Demirel, and A. Rosenhahn.
  Fibroblast adhesion on unidirectional polymeric nanofilms.
  Biointerphases, 6(4):158-163, 2011.

Articles in preparation

- I. Thome, S. Bauer, S. Stuppy, K. Zargiel, M. Alles, M.P. Arpa-Sancet, G. Swain, M. Grunze, and A. Rosenhahn.
  Conditioning of self assembled monolayers and its implication for fouling in the field.
  in preparation.
- M. P. Arpa-Sancet, I. Thome, S. Bauer, K. Zargiel, A. Hucknall, M. Alles, S. Stuppy, A. Chilkoti, G. Swain, M. Grunze, and A. Rosenhahn.
  Early colonization of self assembled monolayers, ethylene glycols and polysaccharides by biofouling organisms studied at the FIT test site.
  in preparation.

List of conferences

- 8.-10. December 2009, St. Petersburg, FL, USA.
  International Workshop on concepts and strategies for surface engineering to control biofouling.
- 13.-15. Mai 2010, Bielefeld, Germany.
  Bunsentagung.
  Poster presentation.
- 18.-20. Mai 2010, Heidelberg, Germany.
  Seacoat Advanced Training Course 1 (Surface Engineering).
- 12.-14. Juli 2010, Zürich, Switzerland.
  Seacoat Advanced Training Course 2 (Surface Analytic).
- 25.-29. Juli 2010, Newcastle, UK.
  15^{th} International Congress of Marine Corrosion and Fouling.
  Poster presentation. Winner of the poster award.
- 7.-9. September 2010, Birmingham, UK.
  Seacoat Advanced Training Course 3 (Bioadhesion).
- 3.-8. April 2011, Buzioz, Brasil.
  7^{th} Brazilian/German Workshop on applied Surface Science.
  Poster presentation.
- 12.-14. October 2011, Heidelberg, Germany.
  Bunsenkolloquium/-diskussionstagung 2011.
  Poster presentation.
- 30. October-4. November 2011, Nashville, TN, USA.
  AVS 58^{th} International Symposium and Exhibition.
  Oral presentation.
- 11.-17. March 2012, St. Christoph, Austria.
  25. Symposium on Surface Science 2012.
  Poster presantation.
- 24.-28. Juni 2012, Seattle, WA, USA.
  16^{th} International Congress of Marine Corrosion and Fouling.
  Poster presentation. Winner of the poster award.

Bibliography

[1] C. M. Magin, S. P. Cooper, and A. B. Brennan.
Non-toxic antifouling strategies.
Materials Today, 13(4):36–44, 2010.

[2] A. Rosenhahn, T. Ederth, and M. E. Pettit.
Advanced nanostructures for the control of biofouling: The FP6 EU Integrated Project AMBIO.
Biointerphases, 3(1):IR1–IR5, 2008.

[3] J. A. Callow and M. E. Callow.
Trends in the development of environmentally friendly fouling-resistant marine coatings.
Nature Communications, 2(244):1–10, 2011.

[4] J. A. Callow.
Some new insights into marine biofouling.
World super yacht, (35):34–39, 2003.

[5] J. A. Callow.
Marine Biofouling: a sticky problem.
Biologist, 49(1):1–5, 2002.

[6] M. Leer-Andersen and L. Larsson.
An experimental/numerical approach for evaluating skin friction on full-scale ships with surface roughness.
Journal of Marine Science and Technology, 8(1):26–36, 2003.

[7] M. P. Schultz.
Effects of coating roughness and biofouling on ship resistance and powering.
Biofouling, 23(5):331–341, 2007.

[8] S. M. Evans, A. C. Birchenough, and M. S. Brancato.
The TBT ban: Out of the prying pan into the fire?
Marine Pollution Bulletin, 40(3):204–211, 2000.

[9] J. J. Corbett and H. W. Koehler.
Updated emissions from ocean shipping.
Journal of Geophysical Research-Atmospheres, 108(D20):1–13, 2003.

[10] T. G. Estes, A. W. Feinberg, M. E. Callow, G. Swain, and A. B. Brennan.
Settlement and release of *Balanus* and *Ulva* as a function of pdms elastomer surface energy.
Polymer Preprints, 45(1):610–611, 2004.

[11] K. A. Dafforn, T. M. Glasby, and E. L. Johnston.
Differential effects of tributyltin and copper antifoulants on recruitment of non-indigenous species.
Biofouling, 24(1):23–33, 2008.

[12] S. M. Evans, T. Leksono, and P. D. McKinnell.
Tributyltin pollution - a diminishing problem following legislation limiting the use of TBT-based antifouling paints.
Marine Pollution Bulletin, 30(1):14–21, 1995.

[13] A. M. Rouhi.
The squeeze on tributyltins.
Chemical & Engineering News, 76(17):41–42, 1998.

[14] E. D. Goldberg.
TBT - an environmental dilemma.
Environment, 28(8):17–44, 1986.

[15] S. M. Evans.
TBT or not TBT?: That is the question.
Biofouling, 14(2):117–129, 1999.

[16] C. Alzieu.
Environmental problems caused by TBT in France - Assessment, Regulations, Prospects.
Marine Environmental Research, 32(1-4):7–17, 1991.

[17] N. Spooner, P. E. Gibbs, G. W. Bryan, and L. J. Goad.
The effect of tributyltin upon steroid titers in the female dogwhelk, *Nucella lapillus*, and the development of imposex.
Marine Environmental Research, 32(1-4):37–49, 1991.

[18] D. M. Yebra, S. Kiil, and K. Dam-Johansen.
Antifouling technology - past, present and future steps towards efficient and environmentally friendly antifouling coatings.
Progress in Organic Coatings, 50(2):75–104, 2004.

[19] A. J. Scardino, E. Harvey, and R. De Nys.
Testing attachment point theory: diatom attachment on microtextured polyimide biomimics.
Biofouling, 22(1):55–60, 2006.

[20] L. K. Ista, M. E. Callow, J. A. Finlay, S. E. Coleman, A. C. Nolasco, R. H. Simons, J. A. Callow, and G. P. Lopez.
Effect of substratum surface chemistry and surface energy on attachment of marine bacteria and algal spores.
Applied and Environmental Microbiology, 70(7):4151–4157, 2004.

[21] S. Schilp, A. Küller, A. Rosenhahn, M. Grunze, M. E. Pettit, M. E. Callow, and J. A. Callow.
Settlement and adhesion of algal cells to hexa (ethylene glycol)-containing self-assembled monolayers with systematically changed wetting properties.
Biointerphases, 2(4):143–150, 2007.

[22] J. A. Callow, M. E. Callow, L. K. Ista, G. Lopez, and M. K. Chaudhury.
The influence of surface energy on the wetting behaviour of the spore adhesive of the marine alga *Ulva linza* (synonym *Enteromorpha linza*).
Journal of the Royal Society Interface, 2(4):319–325, 2005.

[23] T. Ekblad, G. Bergstroem, T. Ederth, S. L. Conlan, R. Mutton, A. S. Clare, S. Wang, Y. L. Liu, Q. Zhao, F. D'Souza, G. T. Donnelly, P. R. Willemsen, M. E. Pettit, M. E. Callow, J. A. Callow, and B. Liedberg.
Poly(ethylene glycol)-containing hydrogel surfaces for antifouling applications in marine and freshwater environments.
Biomacromolecules, 9(10):2775–2783, 2008.

[24] X. Cao, M. E. Pettitt, F. Wode, M. P. Arpa-Sancet, J. Fu, J. Ji, M. E. Callow, J. A. Callow, A. Rosenhahn, and M. Grunze.
Interaction of zoospores of the green alga *Ulva* with bioinspired micro- and nanostructured surfaces prepared by polyelectrolyte layer-by-layer self-assembly.
Advanced Functional Materials, 20(12):1984–1993, 2010.

[25] A. Ulman.
Formation and structure of self-assembled monolayers.
Chemical Reviews, 96(4):1533–1554, 1996.

[26] J. C. Love, L. A. Estroff, J. K. Kriebel, R. G. Nuzzo, and G. M. Whitesides.
Self-assembled monolayers of thiolates on metals as a form of nanotechnology.
Chemical Reviews, 105:1103–1169, 2005.

[27] M. Kind and C. Wöll.
Organic surfaces exposed by self-assembled organothiol monolayers: Preparation, characterization, and application.
Progress in Surface Science, 84(7-8):230–278, 2009.

[28] J. A. Callow and M. E. Callow.
Biofilms.
Marine Molecular Biotechnology, 42:141–169, 2006.

[29] D. L. Kirchman.
The ecology of cytophaga-flavobacteria in aquatic environments.
FEMS Microbiology Ecology, 39(2):91–100, 2002.

[30] S. Krishnan, N. Wang, C. K. Ober, J. A. Finlay, M. E. Callow, J. A. Callow, A. Hexemer, K. E. Sohn, E. J. Kramer, and D. A. Fischer.
Comparison of the fouling release properties of hydrophobic fluorinated and hydrophilic PEGylated block copolymer surfaces: Attachment strength of the diatom *Navicula* and the green alga *Ulva*.
Biomacromolecules, 7(5):1449–1462, 2006.

[31] J. Genzer and K. Efimenko.
Recent developments in superhydrophobic surfaces and their relevance to marine fouling: a review.
Biofouling, 22(5):339–360, 2006.

[32] C. Baum, W. Meyer, R. Stelzer, L. G. Fleischer, and D. Siebers.
Average nanorough skin surface of the pilot whale (*Globicephala melas*, Delphinidae): considerations on the self-cleaning abilities based on nanoroughness.
Marine Biology, 140(3):653–657, 2002.

[33] M. L. Carman, T. G. Estes, A. W. Feinberg, J. F. Schumacher, W. Wilkerson, L. H. Wilson, M. E. Callow, J. A. Callow, and A. B. Brennan.
Engineered antifouling microtopographies - correlating wettability with cell attachment.
Biofouling, 22(1):11–21, 2006.

[34] S. Dürr and J. Thomason.
Biofouling.
Wiley & Sons, 2009.
Chapter 1.

[35] E. Almeida, T. C. Diamantino, and O. de Sousa.
Marine paints: The particular case of antifouling paints.
Progress in Organic Coatings, 59(1):2–20, 2007.

[36] A. Jain and N. B. Bhosle.
Biochemical composition of the marine conditioning film: implications for bacterial adhesion.
Biofouling, 25(1):13–19, 2009.

[37] M. E. Callow and R. L. Fletcher.
The influence of low surface energy materials on bioadhesion - a review.
International Biodeterioration & Biodegradation, 34(3-4):333–348, 1994.

[38] S. Abarzua and S. Jakubowski.
Surface thermodynamics of bacterial adhesion.
Applied and Environmental Microbiology, 46(1):90–97, 1983.

[39] L. D. Chambers, K. R. Stokes, F. C. Walsh, and R. J. K. Wood.
Modern approaches to marine antifouling coatings.
Surface & Coatings Technology, 201(6):3642–3652, 2006.

[40] M. Wahl.
Marine epibiosis. 1. fouling and antifouling: some basic aspects.
Marine ecology progress series, 58(1-2):175–189, 1989.

[41] M. E. Callow, J. A. Callow, J. D. Pickett-Heaps, and R. Wetherbee.
Primary adhesion of *Enteromorpha* (Chlorophyta, Ulvales) propagules: Quantitative settlement studies and video microscopy.
Journal of Phycology, 33(6):938–947, 1997.

[42] D. Roberts, D. Rittschof, E. Holm, and A. R. Schmidt.
Factors influencing initial larval settlement: temporal, spatial and surface molecular components.
Journal of Experimental Marine Biology and Ecology, 150(2):203–221, 1991.

[43] C. Compère, M. N. Bellon-Fontaine, P. Bertrand, D. Costa, P. Marcus, C. Poleunis, C. M. Pradier, B. Rondot, and M. G. Walls.
Kinetics of conditioning layer formation on stainless steel immersed in seawater.
Biofouling, 17(2):129–145, 2001.

[44] G. T. Taylor, D. Zheng, M. Lee, P. J. Troy, G. Gyananath, and S. K. Sharma.
Influence of surface properties on accumulation of conditioning films and marine bacteria on substrata exposed to oligotrophic waters.
Biofouling, 11(1):31–57, 1997.

[45] B. C. van der Aa and Y. F. Dufrene.
In situ characterization of bacterial extracellular polymeric substances by AFM.
Colloids and Surfaces B-Biointerfaces, 23(2-3):173–182, 2002.

[46] R. E. Baier.
Influence of the initial surface condition of materials on bioadhesion.

In *Proc 3rd Int Congr Marine Corrosion and Fouling. Northwestern University Press, Evanston, Illinois*, pages 633–639, 1973.

[47] D. P. Bakker, H. J. Busscher, J. van Zanten, J. de Vries, J. W. Klijnstra, and H. C. van der Mei.
Multiple linear regression analysis of bacterial deposition to polyurethane coating after conditioning film formation in the marine environment.
Microbiology-SGM, 150(6):1779–1784, 2004.

[48] D. L. Kirchman, D. L. Henry, and S. C. Dexter.
Adsorption of proteins to surfaces in seawater.
Marine Chemistry, 27(3-4):201–217, 1989.

[49] G. I. Loeb and R. A. Neihof.
Marine conditioning films.
Advances in Chemistry Series, 145:319–335, 1975.

[50] B. R. Zaidi, R. F. Bard, and T. R. Tosteson.
Microbial specificity of metallic surfaces exposed to ambient seawater.
Applied and Environmental Microbiology, 48(3):519–524, 1984.

[51] D. S. Marszalek, S. M. Gerchakov, and L. R. Udey.
Influence of substrate composition on marine microfouling.
Applied and Environmental Microbiology, 38(5):987–995, 1979.

[52] N. B. Bhosle, A. Garg, L. Fernandes, and P. Citon.
Dynamics of amino acids in the conditioning film developed on glass panels immersed in the surface seawaters of Dona Paula Bay.
Biofouling, 21(2):99–107, 2005.

[53] B. J. Little, P. Wagner, J. S. Maki, M. Walch, and R. Mitchell.
Factors influencing the adhesion of microorganisms to surfaces.
The Journal of Adhesion, 20(3):187–210, 1986.

[54] P. Stoodley, K. Sauer, D. G. Davies, and J. W. Costerton.
Biofilms as complex differentiated communities.
Annual Review of Microbiology, 56:187–209, 2002.

[55] L. Hall-Stoodley, J. W. Costerton, and P. Stoodley.
Bacterial biofilms: from the natural environment to infectious diseases.
Nature Reviews Microbiology, 2(2):95–108, 2004.

[56] P. H. Raven, R. F. Evert, and S. E. Eichhorn.
Biologie der Pflanzen.
De Gruyter, 2006.
Chapter 16.

[57] A. O. Christie and L. V. Evans.
Periodicity in the liberation of gametes and zoospores of *Enteromorpha intestinalis* link.
Nature, 193(4811):193–194, 1962.

[58] R. L. Fletcher and M. E. Callow.
The settlement, attachment and establishment of marine algal spores.
British Phycological Journal, 27(3):303–329, 1992.

[59] J. A. Callow and M. E. Callow.
The Ulva spore adhesive system. In: Smith, A. M. and Callow, J. A., Biological Adhesives.
Springer, 2010.

[60] S. Dobretsov and P.-Y. Qian.
Facilitation and inhibition of larval attachment of the bryozoan *Bugula neritina* in association with mono-species and multi-species biofilms.
Journal of Experimental Marine Biology and Ecology, 333(2):263–274, 2006.

[61] G. Swain, A. C. Anil, R. E. Baier, F.-S. Chia, E. Conte, A. Cook, M. Hadfield, E. Haslbeck, E. Holm, C. Kavanagh, D. Kohrs, B. Kovach, C. Lee, L. Mazzella, A. E. Meyer, P.-Y. Qian, S. S. Sawant, M. Schultz, J. Sigurdsson, C. Smith, L. Soo, A. Terlizzi, A. Wagh, R. Zimmerman, and V. Zupo.
Biofouling and barnacle adhesion data for fouling-release coatings subjected to static immersion at seven marine sites.
Biofouling, 16(2-4):331–344, 2000.

[62] K. A. Zargiel, J. S. Coogan, and G. Swain.
Diatom community structure on commercially available ship hull coatings.
Biofouling, 27(9):955–965, 2011.

[63] G. Swain, S. Herpe, E. Ralston, and M. Tribou.
Short-term testing of antifouling surfaces: the importance of colour.
Biofouling, 22(6):425–429, 2006.

[64] G. M. Whitesides, J. P. Mathias, and C. T. Seto.
Molecular self-assembly and nanochemistry: a chemical strategy for the synthesis of nanostructures.
Science, 254(5036):1312–1319, 1991.

[65] R. G. Nuzzo and D. L. Allara.
Adsorption of bifunctional organic disulfides on gold surfaces.
Journal of the American Chemical Society, 105(13):4481–4483, 1983.

[66] M. Jaschke, H. Schönherr, H. Wolf, H.-J. Butt, E. Bamberg, M. K. Besocke, and H. Ringsdorf.
Structure of alkyl and perfluoroalkyl disulfide and azobenzenethiol monolayers on gold(111) revealed by atomic force microscopy.
The Journal of Physical Chemistry, 100(6):2290–2301, 1996.

[67] G. Liu and M. B. Salmeron.
Reversible displacement of chemisorbed n-alkanethiol molecules on Au(111) surface: an atomic force microscopy study.
Langmuir, 10(2):367–370, 1994.

[68] R. G. Nuzzo, B. R. Zegarski, and L. H. Dubois.
Fundamental studies of the chemisorption of organosulfur compounds on gold(111). Implications for molecular self-assembly on gold surfaces.
Journal of the American Chemical Society, 109(3):733–740, 1987.

[69] C. D. Bain and G. M. Whitesides.
Molecular level control over surface order in self-assembled monolayer films of thiols on gold.
Science, 240(4848):62–63, 1988.

[70] L. H. Dubois and R. G. Nuzzo.
Synthesis, structure, and properties of model organic surfaces.
Annual Review of Physical Chemistry, 43(1):437–463, 1992.

[71] H. Sellers, A. Ulman, Y. Shnidman, and J. E. Eilers.
Structure and binding of alkanethiolates on gold and silver surfaces: implications for self-assembled monolayers.
Journal of the American Chemical Society, 115(21):9389–9401, 1993.

[72] C. D. Bain and G. M. Whitesides.
Modeling organic surfaces with self-assembled monolayers.
Angewandte Chemie International Edition in English, 28(4):506–512, 1989.

[73] H.-J. Himmel and C. Wöll.
Herstellung organischer dünnstschichten.
Chemie in unserer Zeit, 32(6):294–301, 1998.

[74] G. Hähner, M. Kinzler, C. Thümmler, C. Wöll, and M. Grunze.
Structure of self-organizing organic films: A near edge x-ray absorption fine structure investigation of thiol layers adsorbed on gold.
Journal of Vacuum Science Technology A: Vacuum, Surfaces, and Films, 10(4):2758–2763, 1992.

[75] G. E. Poirier and M. J. Tarlov.

The c(4x2) superlattice of n-alkanethiol monolayers self-assembled on Au(111).
Langmuir, 10(9):2853–2856, 1994.

[76] N. Camillone III, C. E. D. Chidsey, G. Liu, and G. Scoles.
Superlattice structure at the surface of a monolayer of octadecanethiol self-assembled on Au(111).
The Journal of Chemical Physics, 98(4):3503–3511, 1993.

[77] P. E. Laibinis, G. M. Whitesides, D. L. Allara, Y. T. Tao, A. N. Parikh, and R. G. Nuzzo.
Comparison of the structures and wetting properties of self-assembled monolayers of n-alkanethiols on the coinage metal surfaces, copper, silver, and gold.
Journal of the American Chemical Society, 113(19):7152–7167, 1991.

[78] M. Himmelhaus, I. Gauss, M. Buck, F. Eisert, C. Wöll, and M. Grunze.
Adsorption of docosanethiol from solution on polycrystalline silver surfaces: an xps and nexafs study.
Journal of Electron Spectroscopy and Related Phenomena, 92(1-3):139 –149, 1998.

[79] O. Alexiadis, V. A. Harmandaris, V. G. Mavrantzas, and L. D. Site.
Atomistic simulation of alkanethiol self-assembled monolayers on different metal surfaces via a quantum, first-principles parametrization of the sulfur-metal interaction.
The Journal of Physical Chemistry C, 111(17):6380–6391, 2007.

[80] D. L. Allara.
In: Feast, W. J. and Munro, H. S. and Richards, R. W., Polymer surfaces and interfaces II.
Wiley & Sons, 1993.

[81] R. E. Baier and V. A. DePalma.
The relation of the internal surface of grafts to thrombosis. In: Dale, W. A., Management of arterial occlusive disease.
Yearbook Medical Publishers Chicago (IL), 1971.

[82] M. E. Schrader.
On adhesion of biological substances to low energy solid surfaces.
Journal of Colloid and Interface Science, 88(1):296–297, 1982.

[83] M. E. Callow, J. A. Callow, L. K. Ista, S. E. Coleman, A. C. Nolasco, and G. P. Lopez.

Use of self-assembled monolayers of different wettabilities to study surface selection and primary adhesion processes of green algal (*Enteromorpha*) zoospores.
Applied and Environmental Microbiology, 66(8):3249–3254, 2000.

[84] A. Rosenhahn, S. Schilp, H. J. Kreuzer, and M. Grunze.
The role of 'inert' surface chemistry in marine biofouling prevention.
Physical Chemistry Chemical Physics, 12(17):4275–4286, 2010.

[85] J. A. Finlay, M. E. Callow, L. K. Ista, G. P. Lopez, and J. A. Callow.
The influence of surface wettability on the adhesion strength of settled spores of the green alga *Enteromorpha* and the diatom *Amphora*.
Integrative and Comparative Biology, 42(6):1116–1122, 2002.

[86] B. Wigglesworth-Cooksey, H. van der Mei, H. J. Busscher, and K. E. Cooksey.
The influence of surface chemistry on the control of cellular behavior: studies with a marine diatom and a wettability gradient.
Colloids and Surfaces B: Biointerfaces, 15(1):71–80, 1999.

[87] J. A. Finlay, S. Krishnan, M. E. Callow, J. A. Callow, R. Dong, N. Asgill, K. Wong, E. J. Kramer, and C. K. Ober.
Settlement of *Ulva* zoospores on patterned fluorinated and PEGylated monolayer surfaces.
Langmuir, 24(2):503–510, 2008.

[88] L. K. Ista and G. P. Lopez.
Interfacial tension analysis of oligo(ethylene glycol)-terminated self-assembled monolayers and their resistance to bacterial attachment.
Langmuir, 28(35):12844–12850, 2012.

[89] C. Christophis, M. Grunze, and A. Rosenhahn.
Quantification of the adhesion strength of fibroblast cells on ethylene glycol terminated self-assembled monolayers by a microfluidic shear force assay.
Physical Chemistry Chemical Physics, 12(17):4498–4504, 2010.

[90] A. Statz, J. Finlay, J. Dalsin, M. E. Callow, J. A. Callow, and P. B. Messersmith.
Algal antifouling and fouling-release properties of metal surfaces coated with a polymer inspired by marine mussels.
Biofouling, 22(6):391–399, 2006.

[91] S. Schilp, A. Rosenhahn, M. E. Pettitt, J. Bowen, M. E. Callow, J. A. Callow, and M. Grunze.

Physicochemical properties of (ethylene glycol)-containing self-assembled monolayers relevant for protein and algal cell resistance.
Langmuir, 25(17):10077–10082, 2009.

[92] K. L. Prime and G. M. Whitesides.
Adsorption of proteins onto surfaces containing end-attached oligo(ethylene oxide) - a model system using self-assembled monolayers.
Journal of the American Chemical Society, 115(23):10714–10721, 1993.

[93] James A. Callow and Maureen E. Callow.
The ulva spore adhesive system.
Biological Adhesives, pages 63–78, 2006.

[94] A. Rosenhahn, J. A. Finlay, M. E. Pettit, A. Ward, W. Wirges, R. Gerhard, M. E. Callow, M. Grunze, and J. A. Callow.
Zeta potential of motile spores of the green alga *Ulva linza* and the influence of electrostatic interactions on spore settlement and adhesion strength.
Biointerphases, 4(1):7–11, 2009.

[95] R. E. Holmlin, X. X. Chen, R. G. Chapman, S. Takayama, and G. M. Whitesides.
Zwitterionic SAMs that resist nonspecific adsorption of protein from aqueous buffer.
Langmuir, 17(9):2841–2850, 2001.

[96] L. Petrone, A. Di Fino, N. Aldred, P. Sukkaew, T. Ederth, A. S. Clare, and B. Liedberg.
Effects of surface charge and Gibbs surface energy on the settlement behaviour of barnacle cyprids (*Balanus amphitrite*).
Biofouling, 27(9):1043–1055, 2011.

[97] A. Kesel and R. Liedert.
Learning from nature: Non-toxic biofouling control by shark skin effect.
Comparative Biochemistry and Physiology Part A: Molecular & Integrative Physiology, 146(4):S130–S130, 2007.

[98] D. S. Baum.
Umweltneutrales Antifouling, eine Delphinhaut für Schiffe.
Biologie in unserer Zeit, 34(5):298–305, 2004.

[99] A. Kesel and R. Liedert.
Antifouling nach biologischem Vorbild.
Forschungsbericht der HS Bremen, 107:107–108, 2006.

[100] J. M. Hills, J. C. Thomason, and J. Muhl.

Settlement of barnacle larvae is governed by euclidean and not fractal surface characteristics.
Functional Ecology, 13(6):868–875, 1999.

[101] A. J. Scardino, J. Guenther, and R. de Nys.
Attachment point theory revisited: the fouling response to a microtextured matrix.
Biofouling, 24(1):45–53, 2008.

[102] M. E. Callow, A. R. Jennings, A. B. Brennan, C. E. Seegert, A. Gibson, L. Wilson, A. Feinberg, R. Baney, and J. A. Callow.
Microtopographic cues for settlement of zoospores of the green fouling alga *Enteromorpha*.
Biofouling, 18(3):229–236, 2002.

[103] J. F. Schumacher, M. L. Carman, T. G. Estes, A. W. Feinberg, L. H. Wilson, M. E. Callow, J. A. Callow, J. A. Finlay, and A. B. Brennan.
Engineered antifouling microtopographies - effect of feature size, geometry, and roughness on settlement of zoospores of the green alga *Ulva*.
Biofouling, 23(1):55–62, 2007.

[104] A. Kumar and G. M. Whitesides.
Patterned condensation figures as optical diffraction gratings.
Science, 263(5143):60–62, 1994.

[105] R. K. Smith, P. A. Lewis, and P. S. Weiss.
Patterning self-assembled monolayers.
Progress in Surface Science, 75(1-2):1–68, 2004.

[106] S. Y. Chou, P. R. Krauss, and P. J. Renstrom.
Nanoimprint lithography.
Journal of Vacuum Science Technology B: Microelectronics and Nanometer Structures, 14(6):4129–4133, 1996.

[107] L. J. Guo.
Nanoimprint lithography: Methods and material requirements.
Advanced Materials, 19(4):495–513, 2007.

[108] B.-J. de Gans, P. C. Duineveld, and U. S. Schubert.
Inkjet printing of polymers: State of the art and future developments.
Advanced Materials, 16(3):203–213, 2004.

[109] A. Bardea and R. Naaman.
Submicrometer chemical patterning with high throughput using magnetolithography.
Langmuir, 25(10):5451–5454, 2009.

[110] T. A. Kumar, A. Bardea, Y. Shai, A. Yoffe, and R. Naaman.
Patterning gradient properties from sub-micrometers to millimeters by magnetolithography.
Nano Letters, 10(6):2262–2267, 2010.

[111] G. P. Lopez, H. A. Biebuyck, and G. M. Whitesides.
Scanning electron microscopy can form images of patterns in self-assembled monolayers.
Langmuir, 9(6):1513–1516, 1993.

[112] C. Vieu, F. Carcenac, A. Pépin, Y. Chen, M. Mejias, A. Lebib, L. Manin-Ferlazzo, L. Couraud, and H. Launois.
Electron beam lithography: resolution limits and applications.
Applied Surface Science, 164(1-4):111–117, 2000.

[113] R. L. Kubena, J. W. Ward, F. P. Stratton, R. J. Joyce, and G. M. Atkinson.
A low magnification focused ion beam system with 8 nm spot size.
Journal of Vacuum Science Technology B: Microelectronics and Nanometer Structures, 9(6):3079–3083, 1991.

[114] A. A. Tseng.
Recent developments in micromilling using focused ion beam technology.
Journal of Micromechanics and Microengineering, 14(4):R15–R34, 2004.

[115] W. Ehrfeld and H. Lehr.
Deep x-ray lithography for the production of three-dimensional microstructures from metals, polymers and ceramics.
Radiation Physics and Chemistry, 45(3):349–365, 1995.

[116] T. Ito and S. Okazaki.
Pushing the limits of lithography.
Nature, 406(6799):1027–1031, 2000.

[117] R. Glass, M. Arnold, J. Blümmel, A. Küller, M. Möller, and J. P. Spatz.
Micro-nanostructured interfaces fabricated by the use of inorganic block copolymer micellar monolayers as negative resist for electron-beam lithography.
Advanced Functional Materials, 13(7):569–575, 2003.

[118] R. D. Piner, J. Zhu, F. Xu, S. Hong, and C. A. Mirkin.
'Dip-pen' nanolithography.
Science, 283(5402):661–663, 1999.

[119] D. S. Ginger, H. Zhang, and C. A. Mirkin.
The evolution of dip-pen nanolithography.
Angewandte Chemie International Edition, 43(1):30–45, 2004.

[120] S. Xu, S. Miller, P. E. Laibinis, and G. Liu.
Fabrication of nanometer scale patterns within self-assembled monolayers by nanografting.
Langmuir, 15(21):7244–7251, 1999.

[121] J.-F. Liu, S. Cruchon-Dupeyrat, J. C. Garno, J. Frommer, and G.-Y. Liu.
Three-dimensional nanostructure construction via nanografting: Positive and negative pattern transfer.
Nano Letters, 2(9):937–940, 2002.

[122] U. Kleineberg, A. Brechling, M. Sundermann, and U. Heinzmann.
Stm lithography in an organic self-assembled monolayer.
Advanced Functional Materials, 11(3):208–212, 2001.

[123] P. C. Hidber, W. Helbig, E. Kim, and G. M. Whitesides.
Microcontact printing of Palladium colloids: Micron-scale patterning by electroless deposition of Copper.
Langmuir, 12(5):1375–1380, 1996.

[124] Y. N. Xia and G. M. Whitesides.
Soft lithography.
Angewandte Chemie-International Edition, 37(5):551–575, 1998.

[125] S. Alom Ruiz and C. S. Chen.
Microcontact printing: A tool to pattern.
Soft Matter, 3(2):168–177, 2007.

[126] A. Gölzhauser, W. Eck, W. Geyer, V. Stadler, T. Weimann, P. Hinze, and M. Grunze.
Chemical nanolithography with electron beams.
Advanced Materials, 13(11):806–809, 2001.

[127] M. Henzler and W. Göpel.
Oberflächenphysik des Festkörpers.
Vieweg & Teubner Verlag, 1994.
Chapter 3.

[128] W. Eck, V. Stadler, W. Geyer, M. Zharnikov, A. Gölzhauser, and M. Grunze.
Generation of surface amino groups on aromatic self-assembled monolayers by low energy electron beams - A first step towards chemical lithography.
Advanced Materials, 12(11):805–808, 2000.

[129] H. U. Müller, M. Zharnikov, B. Völkel, A. Schertel, P. Harder, and M. Grunze.

Low-energy electron-induced damage in hexadecanethiolate monolayers.
The Journal of Physical Chemistry B, 102(41):7949–7959, 1998.

[130] E. Cooper and G. J. Leggett.
Influence of tail-group hydrogen bonding on the stabilities of self-assembled monolayers of alkylthiols on gold.
Langmuir, 15(4):1024–1032, 1999.

[131] N. Ballav, S. Schilp, and M. Zharnikov.
Electron-beam chemical lithography with aliphatic self-assembled monolayers.
Angewandte Chemie-International Edition, 47(8):1421–1424, 2008.

[132] S. Schilp, N. Ballav, and M. Zharnikov.
Fabrication of a full-coverage polymer nanobrush on an electron-beam-activated template.
Angewandte Chemie-International Edition, 47(36):6786–6789, 2008.

[133] W. Geyer, V. Stadler, W. Eck, A. Gölzhauser, M. Grunze, M. Sauer, T. Weimann, and P. Hinze.
Electron induced chemical nanolithography with self-assembled monolayers.
Journal of Vacuum Science Technology B: Microelectronics and Nanometer Structures, 19(6):2732–2735, 2001.

[134] Q. He, A. Küller, M. Grunze, and J. B. Li.
Fabrication of thermosensitive polymer nanopatterns through chemical lithography and atom transfer radical polymerization.
Langmuir, 23(7):3981–3987, 2007.

[135] U. Schmelmer, R. Jordan, W. Geyer, W. Eck, A. Gölzhauser, M. Grunze, and A. Ulman.
Surface-initiated polymerization on self-assembled monolayers: Amplification of patterns on the micrometer and nanometer scale.
Angewandte Chemie-International Edition, 42(5):559–563, 2003.

[136] U. Schmelmer, A. Paul, A. Küller, R. Jordan, A. Gölzhauser, M. Grunze, and A. Ulman.
Surface-initiated polymerization on self-assembled monolayers: Effect of reaction conditions.
Macromolecular Symposia, 217(1):223–230, 2004.

[137] M. Baum and W. J. Brittain.
Synthesis of polymer brushes on silicate substrates via reversible addition fragmentation chain transfer technique.
Macromolecules, 35(3):610–615, 2002.

[138] K. Matyjaszewski, P. J. Miller, N. Shukla, B. Immaraporn, A. Gelman, B. B. Luokala, T. M. Siclovan, G. Kickelbick, T. Vallant, H. Hoffmann, and T. Pakula.
Polymers at interfaces: Using atom transfer radical polymerization in the controlled growth of homopolymers and block copolymers from silicon surfaces in the absence of untethered sacrificial initiator.
Macromolecules, 32(26):8716–8724, 1999.

[139] K. Matyjaszewski and J. H. Xia.
Atom transfer radical polymerization.
Chemical Reviews, 101(9):2921–2990, 2001.

[140] D. M. Jones, J. R. Smith, W. T. S. Huck, and C. Alexander.
Variable adhesion of micropatterned thermoresponsive polymer brushes: AFM investigations of poly (N-isopropylacrylamide) brushes prepared by surface-initiated polymerizations.
Advanced Materials, 14(16):1130–1134, 2002.

[141] S. J. Ahn, M. Kaholek, W.-K. Lee, B. LaMattina, T. H. LaBean, and S. Zauscher.
Surface-initiated polymerization on nanopatterns fabricated by electron-beam lithography.
Advanced Materials, 16(23-24):2141–2145, 2004.

[142] T. L. Sun, G. J. Wang, L. Feng, B. Q. Liu, Y. M. Ma, L. Jiang, and D. B. Zhu.
Reversible switching between superhydrophilicity and superhydrophobicity.
Angewandte Chemie-International Edition, 43(3):357–360, 2004.

[143] R. Advincula.
Polymer brushes by anionic and cationic surface-initiated polymerization (SIP).
In *R. Jordan, Surface-Initiated Polymerization I.* Springer Berlin Heidelberg, 2006.

[144] H. Fujiwara.
Spectroscopic Ellipsometry: Principles and Applications.
Wiley & Sons, 2007.
Chapter 1.

[145] H. G. Tompkins.
A User's Guide to Ellipsometry.
San Diego, CA, Academic Press Inc., 2006.

[146] J. A. Woollam.

Light & Materials - Part 1.
http://www.jawoollam.com/tutorial2.html.
10.03.2013.

[147] V. G. Bordo and H. G. Rubahn.
Optics and Spectroscopy at Surfaces and Interfaces.
Wiley & Sons, 2008.
Chapter 4.

[148] D. H. Goldstein.
Polarized Light.
Optical Engineering Series. Dekker, M., 2003.
Chapter 8.

[149] J. Singh.
Optical Properties of Condensed Matter and Applications.
Wiley Series in Materials for Electronic & Optoelectronic Applications. Wiley & Sons, 2006.
Chapter 1.

[150] W. A. Zisman.
Relation of the Equilibrium Contact Angle to Liquid and Solid Constitution, pages 1–51.
Chapter 2.

[151] P. G. de Gennes.
Wetting: statics and dynamics.
Review of Modern Physics, 57(3):827–863, 1985.

[152] T. Young.
An essay on the cohesion of fluids.
Philosophical Transactions of the Royal Society of London, 95:65–87, 1805.

[153] R. N. Wenzel.
Resistance of solid surfaces to wetting by water.
Industrial & Engineering Chemistry, 28(8):988–994, 1936.

[154] A. B. D. Cassie and S. Baxter.
Wettability of porous surfaces.
Transactions of the Faraday Society, 40:546–551, 1944.

[155] F. M. Hoffmann.
Infrared reflection-absorption spectroscopy of adsorbed molecules.
Surface Science Reports, 3(2-3):107–192, 1983.

[156] R. Winter, F. Noll, and C. Czeslik.
Methoden der Biophysikalischen Chemie.
Vieweg & Teubner Verlag, 2011.
Chapter V 6.

[157] G. Schwedt and J. Schreiber.
Taschenatlas der Analytik.
Wiley VCH Verlag GmbH, 2007.
Chapter 8.5.

[158] R. G. Greenler.
Infrared study of adsorbed molecules on metal surfaces by reflection techniques.
The Journal of Chemical Physics, 44(1):310–315, 1966.

[159] B. L. Frey, R. M. Corn, and S. C. Weibel.
Polarization-Modulation Approaches to Reflection-Absorption Spectroscopy.
In: Chalmers, J.M. and Griffiths, P.R., Handbook of Vibrational Spectroscopy. Wiley & Sons, 2002.

[160] M. E. Pemble and P. Gardner.
Vibrational spectroscopy from surfaces.
In: Vickerman, J. C. and Gilmore, I., Surface Analysis: The Principal Techniques. Wiley & Sons, 2011.
Chapter 7.

[161] B. D. Ratner and D. G. Castner.
Electron spectroscopy for chemical analysis.
In: Vickerman, J. C. and Gilmore, I., Surface Analysis: The Principal Techniques. Wiley & Sons, 2011.
Chapter 7.

[162] J. Blümmel.
Entwicklung biofunktionalisierter Nanostrukturen an Grenzflächen zur Untersuchung der Kinetik des molekularen Motorproteins EG_5.
PhD thesis, Ruprecht-Karls-Universität Heidelberg, 2005.

[163] B. Bhushan.
Part B Scanning probe microscopy.
In: Springer Handbook of Nanotechnology. Springer, 2010.
Chapter 11.3.

[164] F. Braet, R. De Zanger, S. Kämmer, and E. Wisse.
Noncontact versus contact imaging: An atomic force microscopic study on hepatic endothelial cells *in vitro*.

International Journal of Imaging Systems and Technology, 8(2):162–167, 1997.

[165] G. Binnig, C. F. Quate, and Ch. Gerber.
Atomic force microscope.
Physical Review Letters, 56(9):930–933, 1986.

[166] R. Winter, F. Noll, and C. Czeslik.
Methoden der Biophysikalischen Chemie.
Vieweg & Teubner Verlag, 2011.
Chapter IV 1.

[167] H. Hölscher, U. D. Schwarz, and R. Wiesendanger.
Calculation of the frequency shift in dynamic force microscopy.
Applied Surface Science, 140(3-4):344–351, 1999.

[168] S. N. Magonov, V. Elings, and M.-H. Whangbo.
Phase imaging and stiffness in tapping-mode atomic force microscopy.
Surface Science, 375(2-3):L385–L391, 1997.

[169] G. Friedbacher and H. Fuchs.
Classification of scanning probe microscopies.
Pure and Applied Chemistry, 71(7):1337–1357, 1999.

[170] D. Stokes.
Principles and Practice of Variable Pressure: Environmental Scanning Electron Microscopy (VP-ESEM).
RMS - Royal Microscopical Society. Wiley & Sons, 2008.
Chapter 1.

[171] R. F. Egerton.
An introduction to microscopy.
In *Physical Principles of Electron Microscopy*. Springer US, 2005.

[172] P. Walther.
Das Rasterelektronenmikroskop (REM).
http://www.uni-ulm.de/elektronenmikroskopie/2003REM.htm, 2008.
10.03.2013.

[173] W. Senaratne, L. Andruzzi, and C. K. Ober.
Self-assembled monolayers and polymer brushes in biotechnology: Current applications and future perspectives.
Biomacromolecules, 6(5):2427–2448, 2005.

[174] S. Krishnan, C. J. Weinman, and C. K. Ober.
Advances in polymers for anti-biofouling surfaces.
Journal of Materials Chemistry, 18(29):3405–3413, 2008.

[175] G. Albert.
Herstellung und charakterisierung polykristalliner goldschichten zur verwendung in der nanolithographie.
Master's thesis, Institute of Physical Chemistry, University of Heidelberg, 1996.

[176] H. Wang, S. F. Chen, L. Y. Li, and S. Y. Jiang.
Improved method for the preparation of carboxylic acid and amine terminated self-assembled monolayers of alkanethiolates.
Langmuir, 21(7):2633–2636, 2005.

[177] C. D. Bain, E. B. Troughton, Y. T. Tao, J. Evall, G. M. Whitesides, and R. G. Nuzzo.
Formation of monolayer films by the spontaneous assembly of organic thiols from solution onto gold.
Journal of the American Chemical Society, 111(1):321–335, January 1989.

[178] B. Zhu, T. Eurell, R. Gunawan, and D. Leckband.
Chain-length dependence of the protein and cell resistance of oligo(ethylene glycol)-terminated self-assembled monolayers on gold.
Journal of Biomedical Materials Research, 56(3):406–416, 2001.

[179] S. Schilp.
Self-assembled Monolayers and Nanostructured Surfaces as Tools to Design Antifouling Surfaces.
PhD thesis, University of Heidelberg, 2009.

[180] J. Coates.
Interpretation of Infrared Spectra, A Practical Approach.
In: R. A. Meyer, Encyclopedia of Analytical Chemistry. Wiley & Sons, 2006.

[181] S. Krishnan, J. Finlay, A. Hexemer, N. Wang, C. K. Ober, E. J. Kramer, M. E. Callow, J. A. Callow, and D. Fischer.
Interaction of *Ulva* and *Navicula* marine algae with surfaces of pyridinium polymers with fluorinated side-chains.
Polymer Preprints, 46(2):1248–1249, 2005.

[182] R. Valiokas, S. Svedhem, S. C. T. Svensson, and B. Liedberg.
Self-assembled monolayers of oligo(ethylene glycol)-terminated and amide group containing alkanethiolates on gold.
Langmuir, 15(10):3390–3394, 1999.

[183] I. Pasquali, J.-M. Andanson, S. G. Kazarian, and R. Bettini.
Measurement of CO_2 sorption and PEG1500 swelling by ATR-IR spectroscopy.

Journal of Supercritical Fluids, 45(3):384–390, 2008.

[184] F.-G. Wu, J.-J. Luo, and Z.-W. Yu.
Infrared spectroscopy reveals the nonsynchronicity phenomenon in the glassy to fluid micellar transition of DSPE-PEG2000 aqueous dispersions.
Langmuir, 26(15):12777–12784, 2010.

[185] K. Bierbaum, M. Kinzler, C. Wöll, M. Grunze, G. Hähner, S. Heid, and F. Effenberger.
A near edge x-ray absorption fine structure spectroscopy and x-ray photoelectron spectroscopy study of the film properties of self-assembled monolayers of organosilanes on oxidized si(100).
Langmuir, 11(2):512–518, 1995.

[186] A. Gölzhauser, S. Panov, M. Mast, A. Schertel, M. Grunze, and C. Wöll.
Growth of pyromellitic dianhydride on an amino-terminated surface.
Surface Science, 334(1-3):235–247, 1995.

[187] D. R. Kester, I. W. Duedall, D. N. Connors, and R. M. Pytkowic.
Preparation of artificial seawater.
Limnology and Oceanography, 12(1):176–179, 1967.

[188] K. L. Prime and G. M. Whitesides.
Self-assembled organic monolayers - model systems for studying adsorption of proteins at surfaces.
Science, 252(5009):1164–1167, 1991.

[189] S. Herrwerth, W. Eck, S. Reinhardt, and M. Grunze.
Factors that determine the protein resistance of oligoether self-assembled monolayers - Internal hydrophilicity, terminal hydrophilicity, and lateral packing density.
Journal of the American Chemical Society, 125(31):9359–9366, 2003.

[190] D. A. Shirley.
High-resolution x-ray photoemission spectrum of the valence bands of gold.
Physical Review B, 5(12):4709–4714, 1972.

[191] J. H. Scofield.
Hartree-slater subshell photoionization cross-sections at 1254 and 1487 ev.
Journal of Electron Spectroscopy and Related Phenomena, 8(2):129–137, 1976.

[192] J. J. Yeh and I. Lindau.
Atomic subshell photoionization cross sections and asymmetry parameters: $1 \leq Z \leq 103$.

Atomic Data and Nuclear Data Tables, 32(1):1–155, 1985.

[193] I. H. Pratt-Terpstra, A. H. Weerkamp, and H. J. Busscher.
Adhesion of oral streptococci from a flowing suspension to uncoated and albumin-coated surfaces.
Journal of General Microbiology, 133(11):3199–3206, 1987.

[194] S. C. Dexter, J. D. Sullivan, J. Williams, and S. W. Watson.
Influence of substrate wettability on attachment of marine bacteria to various surfaces.
Applied Microbiology, 30(2):298–308, 1975.

[195] T. Miyazawa, K. Fukushima, and Y. Ideguchi.
Molecular vibrations and structure of high polymers. III. Polarized infrared spectra, normal vibrations, and helical conformation of polyethylene glycol.
The Journal of Chemical Physics, 37(12):2764–2776, 1962.

[196] S. P. Cooper, J. A. Finlay, G. Cone, M. E. Callow, J. A. Callow, and A. B. Brennan.
Engineered antifouling microtopographies: kinetic analysis of the attachment of zoospores of the green alga *Ulva* to silicone elastomers.
Biofouling, 27(8):881–891, 2011.

[197] I. Langmuir.
The condensation and evaporation of gas molecules.
Proceedings of the National Academy of Sciences of the United States of America, 3(3):141–147, 1917.

[198] S. M. Bennett, J. A. Finlay, N. Gunari, D. D. Wells, A. E. Meyer, G. C. Walker, M. E. Callow, J. A. Callow, F. V. Bright, and M. R. Detty.
The role of surface energy and water wettability in aminoalkyl /fluorocarbon/hydrocarbon-modified xerogel surfaces in the control of marine biofouling.
Biofouling, 26(2):235–246, 2010.

[199] G. C. Cadée and J. Hegeman.
Seasonal and annual variation in *phaeocystis pouchetii* (haptophyceae) in the westernmost inlet of the Wadden Sea during the 1973 to 1985 period.
Netherlands Journal of Sea Research, 20(1):29–36, 1986.

[200] F. Casse and G. W. Swain.
The development of microfouling on four commercial antifouling coatings under static and dynamic immersion.
International Biodeterioration & Biodegradation, 57(3):179–185, 2006.

[201] A. Myrskog, H. Anderson, T. Aastrup, B. Ingemarsson, and B. Liedberg.
Esterification of self-assembled carboxylic-acid-terminated thiol monolayers in acid environment: A time-dependent study.
Langmuir, 26(2):821–829, 2010.

[202] A. Blume, W. Huebner, and G. Messner.
Fourier transform infrared spectroscopy of 13c:o labeled phospholipids hydrogen bonding to carbonyl groups.
Biochemistry, 27(21):8239–8249, 1988.

[203] R. N. Lewis, R. N. McElhaney, W. Pohle, and H. H. Mantsch.
Components of the carbonyl stretching band in the infrared spectra of hydrated 1,2-diacylglycerolipid bilayers: a reevaluation.
Biophysical Journal, 67(6):2367–2375, 1994.

[204] R. N. Lewis and R. N. McElhaney.
The structure and organization of phospholipid bilayers as revealed by infrared spectroscopy.
Chemistry and Physics of Lipids, 96(1-2):9–21, 1998.

[205] J. W. Costerton, P. S. Stewart, and E. P. Greenberg.
Bacterial biofilms: A common cause of persistent infections.
Science, 284(5418):1318–1322, 1999.

[206] J. H. Pringle and M. Fletcher.
Influence of substratum wettability on attachment of freshwater bacteria to solid surfaces.
Applied and Environmental Microbiology, 45(3):811–817, 1983.

[207] K. M. Wiencek and M. Fletcher.
Effects of substratum wettability and molecular topography on the initial adhesion of bacteria to chemically defined substrata.
Biofouling, 11(4):293–311, 1997.

[208] M. P. Arpa-Sancet, C. Christophis, and A. Rosenhahn.
Microfluidic assay to quantify the adhesion of marine bacteria.
Biointerphases, 7(26):1–9, 2012.

[209] C. Lotz.
Studien zur motilität von pseudomonas aeruginosa in biofilmen.
Master's thesis, Hochschule Fresenius, University of applied science, 2010.

[210] J. Verran and R. D. Boyd.
The relationship between substratum surface roughness and microbiological and organic soiling: A review.
Biofouling, 17(1):59–71, 2001.

[211] M. Wahl, K. Krüger, and M. Lenz.
Non-toxic protection against epibiosis.
Biofouling, 12(1-3):205–226, 1998.

[212] A. V. Bers and M. Wahl.
The influence of natural surface microtopographies on fouling.
Biofouling, 20(1):43–51, 2004.

[213] L. Xiao, S. E. M. Thompson, M. Röhrig, M. E. Callow, J. A. Callow, M. Grunze, and A. Rosenhahn.
Hot embossed microtopographic gradients reveal morphological cues that guide the settlement of zoospores.
Langmuir, 29(4):1093–1099, 2013.

[214] C. J. Long, J. F. Schumacher, P. A.C. Robinson, J. A. Finlay, M. E. Callow, J. A. Callow, and A. B. Brennan.
A model that predicts the attachment behavior of *Ulva linza* zoospores on surface topography.
Biofouling, 26(4):411–419, 2010.

[215] C. M. Magin, C. J. Long, S. P. Cooper, L. K. Ista, G. P. Lopez, and A. B. Brennan.
Engineered antifouling microtopographies: the role of Reynolds number in a model that predicts attachment of zoospores of *Ulva* and cells of *Cobetia marina*.
Biofouling, 26(6):719–727, 2010.

[216] J. F. Schumacher, C. J. Long, M. E. Callow, J. A. Finlay, J. A. Callow, and A. B. Brennan.
Engineered nanoforce gradients for inhibition of settlement (attachment) of swimming algal spores.
Langmuir, 24(9):4931–4937, 2008.

[217] P. Ball.
Engineering shark skin and other solutions.
Nature, 400(6744):507–509, 1999.

[218] M. Tanaka, A. Takayama, E. Ito, H. Sunami, S. Yamamoto, and M. Shimomura.
Effect of pore size of self-organized honeycomb-patterned polymer films on spreading, focal adhesion, proliferation, and function of endothelial cells.
Journal of Nanoscience and Nanotechnology, 7(3):763–772, 2007.

[219] Q. He, A. Küller, S. Schilp, F. Leisten, H. A. Kolb, M. Grunze, and J. B. Li.

Fabrication of controlled thermosensitive polymer nanopatterns with one-pot polymerization through chemical lithography.
Small, 3(11):1860–1865, 2007.

[220] R. R. Bhat, M. R. Tomlinson, T. Wu, and J. Genzer.
Surface-grafted polymer gradients: Formation, characterization, and applications.
In *Surface-Initiated Polymerization II*, pages 51–124. Springer Berlin Heidelberg, 2006.

[221] K. N. Plunkett, X. Zhu, J. S. Moore, and D. E. Leckband.
PNIPAM chain collapse depends on the molecular weight and grafting density.
Langmuir, 22(9):4259–4266, 2006.

[222] J. Zhang and R. Pelton.
The dynamic behavior of poly(N-isopropylacrylamide) at the air/water interface.
Colloids and Surfaces A: Physicochemical and Engineering Aspects, 156(1-3):111–122, 1999.

[223] N. Aldred, A. Scardino, A. Cavaco, R. de Nys, and A. S. Clare.
Attachment strength is a key factor in the selection of surfaces by barnacle cyprids (*Balanus amphitrite*) during settlement.
Biofouling, 26(3):287–299, 2010.

[224] J. F. Schumacher, N. Aldred, M. E. Callow, J. A. Finlay, J. A. Callow, A. S. Clare, and A. B. Brennan.
Species-specific engineered antifouling topographies: correlations between the settlement of algal zoospores and barnacle cyprids.
Biofouling, 23(5):307–317, 2007.

[225] C. J. Long, J. A. Finlay, M. E. Callow, J. A. Callow, and A. B. Brennan.
Engineered antifouling microtopographies: mapping preferential and inhibitory microenvironments for zoospore attachment.
Biofouling, 26(8):941–952, 2010.

Danksagung

Mein großer Dank gilt Prof. Dr. Michael Grunze für die Aufnahme in seine Arbeitsgruppe, die interessante Themenstellung und die Möglichkeit mit vielen Forschern auch international in Kontakt zu treten.

Ganz besonders bedanken möchte ich mich bei Prof. Dr. Axel Rosenhahn für die Betreuung in den letzten Jahren, für die vielen Konferenzen an denen ich teilnehmen durfte und dafür dass er das Beste aus mir herausgeholt hat.

Ich bedanke mich bei apl. Prof. Dr. Hans-Robert Volpp für die Übernahme des Zweit-Gutachters.

Thanks to Prof. Dr. James Callow and Dr. Maureen Callow for the great possibility to spend several weeks at the University of Birmingham and to get to know the last mysteries of the alga *Ulva*.

A great thanks goes to Prof. Dr. Geoffrey Swain and his team for welcoming me three times at the Florida Institute of Technology. I had great times!

I acknowledge the Karlsruhe Nano Micro Facility (KNMF, www.kit.edu/knmf) of the Karlsruhe Institute of Technology for providing access to the e-beam writer at the Institute of Microstructure Technology (IMT). Danke auch an Andrea Bacher für das Strukturieren meiner Proben.

Ein herzliches Dankeschön geht an Silke Kirchen für das gemeinsame Durchführen der Bakterien Assays und das Näherbringen der Mikrobiologie.

Danke auch an Stefan Heissler für die Einführung in die IR Spektroskopie. Peter Lindemann danke ich für den ein oder anderen Background, wenn es bei mir mal wieder zu knapp wurde.

Ein ganz herzliches Dankeschön auch an die AFM Crew Tatjana Ladnorg, Carlos Azucena und Peter Krolla-Sidenstein. Gerade als es am Ende eng wurde, konnte ich mich auf euch verlassen.

Für die Messung und Auswertung der XP Spektren und die zahlreichen fruchtbaren Diskussionen bedanke ich mich bei Nikolaus Meyerbröker und Stella Bauer.

Domenic Kratzer danke ich für die tolle gemeinsame Laborzeit und die Hilfe, wenn es mal wieder um organische Chemie ging.

Ich bedanke mich bei meinen Karlsruher Mädels Tatjana Ladnorg, Maria Girrbach, Anne Lebhard und Maria Buchholz für die herzliche Aufnahme in ihrer

Mitte, für tolle Mittagspausen, Skifahren und alles andere. In euch habe ich neue Freundinnen gefunden.

Natürlich darf auch mein Arbeitskreis nicht vergessen werden. Ich danke euch allen für eine wunderschöne Zeit. Mit Grillen, Schnitzelhaus, Kuchen, Feierabendbier und Co. habt ihr mir die Jahre versüßt! Ein besonderer Dank geht an Stella Bauer, die mir geholfen hat meinen inneren Schweinehund zu überwinden; Stojan Maleschlijski, der immer zur Stelle war, wenn der Computer nicht mehr wollte; Svenja Stuppy für die Waldspatziergänge.

Ein riesen Dankschön geht an Max Hanke für die langjährige Freundschaft und für seine Unterstützung in allen Lebenslagen.

Ich danke meinen Korrekturlesern Stella Bauer, Thomas Gorniak, Max Hanke, Stojan Maleschlijski und natürlich besonders Axel Rosenhahn. Ohne euch wäre die Arbeit heute nicht das, was sie geworden ist.

Meinen drei Liebsten Andrea Back, Melanie Hagenbucher und Jenny Ziriakus danke ich für die jahrelange Freundschaft über alle Ländergrenzen hinaus.

Ich danke Thomas Gorniak für alles.

Der größte Dank gilt natürlich meinen Eltern, meinem Bruder und meiner Oma. Ohne eure finanzielle, moralische und kulinarische Unterstützung wäre ich nie so weit gekommen. DANKE!

Erklärung

Ich erkläre hiermit an Eides Statt, dass ich die vorliegende Dissertation selbst verfasst und mich dabei keiner anderen als der von mir bezeichneten Quellen und Hilfsmittel bedient habe. Ich habe an keiner anderen Stelle ein Prüfungsverfahren beantragt bzw. die Dissertation in dieser oder anderer Form bereits anderweitig als Prüfungsarbeit verwendet oder einer anderen Fakultät als Dissertation vorgelegt.

Heidelberg, den 28.03.2013 .....

(Isabel Thome)